ANALYSIS OF ERC1 CONTRIBUTIONS TO CRANIOFACIAL FORM AND FUNCTION

By

Lauryn N Luderman

Dissertation

Submitted to the Faculty of the

Graduate School of Vanderbilt University

in partial fulfillment of the requirements

for the degree of

DOCTOR OF PHILOSOPHY

in

Neuroscience

May 13, 2022

Nashville, Tennessee

Approved:

Edward Levine, Ph.D.

David Miller, Ph.D.

Heidi Hamm, Ph.D.

Bruce Carter, Ph.D.

Ela W. Knapik, M.D.

DEDICATION

For my family and loved ones

ACKNOWLEDGEMENTS

This work would not have been possible without the support and guidance of many individuals. I would firstly like to thank my mentor, Ela Knapik, for her support over the many years. She took a chance on me, even though I had no cellular or molecular biology experience prior to joining her lab, and allowed me the freedom to follow my passion in neuroscience for my research project. I always knew Ela would have my back and support me in many different scenarios. Working with Ela over the years has taught me so much and has made me a much stronger individual and scientist.

I also want to thank my thesis committee members, Ed Levine, David Miller, Heidi Hamm, Bruce Carter, and former member Rebecca Sappington, for their expertise, time, and guidance. They have undoubtedly strengthened my research by asking me difficult questions to help me recognize the aspects of my project that I've overlooked and to help organize my thoughts and ideas into to testable hypotheses. I am very grateful for their constructive feedback for my thesis work over the years.

I am thankful to the Neuroscience Program for their rigorous training and education that they provided to me. I am especially grateful for Roz Johnson, who could answer any questions I had and was always willing to help. I am very thankful for Chris Wright and the Program in Developmental Biology, who provided me with funding during my first years in graduate school and a great community of scientists and researchers that I could turn to for expertise in developmental biology. Chris is extremely supportive of his trainees, and I have always enjoyed our impromptu elevator and hallway chats. I would also like to thank the Vanderbilt BRET/ASPIRE office for

providing me professional development training and helping me prepare for my future career.

My thesis work would not have been possible without the Vanderbilt Cell Imaging Shared Resource core and the Nikon Center of Excellence. The NCOE became my second home during my time in graduate school, either using the microscopes or analysis workstations. I am thankful to the core for not only providing access to quality hardware and software, but also for allowing me to try out many of the newest microscopes on the market during commercial demos. The people in the core, Jenny Schafer, Kari Seedle, Nick Mignemi, Bryan Millis, were immensely helpful in improving my imaging skills, designing analysis pipelines, and helping me to find my passion for microscopy and image analysis.

I am thankful to my fellow lab members: Dharmendra Choudhary, Dylan Ritter, Mackenzie Michaels, Taylor Nagai, Ali Scalici, Cory Guthrie, Sophia Buzanis, and past members of the Knapik Lab: Daniel Levic, Gokhan Unlu, Amanda Goodrich, Amy Rushing, Kinsey Qi and Joseph Breeyear. I appreciate them for their help to make the Knapik Lab a stimulating, productive and fun environment to work in.

I would not have gotten through all the stress and pressure that comes along with a PhD if it weren't for the love and support of my friends and family. I owe so much to them and cannot thank them enough for everything they've done for me. I am especially thankful for my partner, Adam, who has made me a better, happier person.

TABLE OF CONTENTS

Page

LIST OF FIGURES

CHAPTER I

INTRODUCTION

Overview

The head is one of the most complex structures in vertebrates, consisting of diverse cell types that constitute vasculature, nerves, bone, cartilage, muscles, tendons, and teeth, not to mention the brain. Together these craniofacial tissues perform a variety of functions, such as speaking, breathing, swallowing, chewing, and facial expressions. Over the course of development, craniofacial tissue undergoes growth and morphological changes that are caused by biomechanical processes initiated by either intrinsic or extrinsic cellular forces (Du et al., 2021). Defects in craniofacial morphology, just as in many organ tissues, can have significant impact on function. Understanding the genetic regulation of both craniofacial form and function is currently an understudied aspect of craniofacial biology.

Despite craniofacial function being similar amongst different vertebrate species, craniofacial morphology is quite variable, even within species. This is evident when comparing different types of birds or dogs to one another, but perhaps less evident when comparing facial characteristics of human siblings. In some instances, alteration in craniofacial morphology is a desired trait. For example, certain breeds of dogs have been specifically bred to be brachycephalic, or have a shorten snout/face (i.e., the Bulldog) that is dramatically different from the snout shape of the Labrador retriever. In fact, many domesticated animals are bred for their brachycephalic features, and yet, these changes in

craniofacial morphology are often associated with health conditions (Geiger et al., 2021). For example, Bulldogs and other short snout/face dogs are notorious for having breathing difficulties (Liu et al., 2017a). While morphology can inform function, there are also instances of function influencing craniofacial shape. Throughout evolution, human craniofacial morphology, specifically the mandibular, or jaw region, has undergone pronounced changes in response to diet changes: from the harder diet of hunter-gatherer ancestors to a softer diet that is more agriculturally based (von Cramon-Taubadel, 2011). A softer diet would require less force by the mandible and less stress on the masticatory, or chewing muscles to process the food, and could be an explanation as to why hunter-gatherer ancestors display longer, narrower mandibular shape than current day humans. Similar changes to jaw shape in response to diet has been observed in studies examining the multigenerational effect of consuming a softer diet: soft diet-fed mice have shorter, wider mandibles than hard diet-fed mice (Hassan et al., 2020). These few examples are meant to serve as strong evidence that there is cooperation between form and function when constructing craniofacial tissue. Developmental biologists have discovered many genes that are involved in patterning and structuring craniofacial tissue, and mutations in these genes result in congenital craniofacial abnormalities, which have been confirmed in animal studies. However, craniofacial function, such as jaw movement, is not always examined in these animal disease models, and the role that craniofacial genes play in craniofacial function is not well understood.

The goal of this dissertation is to understand the genetic regulation of craniofacial morphology and function. This introduction describes the biomechanical forces contributing to craniofacial tissue development, and disorders associated with

craniofacial dysfunction. Chapter II describes novel functions of Erc1b in controlling jaw movement in zebrafish by impacting trigeminal nerve growth and craniofacial muscle organization. Chapter III describes a methodology to examine the cell autonomous function of Erc1b in craniofacial tissues. Chapter IV examines the role of zebrafish Erc1 paralogs, Erc1a and Erc1b, in craniofacial development. Chapter V concludes with a discussion of contributions and future implications of this dissertation research to developmental genetics studies and pathophysiology of craniofacial anomalies and jaw dysfunction. Portions of the introduction chapter are adapted from the following review articles:

Luderman, L.N.*, Unlu, G.*****, Knapik, E.W., 2017. Zebrafish Developmental Models of Skeletal Diseases. *Curr Top Dev Biol* 124, 81-124.

*) co-first author.

Luderman, L.N., 2018. Protein interactions in the presynaptic active zone mediate synaptic vesicle docking, voltage-gated calcium channel recruitment to facilitate short-term presynaptic plasticity. *Vanderbilt Reviews Neuroscience*

Mechanobiological inputs contributing to craniofacial morphology

The initial craniofacial morphology of vertebrates begins very early in development, by week 4 gestation in humans or E9.5 in mice, and appears as facial prominences, or outgrowths, and pharyngeal arches. The frontonasal prominence forms the main symmetry of the face, including the midface, forehead, and primary palate, and with the lateral nasal prominences, forms the nose. The pharyngeal arches of vertebrates

will form the rest of the face, including the upper and lower jaw, and neck. The number of pharyngeal arches is species specific, with mammals only having only five pharyngeal arches, while aquatic vertebrates, such as zebrafish, have seven. Each arch is the same structurally, with a layer of ectoderm on the outside, a lining of endoderm internally, and a mesenchyme core containing mesoderm and neural crest cells in between. As each arch contains cells from each germ layer, every arch will form its own associated vasculature, musculature, skeletal, and nervous system structures. In general, cells from the ectoderm form the epidermis, nervous system, and the cranial placodes, such as the lens, olfactory, otic placodes (Schlosser, 2006). The endodermal layer contributes to the pharynx and gland tissue. Voluntary muscles and endothelial cells in the head are produced from the mesoderm and mesenchymal cells (Noden, 1988; Noden and Francis-West, 2006; Trainor and Tam, 1995). Cranial neural crest cells, by far the most diverse cell type in the developing embryo head, differentiate into cartilage, bone, tendons, pigment, and components of the peripheral nervous system (Lumsden et al., 1991; Noden, 1983; Schilling and Kimmel, 1994). At early embryonic stages, neural crest cells and mesenchymal cells are interacting and influencing one another during migration and differentiation (Grenier et al., 2009; Noden and Trainor, 2005). These dynamic interactions between craniofacial tissues during embryonic and post-embryonic development are important for understanding the pathology of congenital craniofacial abnormalities.

While bone and cartilage are considered the foundation of craniofacial morphology, these hard skeletal structures are heavily influenced by soft and connecting tissues, such as muscles, nerves, and tendons. The formation of the endoskeletal system is

unique to vertebrates and its components are highly conserved. The general mechanisms of bone development are classified into two highly conserved processes based on the progression of mesenchymal progenitors: through either cartilage intermediate, endochondral bone formation, or directly to bone by the process of membranous ossification (Berendsen and Olsen, 2015). To begin, mesenchymal stem cells migrate to locations of future bones and condense before differentiating into either chondrocytes or osteoblasts. Endochondral ossification, on the other hand, involves an intermediate step of differentiated chondrocytes secreting cartilage extracellular matrix and forming structural anlage that will ultimately be replaced by bone in areas including the skull base, axial and appendicular skeleton. Mesenchymal stem cells that differentiate into osteoblasts will directly produce bone as part of the membranous neurocranium (the portion of the skeleton skull) and viscerocranium (facial skeleton, including jaw) through intramembranous ossification, these bones including gill covers, shoulder girdle and fin spine rays are often referred to as dermal bones (Miyashita, 2016).

Vertebrate animal models, mainly mouse (Trainor, 2005), chick (Abramyan and Richman, 2018), and zebrafish (Kimmel et al., 2001), have been essential to uncovering the genetics and biochemical signals that underlie craniofacial development. More recently, there has been more of a focus on understanding the interplay between biochemical signals and mechanical forces in the shaping, or morphology of craniofacial tissues, specifically of bone, cartilage, and connective tissue. Here, I will discuss the main mechanical forces driving craniofacial morphogenesis and how they are influenced by genetic or chemical signals. The mechanical forces discussed include 1) proliferation and intrinsic cellular changes, 2) cytoskeleton influences on cell migration, shape, and

polarity, 3) muscle contraction-based stimulation, and 4) the effects of extracellular matrix (ECM).

Cell proliferation as a driver of morphological changes

Intrinsic cellular properties, such as proliferation, apoptosis, and volume changes, play significant roles in morphological changes during embryonic development, and alterations in these properties can lead to developmental malformations, such as hypoplasia. Some of the common developmental morphogens or signaling pathways, such as Hedgehog, bone morphogenetic proteins (BMPs), and Wnt signaling, are involved in proliferation and growth of craniofacial cells. To expand tissues into a particular shape, cells can undergo directional, or anisotropic, cell division. Differential growth and anisotropic division also contribute to species-specific craniofacial morphology.

The cranial neural crest cells are one of the most proliferative cells early in craniofacial development. Following specification and delamination from the ectoderm, cranial neural crest cells migrate in streams towards the facial primordia where they will proliferate and differentiate into numerous tissues, such as bone and cartilage (Szabo-Rogers et al., 2010). Analysis on neural crest cell migration and proliferation in chick embryos found that only a small percentage (<10%) of migrating neural crest cells undergo mitosis during migration, however, once cells have entered the branchial arches, their mitotic activity significantly increases (Ridenour et al., 2014). This finding suggests the presence of mitogenic signals within target pharyngeal arches that influence neural crest cells to begin dividing. This type of controlled proliferation may also assist neural crest cells in their invasion of presumptive pharyngeal arches, much like cancer cells. The

proliferation of neural crest cell populations is important for the expansion of pharyngeal arches and downstream differentiation into various cell tissues.

Facial primordia also contain localized proliferative zones that contribute to morphology. For example, the frontonasal ectodermal zone (FEZ), a region of superficial ectoderm first identified in chick embryos, is important for growth and patterning of the frontonasal process (Hu et al., 2003). This region is defined by non-overlapping *Fibroblast growth factor 8* (*Fgf8*) and *Sonic hedgehog* (*Shh*) expression domains, which contribute to dorsoventral patterning of the frontonasal process and upper beak prior to outgrowth. Transplantation of an ectopic FEZ from a quail embryo onto either the frontonasal process or the mandibular primordia was enough to stimulate ectopic growth mimicking the underlying tissue (Hu et al., 2003). This study not only introduces the idea that there are specific regions of outgrowth that influence craniofacial morphology, but also provides evidence that *Fgf8* and *Shh* are important factors in craniofacial growth and morphology, which has been replicated in other studies (Abzhanov and Tabin, 2004; Chong et al., 2012; Crump et al., 2004; Marcucio et al., 2005; Wada et al., 2005). The FEZ has been identified in both mouse and human embryos, while zebrafish embryos may have a similar structure, based on defects in neurocranium growth in *shh* and *fgf8* mutants (Crump et al., 2004; Hu and Marcucio, 2009; Odent et al., 1999; Wada et al., 2005). Variation in FEZ size is likely one source contributing to species-specific craniofacial morphology differences. For example, bilateral FEZ in a chick embryo merges to form a single midline region of proliferation, resulting in a narrow beak; in contrast, in a duck, the FEZ remains as two separate proliferation zones, contributing to the broader duck bill (Wu et al., 2006). The location of highest proliferation within FEZ

also influences beak curvature in bird species: a more proximal region of proliferation yields a more curved beak in the cockatiel, compared to the flat duck bill, which manifests from a dorsal region of proliferation in the FEZ (Wu et al., 2006).

Other signaling pathways, such as BMP and Wnt signaling, influence cell proliferation and have been linked species-specific morphology. Regulation of BMP signaling by antagonists Noggin (*Nog*) and Chordin (*Chrd*) drives mandible growth in mice (Stottmann et al., 2001). In BMP-deficient mice, mandible outgrowth and development is abolished (Liu et al., 2005); however, in BMP gain-of-function mouse models, either by knockout of Noggin (*Nog-/-)* or overexpression of constitutively active BMP receptors, chondrocyte proliferation was elevated, leading to an enlarged Meckel's cartilage and mandible (Wang et al., 2013). Tissue specific knockouts in mice also demonstrated distinct roles of Noggin during craniofacial development: early expression of *Nog* is important for cranial neural crest survival, whereas at later developmental stages, *Nog* regulates cartilage size by balancing BMP signaling during proliferation (Matsui and Klingensmith, 2014). Further examples of the role of BMP signaling during proliferation comes from bird species, where *Bmp4* expression is enriched in highly proliferative regions and may be a driving factor in species-specific beak morphology (Abzhanov et al., 2004; Wu et al., 2006). Canonical Wnt signaling also plays a prominent role in proliferation during craniofacial morphogenesis. In developing mouse embryos, active Wnt signaling was found at highly proliferative areas, such as the maxillary and lateral nasal prominences, and inhibition of Wnt signaling resulted in craniofacial abnormalities (Brugmann et al., 2007). Wnt-mediated proliferation is also evident in zebrafish embryos, as morpholino knockdown of a Wnt (*wnt9a*), or Frizzled genes (*frzb*

or *frzd7a*) resulted in reduced chondrocyte proliferation and shortened zebrafish ethmoid plate and trabeculae during craniofacial development (Dougherty et al., 2013; Kamel et al., 2013). While the role of Wnt in proliferation during craniofacial development is conserved across vertebrates, differential Wnt signaling may also contribute to species-specific facial outgrowth and morphology. In chick embryos, active Wnt signaling is restricted to a single midline stripe where the protruding beak will form; in contrast, active Wnt patterning in mice is predominant in lateral regions, driving an expanded midface morphology (Brugmann et al., 2007).

Directional cell proliferation contributes to not only elongation and growth, but also to the shape of tissues. For example, in the forming limb bud, mesenchymal cells undergo oriented cell divisions which drive elongation of the limbs (Wyngaarden et al., 2010). Unlike long bones of the limbs, the face is made up of many uniquely shaped skeletal elements, such as curved structures that make up the skull or the jawbone. Regardless, a similar process of anisotropic cell divisions happens in craniofacial morphogenesis, beginning with oriented cell divisions of clonal populations of cranial neural crest cells that will ultimately populate various craniofacial regions (Kaucka et al., 2016). Later in development, chondrocytes also undergo heterogenous anisotropic proliferation, producing localized ‘hot spots’ of growth that contribute to the bending and shaping of cartilaginous structures such as the nasal capsule (Kaucka et al., 2017). Hedgehog signaling may be one pathway involved in directional proliferation as disrupted signaling impacted morphogenesis of the zebrafish opercle, a neural crest-derived dermal bone in the second pharyngeal arch (Huycke et al., 2012). The opercle morphology was smaller in a null mutant for *indian hedgehog a* (*ihha*), a Hedgehog

ligand, compared to wild type zebrafish larvae, specifically due to a reduction in the number of proliferating cells along the posteroventral axis of the growing bone. The opposite opercle morphology was observed a zebrafish mutant for the Hedgehog receptor *patched 1* (*ptch1*), which is a negative regulator of Hedgehog signaling, thus, suggesting that Hedgehog signaling plays a role in directional proliferation and growth in facial bones (Huycke et al., 2012). Planar cell polarity is another pathway likely to be involved in directional growth of craniofacial tissues. Mutations of planar cell polarity pathway genes, including Wnt5a, a non-canonical Wnt, result in shortened craniofacial morphology in both mouse and zebrafish models (LeClair et al., 2009; Yamaguchi et al., 1999). However, these observed morphological defects were not due to a loss of proliferation, but rather, a loss of cellular orientation (Kaucka et al., 2016; Kaucka et al., 2017). This would suggest that proliferation alone is not enough to influence morphology, and that other mechanical inputs, such as those from the cytoskeleton or from muscle contractions, play additional roles in shaping craniofacial tissue.

Although proliferation is a driving force in tissue growth, apoptosis also plays a role in craniofacial morphogenesis. Craniofacial apoptosis is typically found at locations of epithelial fusion, such as during secondary palate fusion (Jin and Ding, 2006). The palate forms the roof of the mouth and separates the oral and nasal cavities. Defects in palatogenesis results in cleft palate, one of the most frequently observed craniofacial abnormalities (Dixon et al., 2011). Secondary palatogenesis begins as mesenchymal shelves extend vertically towards the mandible along either side of the tongue, before reorienting themselves to a horizontal position above the tongue. The two palatal shelves grow towards each other and make contact at the medial edge epithelium, which triggers

a fusion process to create the midline epithelial seam. This seam degenerates to give rise to a single, continuous palate. Programmed cell death is a popular mechanism driving degeneration of the midline epithelial seam (Cuervo and Covarrubias, 2004). Apoptosis at the midline seam has been shown to be triggered by retinoic acid, Tgfβ3, and Irf6 signaling in order to induce palate fusion (Cuervo et al., 2002; Lane et al., 2015; Richardson et al., 2009). Additionally, a significant portion of animals exhibited cleft palate in a mouse triple knockout of intrinsic apoptotic genes (*Bok, Bax*, *Bak*) (Ke et al., 2018). However, other studies have identified cell migration as another possible mechanism underlying palate fusion and medial seam degeneration (Carette and Ferguson, 1992; Jin and Ding, 2006). While palate fusion is an example of appropriate apoptosis function, there are also instances of aberrant apoptosis leading to craniofacial abnormalities, which will be discussed further in another section (Compagnucci et al., 2021).

Cytoskeleton influences cell migration, shape, and polarity

The cytoskeleton system drives several processes that are important during morphogenesis including cell migration, shape, and polarity. Actin and microtubules are dynamic cytoskeletal structures that generate pushing and contractile forces through crosslinking and interacting with associated proteins. Defects in cytoskeleton dynamics and assembly, or in cytoskeleton associated proteins can cause craniofacial abnormalities in vertebrates (Larson et al., 2010; Nie et al., 2011; Saadi et al., 2011).

Cell migration requires crosstalk between cytoskeleton structures and intracellular and extracellular cues in order to drive movement. In general, cell migration can be broken down into five steps: establishment of a front-rear polarity axis, extension of a

leading edge by actin polymerization, adhesion to a substrate or other cells through focal adhesion complexes, cell body contraction by interactions between actin and myosin motor proteins, and rear retraction. Cranial neural crest cells migration requires cytoskeleton dynamics in order to move from the neural tube into target pharyngeal arches, however, the mechanism of migration, either through individual migration or collective migration, has been up for debate (Richardson et al., 2016; Szabó and Mayor, 2018). Actin binding proteins are expressed in both pre-migratory and migratory neural crest cells (Vermillion et al., 2014). Impaired actin dynamics through loss of either actin depolymerizing factors or stabilizing proteins, such as Caldesmon, results in decreased neural crest cell migration (Gurniak et al., 2005; Nie et al., 2011; Vermillion et al., 2014). Migration defects are due to loss of protrusions from the leading cell edge and disrupted adhesions (Nie et al., 2011). Knockdown of an unconventional myosin, Myosin-X, that interacts with actin to induce cell contractility, also results in neural crest cell migration defects (Nie et al., 2009). Defects in neural crest migration into the pharyngeal arches ultimately causes missing or abnormal cartilage formation in vertebrates (Nie et al., 2009, 2011).

The cytoskeleton also influences cell shape. In the cell migration studies mentioned above, loss of Caldesmon or Myosin-X resulted in loss of leading-edge protrusions in migrating neural crest cells, changing the overall cell morphology. Cytoskeleton dynamics also affect the cells shape of non-migrating cells, predominantly through actomyosin-based contraction (Mao and Baum, 2015; Martin et al., 2009). The function of actomyosin contraction in morphogenesis has been best demonstrated during apical constriction during epithelial sheet invagination (Martin et al., 2009). In short,

signaling cues organize actomyosin cables around the apical surface of cells in an epithelial monolayer, and contraction of the actomyosin system will shrink the apical surface like pulling on purse strings, thus causing the epithelial layer to buckle. Similar mechanisms of apical constriction are involved in the folding of the lens and inner ear placodes during craniofacial morphogenesis (Houssin et al., 2020; Sai et al., 2014). Microtubules can also contribute to cellular morphogenetic changes, such as changes in cell length during myoblast elongation and fusion (Straube and Merdes, 2007). Although microtubules are bendable yet rigid structures, they are not often considered the main generators of force on the cell cortex, like actin. However, orientation of microtubules towards the cell cortex allows for trafficking of cellular components that would be necessary for morphology changes. While cell shape regulation in mesenchymal cells (e.g. fibroblasts, chondrocytes, neural crest stem cells), or other isolated cells remains poorly understood, they are likely influenced by forces other than the cytoskeleton, such as the extracellular matrix.

Polarity is manifested in cells as asymmetric distribution of organelles, intracellular trafficking, plasma membrane allocations, and the cytoskeleton. The cytoskeleton itself is polarized in its structure: actin and microtubules are made up of asymmetric monomers (globular actin or α/β tubulins, respectively), that line up head to tail, resulting in two structurally different ends on the filaments, with the barbed (actin) or plus (microtubule) end having higher monomer association rates, and the pointed (actin) or minus (microtubule) end having higher monomer dissociation rates (Li and Gundersen, 2008). The cell capitalizes on the inherent polarity of cytoskeletal structures through numerous cytoskeleton-associated proteins, such as motor proteins, which can function in

polarized membrane-bound vesicle trafficking. As mentioned above, the cytoskeleton is involved in establishing polarity during cranial neural crest cell migration and is necessary for craniofacial morphogenesis. Another type of polarity that is important for craniofacial development is planar cell polarity, which drives a number of cell behaviors during development, such as polarized cell migration, oriented cell divisions, cell shape changes and intercalation in both vertebrates and invertebrates (Gong et al., 2004; Kiefer, 2005; Marlow et al., 2002; Wansleeben and Meijlink, 2011). All of these polarizing behaviors suggests some influence by the cytoskeleton. Studies have discovered interactions between the planar cell polarity components and the microtubule organizing center, which imbues polarity based on its intracellular position (Sepich et al., 2011). During craniofacial development, planar cell polarity signaling functions in intercalating newly differentiated chondrocytes into columns of disk-like cells that closely resemble a stack of coins (Kimmel et al., 1998). In zebrafish, the microtubule organizing center position, and therefore cellular polarity, within pharyngeal arch 1 chondrocytes is altered during the intercalation phase (Le Pabic et al., 2014). This pattern of cartilage polarity and chondrocyte stacking is conserved between both zebrafish and mice (Le Pabic et al., 2014). Morpholino knockdown of two planar cell polarity components, Fat3 and Dachsous-2, in zebrafish causes both a loss of chondrocyte stacking and loss of cell polarity, assessed by microtubule organizing center location (Le Pabic et al., 2014). Surprisingly, this group also found that influencing the planar cell pathway also affected chondrocyte differentiation, suggesting additional roles for planar cell pathways beyond that of coordinating morphogenesis.

Muscle contraction stimulation is important for chondrocyte intercalation, joint formation

It is well known that there is a strong relationship between muscles and the skeletal system. This relationship is just as important at elderly stages, when muscle mass is decreased and bones become brittle, as it is during development, when muscle contraction provides important mechanical signals for morphogenesis of skeletal structures, connective tissue, and joints (Shwartz et al., 2013). The craniofacial muscles are derived from the mesoderm, whereas the craniofacial skeletal elements (bone, cartilage, tendons) are derived from the cranial neural crest cells (Noden, 1983). For the most part, the scope of this section will be limited to the musculoskeletal crosstalk involved in morphology of the masticatory system. The masticatory system in humans is comprised of the mandible (lower jawbone) and maxillae (upper jawbone), the masticatory muscles (temporalis, pterygoids, and masseter), and the temporomandibular joint among other craniofacial tissues, including neurovascular elements (Buvinic et al., 2021). This system is responsible for jaw movements that comprise many craniofacial functions, such as chewing, sucking, swallowing, and speech. There are several key biochemical and anatomical differences between masticatory muscles and trunk/limb muscles, including muscle myosin composition, fiber diameter, and contraction dynamics (Isola et al., 2018; Korfage et al., 2005; van Eijden and Turkawski, 2001). These differences provide the jaw muscles the ability to take on high contraction forces while resisting fatigue to perform the aforementioned craniofacial functions. However, before jaw muscle contractions are used for eating food, such contractions play a role in forming the jaw shape.

Spontaneous movements are evident very early in development. In humans, movement can be observed as early as 7 weeks, and zebrafish embryos can begin moving as early as 24 hours post-fertilization (Kimmel et al., 1995b; Lüchinger et al., 2008). Most of these movements are elicited by active skeletal muscle contractions following coordinated electrical firing of innervating motor neurons through a specialized synapse, the neuromuscular junction (NMJ). However, there are examples of passive movements in embryonic development that are caused by maternal movement, for example (Nowlan et al., 2012). Active muscle contraction, and passive movement to a lesser extent, can produce mechanical forces necessary for skeletal morphogenesis. Numerous vertebrate studies have examined the effect of 'muscle-less' or paralysis on the skeletal system, all of which demonstrate significant defects in craniofacial morphology (Hall and Herring, 1990; Hinits et al., 2011; Nowlan et al., 2010). These findings are clinically relevant as decreased or absent spontaneous fetal movements in utero leads to the lethal condition fetal akinesia deformation sequence (FADS, OMIM #208150), characterized by severe abnormalities, including craniofacial defects, joint contractures, and tissue hypoplasia (Adam et al., 2018; Nayak et al., 2014). FADS pathogenesis may be myogenic or neurologic in nature (Adam et al., 2018). There have been several NMJ and synaptogenesis gene mutations linked to FADS including acetylcholine receptor subunits and associated genes (*CHRNA1* OMIM #100690*, CHRND* OMIM #100720), *RAPSN* (OMIM #601592), *MuSK* (OMIM #601296), and *DOK7* (OMIM 610285) (Michalk et al., 2008; Vogt et al., 2009; Wilbe et al., 2015). Although mutations in NMJ genes result in craniofacial abnormalities, including cleft palate, hypertelorism, depressed nasal bridge,

micrognathia, and low-set ears, very few studies have investigated the specific roles of these genes or the NMJ in craniofacial morphogenesis.

Animal studies can help understand that pathogenesis of the craniofacial defects observed in FADS patients. For example, micrognathia could be due to defects in chondrocyte intercalation and extension of the craniofacial skeleton. This was observed in zebrafish where muscle paralysis, from chemical treatment or genetic mutations, prevented proper chondrocyte stacking during the intercalation phase of cartilage morphogenesis, resulting in shorter, thicker Meckel's cartilage and alterations to jaw shape (Shwartz et al., 2012). Additionally, muscle activity is also required for joint morphology and integrity during development, which may explain joint contractures observed in FADS. Loss of muscle activity in zebrafish caused morphological changes to the jaw joint that forms between the Meckel's and the palatoquadrate cartilage and leads to defects in jaw movement (Brunt et al., 2015; Brunt et al., 2016). However, a hyperactive zebrafish model also caused alterations to jaw joint shape, thus suggesting that there is an optimal level of muscle activity needed for morphogenesis (Brunt et al., 2016). Lastly, mechanical force generated by muscle contraction plays a role in development and maturation of tendon connective tissue (Peterson et al., 2021). Although tendons have not been exclusively examined in FADS, connective tissue abnormalities can restrict fetal movement that can lead to congenital contractures such as those observed in FADS (Hall, 2014). Onset of muscle contraction in zebrafish leads to changes in tenocyte morphogenesis located in the myotendinous junction of craniofacial muscles, which becomes defective in a paralysis model (Subramanian et al., 2018). Defects in muscle activity also significantly altered the extracellular matrix surrounding

tenocytes, which would impact the function of the myotendinous junction in maintaining connection between muscle and bone (Subramanian et al., 2018; Subramanian and Schilling, 2015). These findings further illustrate the role of extracellular matrix in the morphology and function of craniofacial tissues, which will be further discussed in the section below.

ECM properties and composition affect craniofacial morphology

The extracellular matrix (ECM) is a dynamic structure that provides a mechanical context to cells while maintaining gradients of growth factors and morphogens necessary for migration, proliferation and differentiation of progenitor cells to mature tissue. The components of ECM, including bound water, proteins and polysaccharides, are synthesized and are secreted to the extracellular milieu by exocytic machinery in an organized, regulated fashion. ECM composition is unique to each tissue. For example, chondrocytes and osteoblasts secrete type II and type I collagens that are characteristic of mature cartilage and bone, respectively (Gay et al., 1976; Li et al., 1995; Reddi et al., 1977). Secreted extracellular cargos are synthesized in the ER, the gateway of the secretory pathway, and are carried forward to the central processing and sorting station, the Golgi complex, from which the post-Golgi system of specialized vesicular coats direct them to their final destinations (Schekman and Orci, 1996). COPII (coat protein II complex) mediates the first leg of the secretory pathway from the ER to the ER-to-Golgi Intermediate Compartment (EGRIC) and then to the Golgi complex during secretion of ECM components. Details on this process were recently reviewed by our lab and others (Brandizzi and Barlowe, 2013; Melville and Knapik, 2011; Szul and Sztul, 2011; Unlu et al., 2014). In brief, COPII complex assembly begins when Sar1, a cytoplasmic GTPase,

is activated through GTP binding (Barlowe et al., 1993). Sar1 recruits heterodimers, Sec23/Sec24, to form the "inner coat" (Bi et al., 2002) and Sec12, a guanine nucleotide exchange factor (GEF) for Sar1, cooperates with Sec16, a scaffold protein, to assist with vesicular carrier formation. Sec24 acts as cargo loading adaptor (Barlowe and Schekman, 1993). When the vesicle is ready to dissociate from ER membrane, Sec23, a GTPase activating protein (GAP), deactivates Sar1 (Yoshihisa et al., 1993). Following assembly of the inner coat, Sec13/Sec31 heterotetramer assists in the formation of an outer coat that stabilizes the entire complex as it travels from the ER to the EGRIC (Copic et al., 2012). The importance of COPII proteins in the craniofacial skeleton morphology has been highlighted by studies in patients with craniofacial dysmorphology syndromes and zebrafish with mutations in COPII genes.

The physical properties of the ECM changes over the course of development, and how cells sense and respond to these physical changes will ultimately affect tissue morphogenesis. Cells rely on integrins, which are transmembrane heterodimeric receptors, to attach to the ECM and sense changes to induce downstream signaling to drive migration, differentiation, and proliferation within the cell (Geiger et al., 2001). While the extracellular domains of integrins bind to ECM ligands such as fibronectin, the intracellular face of the protein associates with focal adhesion complexes that connects to the actin cytoskeleton to control contractility of the cell. This crosslinking of ECM to cytoskeleton through integrin-mediated focal adhesion complexes allows the cell not only sense the ECM, but also to respond in turn by altering ECM stiffness through actomyosin contractions or by modulating ECM composition and crosslinking (Muncie and Weaver, 2018). The balance of ECM stiffness and cell-ECM adhesion is important for neural crest

cell migration. During the migratory phase, there is a gradual increase in stiffness of ECM ahead of migrating cranial neural crest cells in vivo (Barriga et al., 2018). Furthermore, ECM stiffness and therefore neural crest cell migration are affected by directly interfering with actomyosin contractility of neural crest cells (Barriga et al., 2018). Perturbing the mechanosensing ability of neural crest cells by inhibiting integrin signaling also significantly impacts neural crest cell migration. Conditional knockout of β1 integrin in mouse neural crest cells not only inhibited neural crest cell migration, but also compromised deposition of ECM components, such as fibronectin, laminin, and collagen IV (Pietri et al., 2004). This suggests an iterative role of ECM sensing and deposition by neural crest cells during development.

The ECM also plays a role in controlling where and how quickly neural crest cells can migrate. As neural crest cells migrate, they encounter physical barriers of ECM that influence their migration stream. These ECM barriers are broken down and remodeled by Matrix Metalloproteinases (MMPs) and A Disintegrin and Metalloproteinases (ADAMs). Expression of these proteases are required for cranial neural crest cell migration and craniofacial morphology. In a mouse model, conditional knockout of ADAM10 from cranial neural crest cells led to craniofacial dysmorphia, including shortened mandibular and maxilla bones (Tan et al., 2016). In Xenopus cranial neural crest cells, defective protease function of ADAM13 prohibits cell migration; however, ectopic expression of wild-type protein resulted in mislocalization of cells due to a breakdown in the migration pathways (Alfandari et al., 2001). This gain-of-function phenotype suggests that protease expression and/or function is regulated based on cranial neural crest migration pathways to specific pharyngeal target. ECM components themselves can function as permissive

and non-permissive signals in order to maintain migratory pathways of cranial neural crest cells (Perris and Perissinotto, 2000). Permissive ECM components, such as fibronectin and laminin, support strong cell-ECM adhesion and migration, likely due to expression of integrins and other laminin receptors on the neural crest cell surface (Perris and Perissinotto, 2000; Strachan and Condic, 2003; Strachan and Condic, 2008). Non-permissive or inhibitory ECM components, including aggrecan and versican proteoglycans, are expressed in barrier tissues that exclude migrating neural crest cells and help to define and maintain neural crest cell migration streams (Perissinotto et al., 2000). Knockdown of versican in Xenopus resulted in slow, disorganized neural crest cell migration that affects neural crest derivatives such as craniofacial cartilage (Szabó et al., 2016). During migration, cranial neural crest cells are subject to a gradient of permissive and non-permissive ECM molecules, and must regulate dynamic expression of integrins and other ECM receptors in order to navigate to target pharyngeal arches (Strachan and Condic, 2004).

Beyond its role in migrating neural crest cells, the ECM also functions in differentiation, cell shape, and tissue homeostasis during morphogenesis (Muncie and Weaver, 2018; Scott, 2003; Wang et al., 2015). The importance of the ECM during development is further illustrated in the number of congenital skeletal disorders associated with defects in ECM trafficking, composition, and processing (Luderman et al., 2017). The use of vertebrate models has furthered our understanding of the role of ECM and its interactions during development, as well as the pathology that underlies craniofacial dysmorphology and dysfunction.

Craniofacial abnormalities in patients illustrate the interplay between morphology and function

Craniofacial abnormalities comprise over one-third of congenital birth defects and affect the shape of craniofacial structures including the palate, jaw, temporomandibular joint, nose, forehead, skull, and ear to varying degrees (Twigg and Wilkie, 2015). Congenital craniofacial abnormalities arise from mutations in genes that are linked to cranial neural crest cell formation, migration, and differentiation, some of which have been discussed in earlier sections. In addition to genetic mutations, malformations of craniofacial tissue can also emerge following teratogen exposure during development (Liu et al., 2020). The use of vertebrate models has been pivotal in uncovering not only genes involved in craniofacial development, but also in understanding the pathogenicity of congenital craniofacial disorders. Here, I will briefly discuss how morphological phenotypes associated with a few congenital craniofacial disorders affects the function of craniofacial tissues, including feeding, breathing, and other jaw movement functions. Table 1.1 provides further information on these craniofacial disorders including associated genes, phenotypes, and available animal models to examine gene function.

Cleft lip and palate (CLP) is the most common facial deformity and is caused by disruptions in the development and fusion of the tissues that make up the lip and palate (Dixon et al., 2011). The palate plays a crucial role during feeding, speech and breathing, therefore disruptions in its morphology can have detrimental effects on these crucial craniofacial functions (Matsuo and Palmer, 2008). CLP is an observable phenotype in a range of craniofacial malformation syndromes, including more than 500 Mendelian disorders, and yet, approximately 70% of CLP cases are considered non-syndromic

(Dixon et al., 2011; Martinelli et al., 2020). Nonetheless, genes associated with CLP are involved in developmental pathways that control cell growth and proliferation, cell adhesion, cytoskeleton interactions, and the extracellular matrix (Burg et al., 2016; Dixon et al., 2011; Martinelli et al., 2020). Two craniofacial functions most impacted by CLP are feeding and speech. Feeding deficits are of most concern immediately after birth as inadequate feeding can lead to malnutrition and delayed growth and development. CLP can impact the formation of a seal by the lips and the intraoral pressure that is needed for suckling and swallowing (Duarte et al., 2016). For this reason, feeding intervention is critical during early childhood (Bessell et al., 2011). Movement of the jaw is also a concern during feeding in CLP patients. Malocclusions, such as anterior and/or posterior crossbite, are often observed in CLP patients following surgery repair due to defects in maxillary growth (Paradowska-Stolarz and Kawala, 2014). Studies have shown that masticatory muscle activity varies in CLP patients compared to controls during rest and masticatory muscle clenching (Szyszka-Sommerfeld et al., 2020; Szyszka-Sommerfeld et al., 2018). These studies indicate CLP patients with malocclusions have difficulty in mastication, however, it is unclear whether this is a defect that is specific to CLP, or a side effect of surgical procedures. Later in life, speech becomes another concern related to CLP. The soft palate and roof of the mouth functions in speech to produce the sound of certain constants and vowels, and CLP can result in defects in articulation, resonance, and voice volume, which can be addressed in speech therapy (Mildinhall, 2012). In general, management and treatment of CLP involves a multi-disciplinary team of healthcare professions to address both the facial aesthetics and functional deficits through different therapies.

The morphology of the lower jaw, or mandible, can also have significant impact on craniofacial function. The mandible is the largest bone in the human skull and is one of the few skull bones subject to movement. Movement of the mandible is especially important during feeding, breathing and speech. Congenital defects in the mandible include micrognathia (also known as mandibular hypoplasia) and prognathia, or jaw protrusion. Mandibular prognathism is most often associated with Class III malocclusions and reduced masticatory efficiency (Chang et al., 2006; Iwase et al., 2006; Kobayashi et al., 2001). Additionally, mandibular prognathism patients also exhibit decreased masticatory muscle activity during clenching tasks, which likely contributes to masticatory defects (Kanzaki et al., 2019). Micrognathia is associated with many craniofacial syndromes including Pierre Robin Sequence, Treacher Collins syndrome, and hemifacial microsomia syndromes. Micrognathia can cause difficulties in breathing due to a smaller oral cavity area for the tongue to sit (Poets and Bacher, 2011). Patients with micrognathia often have feeding difficulties related to swallowing impairment (Paes et al., 2017; Van De Lande et al., 2018). However, it's currently unknown whether these feeding defects are due directly to the small mandible or due to a neuromuscular defect.

As discussed early, muscular activity has important function in craniofacial morphogenesis, and lack of muscle contraction leads to lethal syndromes such as Fetal Akinesia Deformation (FADS). Less severe examples of congenital muscular defects affecting craniofacial morphology are muscular dystrophies and myasthenic syndromes. Muscular dystrophies, such as Duchenne muscular dystrophy and myotonic dystrophy, are progressive muscle weakness disorders that affect a number of muscles, including facial and jaw muscles (Kiliaridis and Katsaros, 1998). Malocclusion is a common

craniofacial characteristic of muscular dystrophies, likely due to the progressive weakness of the craniofacial muscles (Fontinha et al., 2018; Kiliaridis and Katsaros, 1998). Progressive weakening of masticatory muscles in patients leads to increased difficulty in chewing, and swallowing, requiring specialized dietary interventions (Umemoto et al., 2009). Muscular dystrophy patients also present with other impaired facial motor dysfunction including facial expression and speech difficulties as a result of their conditions (Sjögreen et al., 2006). Other congenital facial weakness syndromes, including congenital myasthenic syndromes, are also associated with craniofacial dysmorphologies and craniofacial dysfunction (Mihaylova et al., 2009; Webb et al., 2021). The clinical presentation of these conditions further illustrate the interplay between craniofacial morphology and function.

Craniofacial disorders affect critical craniofacial functions such as breathing, eating, and speech. Because of this, interventions, such as surgery, orthodontics or other therapy, are needed to assist with, or restore craniofacial functions. Most CLP patients will undergo surgeries to fix the morphological defect and improve speech and feeding (Burg et al., 2016). Typically, CLP repair surgeries are performed prior to age 7, as it's believed there is little benefit to improved speech functions after this stage, and surgery may hinder any speech progress made from therapy (Burg et al., 2016; Katzel et al., 2009). However, CLP surgery most often leads to malocclusions due to disruptions in midface growth and to velopharyngeal insufficiency, a speech deficiency caused by structural or functional defects in the velopharyngeal valve (Burg et al., 2016; Paradowska-Stolarz and Kawala, 2014). CLP repair requires long-term orthodontic care speech therapy to maintain proper function. To relieve some of the functional

consequences associated with micrognathia, patients can undergo a mandibular distraction procedure to lengthen the mandible. The mandibular distraction procedure is an alternative to tracheostomy, providing relief to upper respiratory obstructions in patients (Breik et al., 2016a). This procedure can also improve feeding in patients with micrognathia (Breik et al., 2016b). While craniofacial abnormalities can vary from mild to severe defects which may influence the level of required interventions, patients can be affected psychologically by their appearance (Singh and Moss, 2015). Overall, craniofacial abnormalities lead to defects that drastically affect the quality of life of patients, both physically and psychologically. Understanding the genetic causes and the pathophysiology of craniofacial disorders can help inform physicians on treatment and management plans.

Table 1.1. Craniofacial disorders and associated disrupted functions
Adapted from Luderman et al., 2017

Syndromes (OMIM)	Gene(s)	Craniofacial phenotypes	Functional deficits	Animal models	References
Osteogenesis imperfecta, type III (259420)	*COL1A1*	Triangular face Frontal bossing Micrognathia Malocclusions Open bite	Reduced jaw opening Open bite	Zebrafish Mouse	(Fisher et al., 2003), (Chetty et al., 2017), (Bendixen et al., 2018)
Raine syndrome (259775)	*FAM20C*	Narrow prominent forehead Proptosis Low nasal bridge Midface hypoplasia	Feeding, breathing difficulty	Zebrafish Mouse	(Eames et al., 2011), (Liu et al., 2017b), (Mameli et al., 2020)
Cranio-lenticulo-sutural dysplasia (CLSD, 607812)	*SEC23A*	Frontal bossing Midface hypoplasia Prominent supraorbital ridge Macrocephaly	-	Zebrafish	(Lang et al., 2006), (Boyadjiev et al., 2006)
CATIFA syndrome (618761)	*RIC1*	Microcephaly Elongated face Small ears Cleft lip and/or palate Tooth eruption problems	-	Zebrafish	(Unlu et al., 2020)
Treacher Collins (154500)	*TCOF1*	Narrow palate Mandibular hypoplasia Macrostomia Malformed auricle Dental anamolies	Limitations in mouth opening Open bite	Mouse	(Jones et al., 2008), (Trainor, 2010), (Martelli-Junior et al., 2009)
Pierre Robin sequence (261800)	*SOX9*	Micrognathia Cleft palate	Feeding difficulties Respiratory problems	Mouse	(Paes et al., 2017), (Motch Perrine et al., 2020)

Table 1.1 continued

Syndromes (OMIM)	**Gene(s)**	**Craniofacial phenotypes**	**Functional deficits**	**Animal models**	**References**
Hemifacial microsomia (164210)	Multiple (*MYT1*, *OTX2*, *ROBO1*, *GATA3*, *FGF3*)	Microtia Mandibular hypoplasia Maxillary hypoplasia Macrostomia Cleft lip/palate Retrognathia	Feeding, breathing, swallowing difficulties	-	(Singh and Bartlett, 2005), (Van De Lande et al., 2018)
Robinow syndrome (180700)	*WNT5A*	Macrocephaly Frontal bossing Micrognathia Midface hypoplasia Retrognathia Hypertelorism Prominent eyes Low-set ears	-	Mouse	(Yamaguchi et al., 1999)
DiGeorge syndrome (188400)	22q11.2 deletions	Micrognathia Low-set ears Hypertelorism High arched palate Cleft palate Malocclusions	Feeding, swallowing deficits Open bite	Mouse	(Welby et al., 2020)

Utilizing a vertebrate model to investigate the genetic regulation of craniofacial morphology and function

Craniofacial disorders represent a large class of abnormalities that can disrupt normal craniofacial function. Many craniofacial disorders have been identified through collaborative analysis of clinical data and vertebrate model systems. Yet, geneticists, clinicians, and biologists continue to identify new craniofacial disorders (Unlu et al., 2020).

Zebrafish is an amenable model to examine the genetic basis of craniofacial morphology and function. As a model organism, the zebrafish offers multiple gene depletion strategies including classical chemical mutagenesis with N-ethyl-N-nitrosourea (ENU), insertional mutagenesis, gene knockdown via morpholino-oligonucleotide injection, and newer techniques such as TALEN, zinc-finger nuclease (ZFN) and CRISPR/Cas9 genome editing approaches (Vacaru et al., 2014). ENU-based forward genetics screens have been instrumental in identifying skeletal development models in zebrafish (Andreeva et al., 2011; Driever et al., 1996; Knapik, 2000; Neuhauss et al., 1996). These unbiased screens revealed previously unidentified factors essential for craniofacial and vertebral development. Craniofacial development, including signaling processes, differentiation of craniofacial muscles and cartilage, branchiomotor neuron axonogenesis, and craniofacial muscle innervation in zebrafish mirrors that of other vertebrate species, including mouse and human (Chandrasekhar et al., 1997; Goody et al., 2017; Schilling and Kimmel, 1997). These developmental processes can be easily observed in the developing zebrafish through live imaging of transgenic animals, transient expression of fusion proteins, or by whole-mount immunofluorescence (Figure

1.1). Jaw movement is a commonly shared craniofacial function in humans and zebrafish and can be easily assessed in the zebrafish as spontaneous jaw muscle contractions begin as early as 3 days post-fertilization (Subramanian et al., 2018). For these reasons, the zebrafish vertebrate model is a simple, yet efficient system to investigate the cellular and molecular mechanisms driving craniofacial morphology and function, such as jaw movement.

The zebrafish field previously isolated numerous genetic mutants that disrupt craniofacial morphogenesis (Neuhauss et al., 1996). The Knapik laboratory identified many of these mutants disrupt genetic pathways involved in neural crest cell induction and specification (Barrallo-Gimeno et al., 2004; Montero-Balaguer et al., 2006), COPII vesicle transport and differentiation (Lang et al., 2006; Melville et al., 2011; Sarmah et al., 2010), and Rab6 vesicle interactions (Unlu et al., 2020), among others. One of the zebrafish lines isolated from the pool of craniofacial dysmorphology mutants, *kimble* (*kim*^{m533}), was of particular interest because it carries a nonsense mutation in *erc1b* that results in a global loss of Erc1b protein expression (D. Levic, unpublished). Zebrafish Erc1b is homologous to human ERC1, which has gained a lot of attention in the last few years because of its numerous functions identified in both neuronal and nonneuronal cells. Curiously, although there are no known human syndromes directly related to *ERC1* mutations or loss of function, *ERC1* is found within the smallest region of overlap in patients with chromosome 12p microdeletions that present both facial dysmorphology and functional, or neurologic, deficits (Silva et al., 2014). Currently, there are no other known *in vivo* vertebrate models to investigate *ERC1* as a candidate gene underlying the pathophysiology of the craniofacial and neurologic deficits in chromosome 12p

microdeletion patients. Therefore, I propose using the zebrafish *erc1b*/*kim*^{m533} global loss of function to investigate the role of ERC1/Erc1b in craniofacial and neuronal development.

The *ERC1* gene was originally discovered as *ELKS*, a novel gene that activates RET tyrosine kinase in papillary thyroid carcinomas (Nakata et al., 1999). Later rediscovered as a Rab6-interacting protein (Rab6IP2) (Monier et al., 2002) and as a core presynaptic active zone component named CAST (Ohtsuka et al., 2002), ERC1 was renamed as an acronym of its previously reported names: ELKS, Rab6IP2, and CAST (Wang et al., 2002). Vertebrate species contain two *ERC* paralogous genes, *ERC1* and *ERC2*, whereas *C. elegans* and *Drosophila* contain a single homologous gene known as *ELKS* and *bruchpilot*, respectively (Deken et al., 2005; Wagh et al., 2006). *ERC1* in vertebrates has alternative splice sites, and the resulting isoforms are differentially expressed: a shorter ERC1 isoform is primarily expressed in neuronal cells whereas a longer isoform is found in nonneuronal tissues (Wang et al., 2002). ERC1 is predicted to be composed of multiple coiled-coil domains and a Rab-binding domain at its C-terminus (Hida and Ohtsuka, 2010). In non-neural cells, ERC1 functions as a modulator of vesicle exocytosis, mainly through its Rab-binding domain (Grigoriev et al., 2007; Monier et al., 2002). Recent findings also identified a role for ERC1 in modulating focal cell adhesion turnover during migration in *in vitro* cell culture analysis (Astro et al., 2016; Sala et al., 2019). ERC1 also localizes with focal cell adhesion complexes at the tips of growing axons in neuronal cell culture (Franchi et al., 2016). However, the most well-known functions of ERC1 are within the presynaptic active zone of neurons, where ERC1 plays a role in ensuring fast, efficient synaptic vesicle release (Held et al., 2016; Kawabe et al.,

2017; Liu et al., 2014; Sudhof, 2012; Wang et al., 2016). Despite these findings, it is unclear the role of ERC1 *in vivo* during development, as global knockout of *ERC1* in a mouse model is embryonic lethal (Liu et al., 2014; Nyitrai et al., 2020).

In this thesis study, I used the global loss of function zebrafish mutant, *kimble*, to discover novel contributions to craniofacial tissue morphology, organization, and jaw function by ERC1, a previously identified candidate gene for craniofacial dysmorphology. Using the zebrafish model, I sought to understand the cell autonomous function of ERC1 in cranial motor nerves and craniofacial muscles that drive jaw movements. Additionally, I took advantage of the evolutionary genome duplication event in zebrafish to further understand the roles of human ERC1 isoforms in craniofacial and neural development.

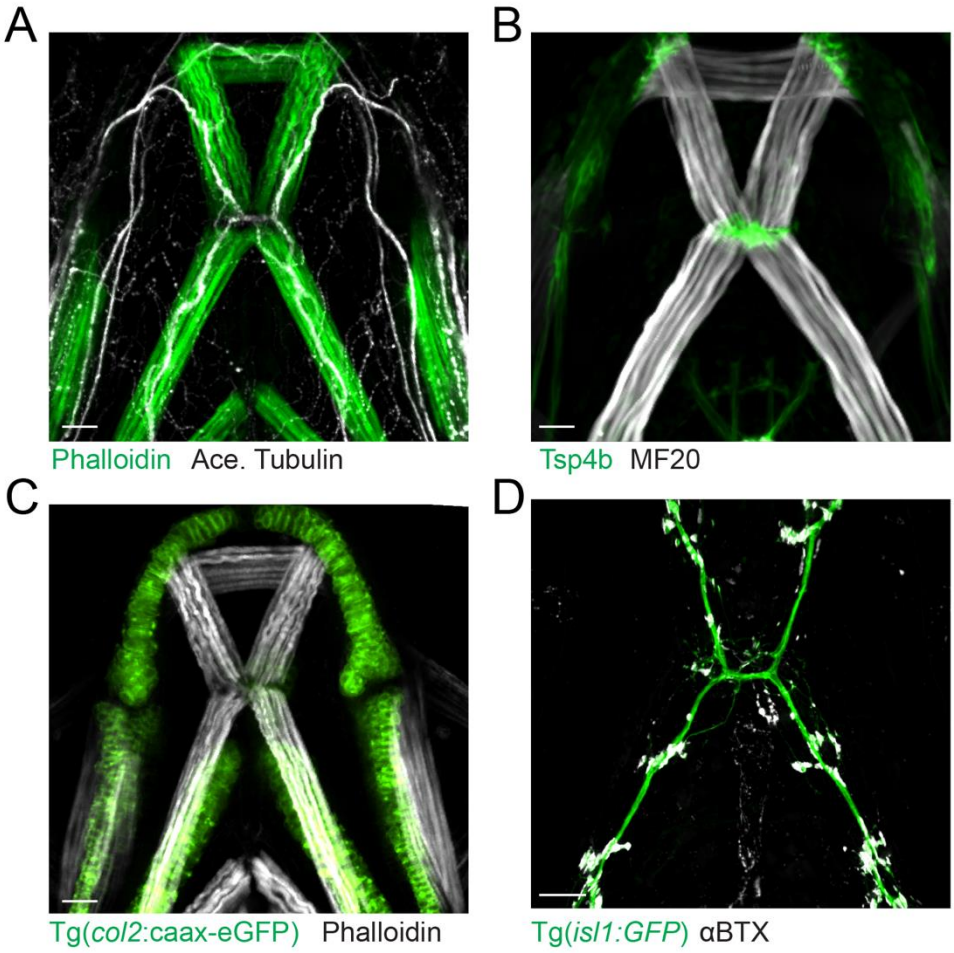

Figure 1.1. Zebrafish model system can be used to examine the biology of craniofacial tissue

Representative images of 4 days post-fertilization (dpf) wild-type zebrafish larvae to visualize ventral craniofacial tissue including **(A)** muscles (phalloidin, green) and nerves (acetylated tubulin, white); (**B)** muscles (MF20, white) and myotendinous junctions (Tsp4b, green); (**C)** cartilage (Tg(*col2*:caax-eGFP), green) and muscles (phalloidin, white); (**D)** cranial motor neurons (Tg(*isl1:GFP*), green) and acetylcholine receptors (alpha-Bungarotoxin (αBTX), white). All images maximum intensity projections. Scale bar = 25 μm.

CHAPTER II

ZEBRAFISH Erc1b MEDIATES MOTOR INNERVATION AND ORGANIZATION OF CRANIOFACIAL MUSCLES IN CONTROL OF JAW MOVEMENT

Lauryn N. Luderman[1,2], Mackenzie T. Michaels[2], Daniel S. Levic[2,3,4], and Ela W. Knapik[1,2,3]

[1]Neuroscience Graduate Program, Vanderbilt Brain Institute, Vanderbilt University, Nashville, TN, USA. [2]Division of Genetic Medicine, Department of Medicine, Vanderbilt University Medical Center, Nashville, TN, USA. [3]Department of Cell and Developmental Biology, Vanderbilt University, Nashville, TN, USA.

[4]Present address: Department of Cell Biology, Duke University Medical Center, Durham, NC, USA.

This chapter is currently undergoing revisions for publication *Developmental Dynamics* (Luderman, et al., In Revisions).

Abstract

Background

Movement of the lower jaw a common behavior observed among vertebrates that is required for eating and processing food. This movement is controlled by signals sent from the trigeminal motor nerve through neuromuscular junctions (NMJs) to the masticatory muscles. Dysfunctional jaw movements contribute to craniomandibular disorders, yet the pathophysiology of these disorders is not well understood, as limited studies have been conducted on the molecular mechanisms of jaw movement.

Results

Using *erc1b/kim*^{m533} genetic loss of function mutant, we evaluated lower jaw muscle organization and innervation by the trigeminal motor nerve in developing zebrafish. Using time-lapse confocal imaging of the *erc1b* mutant in a transgenic fluorescent reporter line, we found delayed trigeminal nerve growth and disrupted branching architecture during muscle innervation. By automated 3D image analysis of NMJ distribution, we identified an increased number of small, disorganized NMJ clusters in *erc1b* mutant larvae compared to WT siblings. Using genetic replacement, we determined that the Erc1b-Rab GTPase binding domain is required for trigeminal nerve branching, but not NMJ organization or muscle attachment.

Conclusions

We identified Erc1b/ERC1 as a novel component of a genetic pathway contributing to muscle organization, trigeminal nerve outgrowth, and NMJ spatial distribution during development that is required for jaw movement.

Introduction

Movement of skeletal elements requires coordinated firing of multiple motor units, each one made of a motor neuron connected to multiple skeletal muscle fibers by neuromuscular junctions (NMJs). The process of motor neuron innervation of skeletal muscles is well studied, particularly for vertebrate trunk (Flanagan-Steet et al., 2005; Panzer et al., 2005; Szokol et al., 2008), and limb (Phelan and Hollyday, 1990; Walker et al., 2021) muscles. For example, it is generally accepted that before the onset of movement, extracellular cues guide motor axons toward the muscles, and upon reaching the target for innervation, transcellular signaling between muscles and motor axons begin the process of NMJ synaptogenesis (Darabid et al., 2014; Wu et al., 2010). NMJs also undergo a maturation step, where multiple NMJs are recruited into organized clusters in order to produce synchronized contraction of a muscle group and generate the force needed for movement (Harris, 1981; Sanes and Lichtman, 2001). Previous studies identified the Agrin-Lrp4-MuSK signaling axis (Jing et al., 2010; Kim and Burden, 2007; Kim et al., 2008; Lin et al., 2001; Ono et al., 2001; Wu et al., 2010) to be involved in motor axon outgrowth and muscle innervation. An outstanding question in the field remains what additional molecules are involved in genetic pathways needed for movement.

In contrast to considerable knowledge on innervation of trunk and limb skeletal muscles, significantly less is known about the process of craniofacial muscle innervation that is required for jaw movement. The motor branch of the trigeminal cranial nerve controls movement of the masticatory muscles, which include the temporalis, medial pterygoid, lateral pterygoid, and masseter muscle groups in humans, with homologous

muscle groups present in most vertebrates (Akita et al., 2019; Shankland, 2001). There are several differences between masticatory muscles and the trunk and limb muscles, including fiber composition and size (Isola et al., 2018; Korfage et al., 2005; van Eijden and Turkawski, 2001). These differences illustrate the unique requirements for movement of the jaw compared to movement of other skeletal elements. Therefore, it's reasonable to suspect there may be other important differences relating to cranial motor innervation and the formation of NMJs, although this question has been sparsely addressed in a vertebrate model. Understanding how alterations in innervation of jaw muscles affect movement can help explain the pathophysiology of craniomandibular disorders and other jaw dysfunction. These disorders are prevalent in the general population, with approximately 75% of individuals reporting some jaw related dysfunction in their lifetime(Bourzgui et al., 2013; Tjakkes et al., 2010).

Zebrafish is a tractable vertebrate model system to assess not only jaw movement behavior, but also the development of the musculature and cranial motor nerves that contribute to movement. The jaw musculature of developing zebrafish has been described and includes several functionally homologous muscle groups found in other tetrapods (Diogo et al., 2008; Schilling and Kimmel, 1997). External development of zebrafish embryos allows for visualization of spontaneous jaw muscle contractions, which begin as early as 72 hours post-fertilization (hpf) (Subramanian et al., 2018) following cranial motor innervation. This simple, yet efficient vertebrate model has been used for years to examine craniofacial tissue development through live imaging of transgenic animals and genetic manipulation (Luderman et al., 2017). There is a wealth of ENU-induced mutations in genes that disrupt craniofacial development in the zebrafish field (Neuhauss

et al., 1996; Schilling et al., 1996); however, how these genetic mutations affect jaw movement remains largely unexplored.

In this study, we identified that the craniofacial zebrafish mutant *kimble* (*kim*^{m533}) (Neuhauss et al., 1996), carrying a nonsense variant in *erc1b*, exhibits defects in jaw movements compared to wild-type (WT) siblings. To explore the underlying causes of jaw movement defects, we evaluated organization of lower jaw movement muscles and innervation by the trigeminal motor nerve in developing zebrafish. We found that tendon condensation defects in *kim*^{m533} mutants result in poorly organized lower jaw muscle groups. Using live imaging, we determined that *kim* ^{m533} mutants exhibit trigeminal nerve growth delays, followed by expansive nerve branching later in development. Automated 3D analysis of trigeminal motor innervation of jaw muscles in whole zebrafish revealed that while NMJs form in *kim* ^{m533} mutants, synaptic markers, SV2 and αBTX, are disorganized in their spatial distribution. Through genetic replacement experiments, we determined that the Rab GTPase binding domain of Erc1b contributes to trigeminal nerve branching.

Methods

Zebrafish maintenance and breeding

Zebrafish were raised under standard laboratory conditions as previously described (Liu et al., 2011; Unlu et al., 2020; Westerfield, 2000). All experiments were conducted according to the guidelines established by the Institutional Animal Care and Use Committee at Vanderbilt University Medical Center (protocol number M1700020-00). The *kimble* allele m533 was previously described (Neuhauss et al., 1996) and was

characterized as a nonsense mutation (G253X) by positional cloning (Levic et al, unpublished). Adult zebrafish lines were kept in the AB or Tg(*isl1*:GFP)^{rw0} (Higashijima et al., 2000) background for phenotypic analysis. Throughout the manuscript, we refer to zebrafish as embryos during the period of development prior to hatching (typically <72 hpf), and as larvae thereafter (>72 hpf). Zebrafish were imaged live or were fixed at indicated developmental stages (hours or days post-fertilization). Embryos used for subsequent live imaging were grown in 0.003% 1-phenyl-2-thiourea (PTU, Sigma-Aldrich, P7629) to prevent pigmentation, otherwise fish were raised to indicated stages in embryo medium (Müller et al., 2013; Westerfield, 2000).

Genotyping analysis of imaged embryos

Embryo genotypes were confirmed post-imaging by PCR and enzymatic digestion. Single embryos were incubated in lysis buffer (50 μM KCl, 10 μM Tris-HCl pH 8.0, 0.3% Tween-20) at 100°C for 10 minutes, followed by proteinase K digestion (Roche, 0.1 μg/μl) at 55°C for 30 minutes to extract DNA. Proteinase K was inactivated by 10 minute incubation at 100°C. DNA was amplified using PCR primers (Forward: 5'-GACCTGAACCAGCTCTTCCCG-3'; Reverse: 5'-AAGGTTGGCTAAGCGTTGTG-3') designed using a web-based program (dCAPS) (Neff et al., 2002). PCR product was digested by AciI (NEB, no. R0551S), which cuts only wild type allele, and PstI-HF (NEB, no. R3140S), which helps to resolve the digested bands on a 3% agarose gel. Gel-based genotyping results were further confirmed by Sanger sequencing.

Jaw movement live videos and analysis

6 dpf WT and *erc1b*$^{-/-}$ larvae were lightly anesthetized in 1x (0.2 g/L) Tricaine-S (MS-222, Pentair AES) before being embedded laterally in 2% low-melt agarose on a microscope slide. After the agarose solidified, a scalpel was used to carefully remove agarose from around the head, allowing free movement of the lower jaw. Anesthetized embryos were rinsed multiple times with fresh embryo media until jaw movements resumed. A coverslip was placed on top of the embryos before imaging under transmitted light on a Zeiss AxioImager Z1 equipped with a x10 objective and Flash4.0 camera (Hamamatsu). Videos were recorded for 30 seconds, at 20 ms exposure using ZEN2 software (blue edition) and opened in ImageJ for manual analysis. A jaw movement event was defined as any deflection of the lower jaw. The total number of jaw movement events and frequency of openings per second were calculated for each embryo over the entire 30 second video. The minimum and maximum distance between the lower and upper jaw (mouth gape) was measured for three independent jaw movement events in each embryo. Mean gape magnitude was calculated as difference in gape size during the 3 jaw movement events.

Live imaging of Tg(isl1:GFP) zebrafish

All live imaging of WT and *erc1b*$^{-/-}$ transgenic zebrafish was performed on a Nikon Spinning Disk confocal microscope equipped with a motorized, multi-point stage and an Andor iXon DU-897 EMCCD camera. GFP+ zebrafish at specified stages were lightly anesthetized, embedded in 0.9% low-melt agarose on glass-bottom confocal dishes overlaid with embryo media containing Tricaine. For images taken of single developmental timepoints, Z-stack images were acquired under a Plan Apo Lambda 40x

oil objective (1.3 NA, 0.3 μm slice depth). For time-lapse imaging, GFP+ embryos were imaged under a Plan Apo Lambda 20x (0.75 NA) objective with Perfect Focus System. Z-stack images (100 μm total depth, 0.9 μm slice depth) were collected automatically every 15 minutes over 20 sequential hours using Nikon Elements software. Images and videos were deconvolved using Nikon Elements software and presented as maximum intensity Z-projections.

3D filament tracing of trigeminal nerve

Confocal z-stack images from live transgenic imaging were analyzed in Imaris 9.7.2 (Bitplane). 3D tracing of trigeminal nerve filaments was generated by the automated Filaments and the semi-automated Autopath algorithms provided in the software package. Dendrite diameter was calculated based on the absolute intensity of the fluorescent signal. Sholl intersections (1.0 μm radius) were measured from the midpoint of each image. Branching quantification was calculated automatically under the statistics analysis package provided in the Imaris software.

Whole-mount immunofluorescence (IF)

MF20 & Tsp4b staining. Zebrafish whole-mount IF to visualize craniofacial muscles and myotendinous junctions was performed as previously described (Unlu et al., 2020). Primary antibodies anti-myosinHC (Developmental Studies Hybridoma Bank, MF20, 1:250) and anti-thrombospondin-4b (Abcam, ab211143, 1:250) were incubated overnight at 4˚C in 10% normal goat serum, 1% DMSO, 1% BSA, PBS 0.1% Triton X-100. Secondary antibodies used were anti-Mouse Alexa Fluor 555 (Thermo Fisher Scientific, no. A21147) and anti-Rabbit Alexa Flour 488 (Thermo Fisher Scientific, no. A11034), diluted 1:300 as above and incubated overnight 4˚C. Following post-fixation with 4%

paraformaldehyde (PFA) for 10 min, embryos were cleared and stored in 90% glycerol until imaging.

Acetylated tubulin & NMJ (SV2 & αBTX) staining. WT and *erc1b*$^{-/-}$ zebrafish at specified stages were fixed in 4% PFA overnight at 4˚C. PFA was washed off with multiple rinses of PBS-0.1% Tween-20 (PBT). Under a dissecting microscope, the tip of the tail was removed from each animal. Next, samples were bleached in 1.5% H_2O_2/1% KOH, rinsed multiple times in PBT, and then permeabilized in ice-cold acetone for 7 minutes at -20˚C. Samples were blocked in 2% normal goat serum, 1% BSA in PBS-0.5% Triton X-100. Primary antibodies were diluted in the blocking solution (1:100 anti-SV2, DSHB; 1:300 anti-acetylated tubulin, Sigma, no. T7451) and incubated overnight at 4˚C with gentle rocking. Alexa Fluor 488 conjugated αBTX (1:250, 1 mg/mL, Thermo Fisher Scientific, no. B13422) and secondary antibodies (1:1000 anti-Mouse Alexa Fluor 555; anti-Mouse Alexa Flour 633, Thermo Fisher Scientific, no. A21126) were diluted in blocking solution and incubated overnight at 4˚C with gentle rocking. Following incubation, antibodies were rinsed several times in PBS-0.5% Triton X-100 before clearing and storage in 90% glycerol until imaging.

Phalloidin staining. For visualization of muscles, animals were fixed in 4% PFA, as described above. Following bleaching in 1.5% H_2O_2/1% KOH, samples were incubated in rhodamine phalloidin (1:250, Thermo Fisher Scientific, no. R415) diluted in PBS-0.1% Triton overnight at 4˚C with gentle rocking. Phalloidin was washed off by several rinses of PBS-0.1% Triton. Embryos were cleared and stored in 90% glycerol until imaging. For imaging of whole-mount IF samples, zebrafish were embedded in 0.9% low-melt agarose on glass-bottom confocal dishes and imaged on a Nikon Spinning Disk confocal

microscope with Plan Apo Lambda 40x oil objective (1.3 NA, 0.3 μm slice depth). Images were deconvolved using Nikon Elements software and presented as maximum intensity Z-projections.

NMJ analysis and colocalization

Automated quantification of NMJs was performed on zebrafish that underwent NMJ and phalloidin co-staining. 3D surfaces representing SV2 and αBTX channels were generated using Imaris (9.7.2) surface rendering with automatic thresholding. SV2 and αBTX surfaces were filtered for an approximate distance ≤0.05 μm, which was used to represent the distance between pre- and postsynaptic NMJ components (Nishimune and Shigemoto, 2018; Slater, 2017), and to identify closely opposed surfaces that were then merged into a single NMJ surface. The size of an NMJ was measured as the combined volume of both SV2 and αBTX surfaces. For each image, a reference point representing the mandibulohyoid junction (mhj) was placed at the intersection of the intermandibularis posterior and interhyal muscles as observed by phalloidin staining. NMJ quantification, including object count, volume, distance from the mhj reference point, and surface overlapped volume were automatically calculated by the Imaris software. Colocalization of SV2 and αBTX channels was assessed based on voxel intensity and automatic thresholding using Imaris Coloc to calculate Pearson's coefficient in colocalized volume.

Fluorescent αBTX staining in live Tg(isl1:GFP) zebrafish and image analysis

Live labeling of acetylcholine receptors was modified from previously published work(Panzer et al., 2006). GFP+ WT and *erc1b*$^{-/-}$ zebrafish were collected at specified timepoints and briefly anesthetized in Tricaine. The most caudal region of the tail was removed from each animal by a scalpel under a dissecting microscope. Samples were

rinsed briefly in Hank's solution (in mM: 137 NaCl, 5.4 KCl, 0.25 Na_2HPO_4, 0.44 KH_2PO_4, 1.3 $CaCl_2$, 1.0 $MgSO_4$, 4.2 $NaHCO_3$), followed by incubation in Alexa Fluor 555 αBTX (15 mg/ml; Thermo Fisher Scientific, no. B13422) diluted in Hank's solution for 1.5 hours at room temperature with gentle rocking. Samples were extensively washed in embryo media before embedding in 0.9% low-melt agarose for imaging on a Nikon Spinning Disk confocal microscope. Zebrafish were genotyped post-imaging. 3D surfaces of αBTX staining were automatically generated and quantified using Imaris (9.7.2) surface rendering with automatic thresholding.

mRNA overexpression and phenotypic assessment

Zebrafish Erc1b cDNA was previously cloned from wild-type zebrafish embryos (Levic et al. unpublished) and inserted into a pCS2+ vector. The Rab-binding domain was removed from wild-type Erc1b cDNA by inserting a stop codon through site-directed mutagenesis(Granero-Moltó et al., 2008). cDNA vectors were linearized by NotI digestion and synthesized capped mRNA transcripts were produced via in vitro transcription with mMESSAGE mMACHINE SP6 transcription kit (Thermo Fisher Scientific). 1200 pg of mRNA diluted in 0.3x Danieau buffer was micro-injected into single cell-stage embryos. As a control, an eGFP-Erc1b fusion mRNA construct was injected at the same concentration into single cell-staged embryos to assess protein translation (Fig. 2.1). Embryos were grown to indicated stages for subsequent fixation, staining, imaging, and post-imaging genotyping. An observer blinded to both genotype and injection scored images and videos for phenotypic analysis. For jaw movement analysis, video recordings were assessed for the number of jaw openings, opening frequency, and mouth gape magnitude using ImageJ, as described above. For muscle

phenotype analysis, the number of ectopic intermandibularis posterior (imp) or interhyal (ih) muscle fibers projecting between the mandibulohyoid (mhj) and hyohyal (hhj) junctions was manually counted in images of phalloidin stained larvae following mRNA injection, and the percent of larvae for genotype and injection type displaying zero, 1-2, or >3 ectopic muscle fibers was calculated. For trigeminal nerve branching phenotype analysis, ImageJ was used to linearly segment the nerve at 3 locations along the vertical axis and 3 locations along the horizontal axis of each image. Plot profiles of each segment were automatically assessed for the number of peaks using a script provided within ImageJ (BAR). The number of peaks from the six individual line plots was averaged for each embryo to produce a branching index. NMJ organization phenotype was analyzed using Imaris (9.7.2) surface rendering with automatic thresholding to generate 3D surfaces representing SV2 and αBTX channels which were then filtered for an approximate distance ≤0.05 μm to identify closely opposed surfaces. Surfaces were then merged into a single NMJ surface, and NMJ object count was calculated automatically by the software.

Statistics

Statistical analyses were performed with GraphPad Prism v.7.0. Statistical significance between WT and *erc1b*$^{-/-}$ zebrafish was assessed by Mann-Whitney U-test (two-tailed) with 95% confidence intervals. Trigeminal nerve branching index and NMJ analysis following mRNA overexpression was analyzed using 2-way ANOVA with Sidak's multiple comparison test. Symbols on graphs represent individual animals with lines representing mean ± SEM.

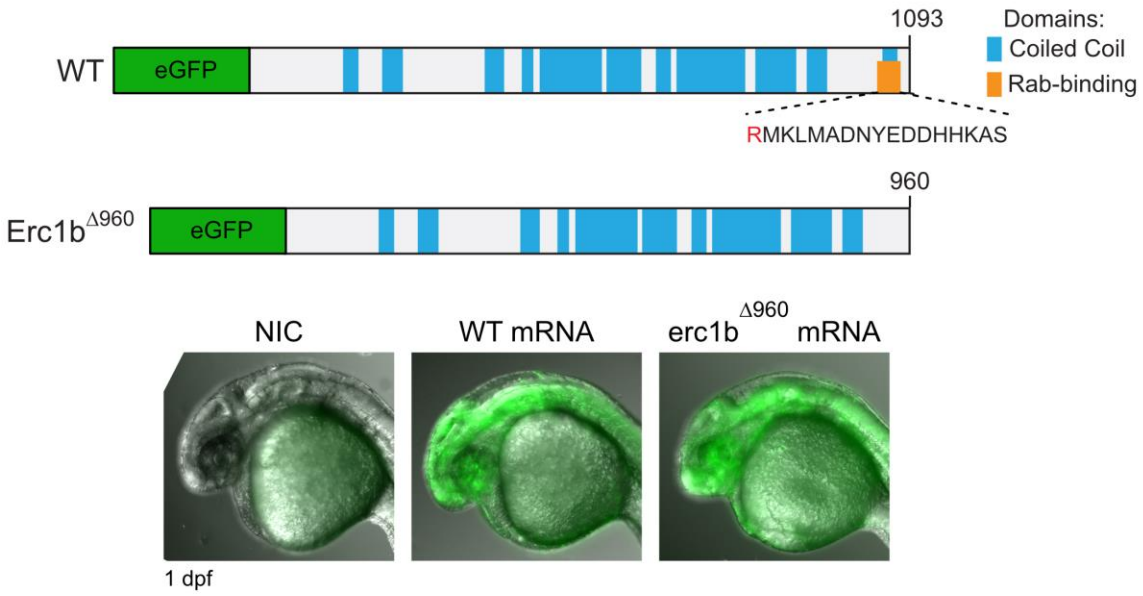

Figure 2.1. Expression of eGFP-Erc1b fusion proteins.
N-terminal eGFP fusion constructs (WT and Erc1b$^{\Delta 960}$) were generated to test translation of injected mRNA into protein. Both WT *erc1b* and *erc1b*$^{\Delta 960}$ mRNA injected embryos express eGFP globally at 1 day post-fertilization (dpf) compared to non-injected control (NIC).

Results

Kimble (kim^{m533}) mutant zebrafish display reduced mouth gape magnitude and number of jaw openings.

Zebrafish begin active feeding and increase jaw opening frequency between 5-7 days post-fertilization (dpf) (Asante et al., 2021). We evaluated lower jaw movements of 6 dpf zebrafish larvae embedded laterally, with excess agarose removed to allow free movement of the head. To assess jaw movements, we measured mouth gape, or the distance between the lower and upper jaw during minimal (Fig. 2.2A) and maximal jaw displacement (Fig. 2.2B), and calculated the change in jaw displacement as gape magnitude. WT zebrafish displayed two distinct patterns of jaw movement during the video recordings (Movie 1A): bursts of jaw movements with frequent opening events, and more evenly distributed jaw openings, as has been previously reported (Asante et al., 2021). In our collection of craniofacial zebrafish mutants, we identified *kimble* (*kim*^{m533}) (Neuhauss et al., 1996) as a line that displays jaw movement defects. Compared to WT, *kim*^{m533} mutants displayed defects specifically in jaw closure as the lower jaw of mutants do not contact the upper jaw (Movie 1B). Jaw movements in *kim*^{m533} mutants were more twitch-like compared to movements observed in WT siblings, resulting in significantly smaller gape magnitude than WT (Fig. 2.2C), fewer total jaw openings (Fig. 2.2D), and reduced opening frequency (Fig. 2.2E) over the 30 second recordings.

We previously determined that the *kim*^{m533} mutant line carries a nonsense variant in the zebrafish *erc1b* gene that is predicted to cause early truncation of the Erc1b protein (Q253X) (Fig. 2.2F) (Levic et al, unpublished). To determine if an Erc1b deficit is responsible for the observed jaw movement phenotype, we performed a replacement

experiment by injecting wild-type zebrafish *erc1b* mRNA into single-cell stage embryos (Fig. 2.2G) and evaluated live video recordings of jaw movements at 6 dpf. Overexpression of WT *erc1b* mRNA in *kim*^{m533} mutants restored normal jaw closure state (Fig. 2.2H, Movie 2), and increased mean gape magnitude to approximately WT levels (Fig. 2.2J). Total jaw openings (Fig. 2.2K) and opening frequency (Fig. 2.2L) in *kim*^{m533} mutants were also similar to WT following replacement of Erc1b. We conclude from the global genetic replacement experiment that the Erc1b deficit in *kim*^{m533} mutants is responsible for the jaw movement phenotype. We therefore will refer to *kim*^{m533} mutants as *erc1b*$^{-/-}$ mutants throughout this report.

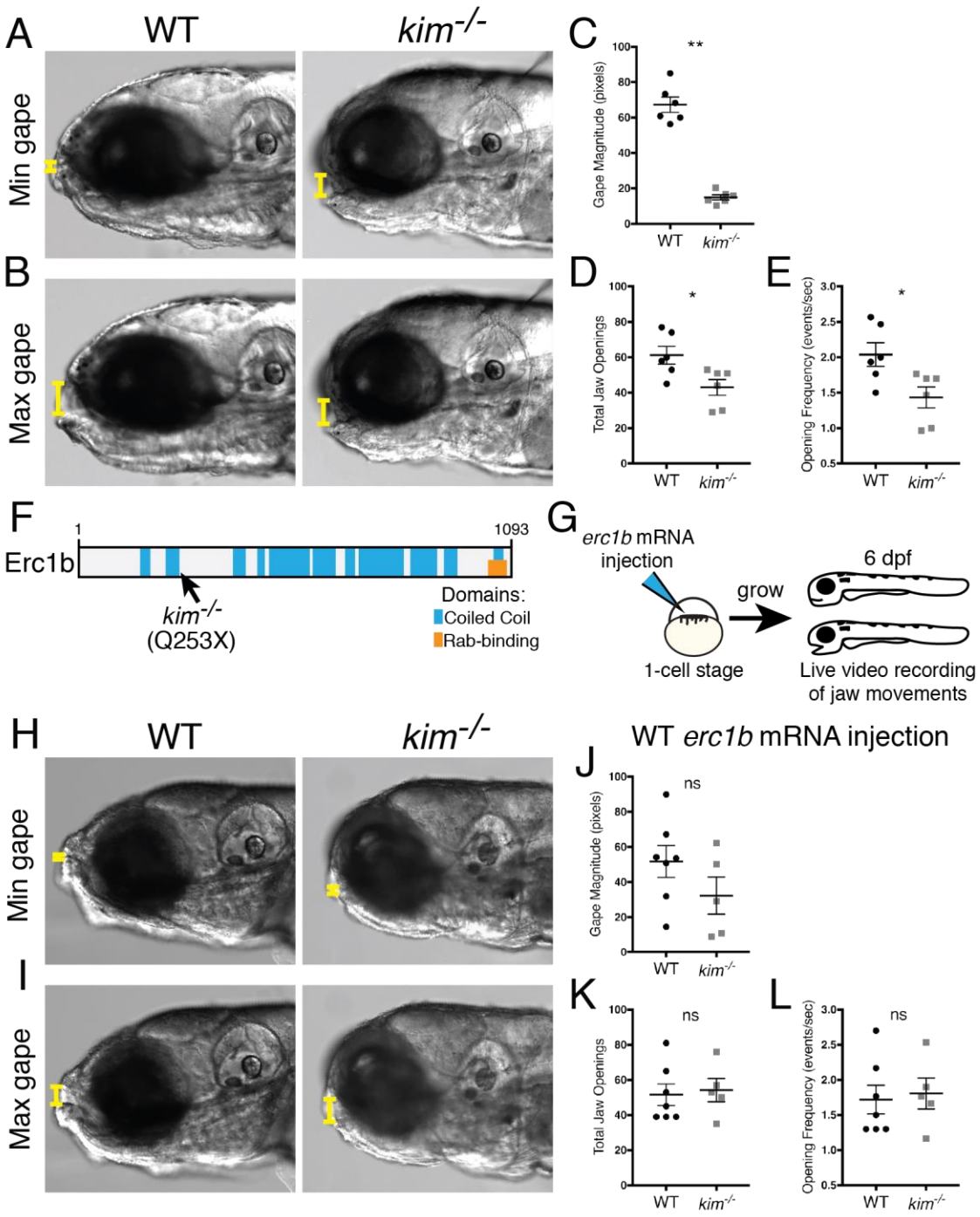

Figure 2.2. Erc1b deficiency in *kim*^{m533} mutant larvae results in jaw movement defects.

Minimal **(A)** and maximal **(B)** lower jaw displacement from 30 second recordings of jaw movements in 6 dpf WT and *kim*$^{-/-}$ larvae. Brackets indicate mouth gape. **(C)** Quantification of mean mouth gape magnitude, **(D)** total number of jaw openings, and **(E)** jaw opening frequency (opening per second) in WT (n=6) and *kim*$^{-/-}$ (n=6) larvae. **(F)**

Schematic of zebrafish Erc1b protein structure, depicting coiled-coil regions and a C- terminal Rab-binding domain; location of *kim*^{m533} mutation indicated. **(G)** Experimental design for replacement experiment with wild-type (WT) zebrafish *erc1b* mRNA (see Methods). Minimum **(H)** and maximum **(I)** lower jaw displacement of 6 dpf WT *erc1b* mRNA injected WT and *kim*$^{-/-}$ larvae. **(J)** Quantification of mean mouth gape magnitude, **(K)** total number of jaw openings, and **(L)** jaw opening frequency in WT (n=7) and *kim*$^{-/-}$ (n=5) larvae injected with WT *erc1b* mRNA. Symbols indicate individual animals, lines indicate mean with SEM. Mann-Whitney U t-test (two-tailed) was used for statistical analysis, 95% confidence interval, *p<0.05, **p<0.01.

Craniofacial muscles fibers are disorganized in erc1b$^{-/-}$ mutants.

We sought to understand the cellular mechanisms that contribute to the jaw movement defects observed in *erc1b* mutant larvae. The force needed to power jaw movements requires tendon attachment of craniofacial muscles to corresponding skeletal elements (Chen and Galloway, 2014; Koolstra and van Eijden, 1997; Sugimoto et al., 2013). To determine if defects in muscles and tendons contribute to jaw dysfunction, we evaluated ventral craniofacial muscles and tendon attachments by whole-mount immunofluorescence (IF) with antibodies against muscle myosin (MF20) and thrombospondin-4b (*Tsp4b*), an extracellular matrix protein present at myotendinous junctions (MTJ) (Subramanian and Schilling, 2014). We examined WT and *erc1b*$^{-/-}$ zebrafish larvae at two developmental timepoints: early in jaw movement at 4 dpf, and at 6 dpf, when movements are more prevalent (Asante et al., 2021). In WT larvae, the intermandibularis anterior (ima), intermandibularis posterior (imp), and interhyal (ih) muscles, which are involved in lower jaw movement (Diogo et al., 2008; Hernandez, 2002), were well-organized with condensed MTJs at the tips of each muscle group, as shown by Tsp4b labeling (Fig. 2.3A, white arrows). In *erc1b*$^{-/-}$ larvae, Tsp4b labeling revealed less organized muscle groups and tendon attachments, including the presence of ectopic fibers at both developmental stages (open yellow arrowheads, Fig. 2.3C-D'). For

example, in *erc1b*$^{-/-}$ larvae, a few imp muscle fibers extended beyond the mandibulohyoid junction (mhj) to the hyohyal junction (hhj) (Fig. 2.3C-D', yellow arrowheads). Also, we did not observe major defects to the adductor mandibulae fiber organization in *erc1b*$^{-/-}$ larvae. Despite improper attachments and loose condensation, tendons in *erc1b*$^{-/-}$ appear stable as we did not observe muscle fiber detachment even at 6 dpf. Furthermore, based on the striation pattern in MF20 staining, sarcomere organization in WT and *erc1b*$^{-/-}$ larvae appear similar. Although all *erc1b*$^{-/-}$ larvae consistently display jaw movement deficits, we observed a spectrum of lower jaw muscle phenotypes, from larvae with no ectopic muscle fibers to few ectopic fibers (Fig. 2.3C-D', G).

To test whether the muscle organization defect observed in the mutants is caused by Erc1b deficiency, we performed a replacement experiment by injecting WT zebrafish *erc1b* mRNA into single-cell embryos and assessed muscle organization in 4 dpf larvae by labeling craniofacial muscles with phalloidin (Fig. 2.3E). Zebrafish were genotyped following imaging, and a blinded observer scored the number of ectopic muscle fibers present. Overexpression of WT *erc1b* was sufficient to rescue ectopic muscle fiber phenotype in *erc1b*$^{-/-}$ larvae to a level comparable to WT (Fig. 2.3F-G). This result provides evidence that Erc1b is involved in jaw musculature organization. Approximately 50% of non-injected control (NIC) *erc1b*$^{-/-}$ larvae display a few (1-2) ectopic muscle fibers while approximately 25% show WT phenotype (Fig. 2.3G), therefore, in addition to muscle defects, we suspected that muscle innervation may contribute to the aberrant jaw movement in *erc1b*$^{-/-}$ mutants.

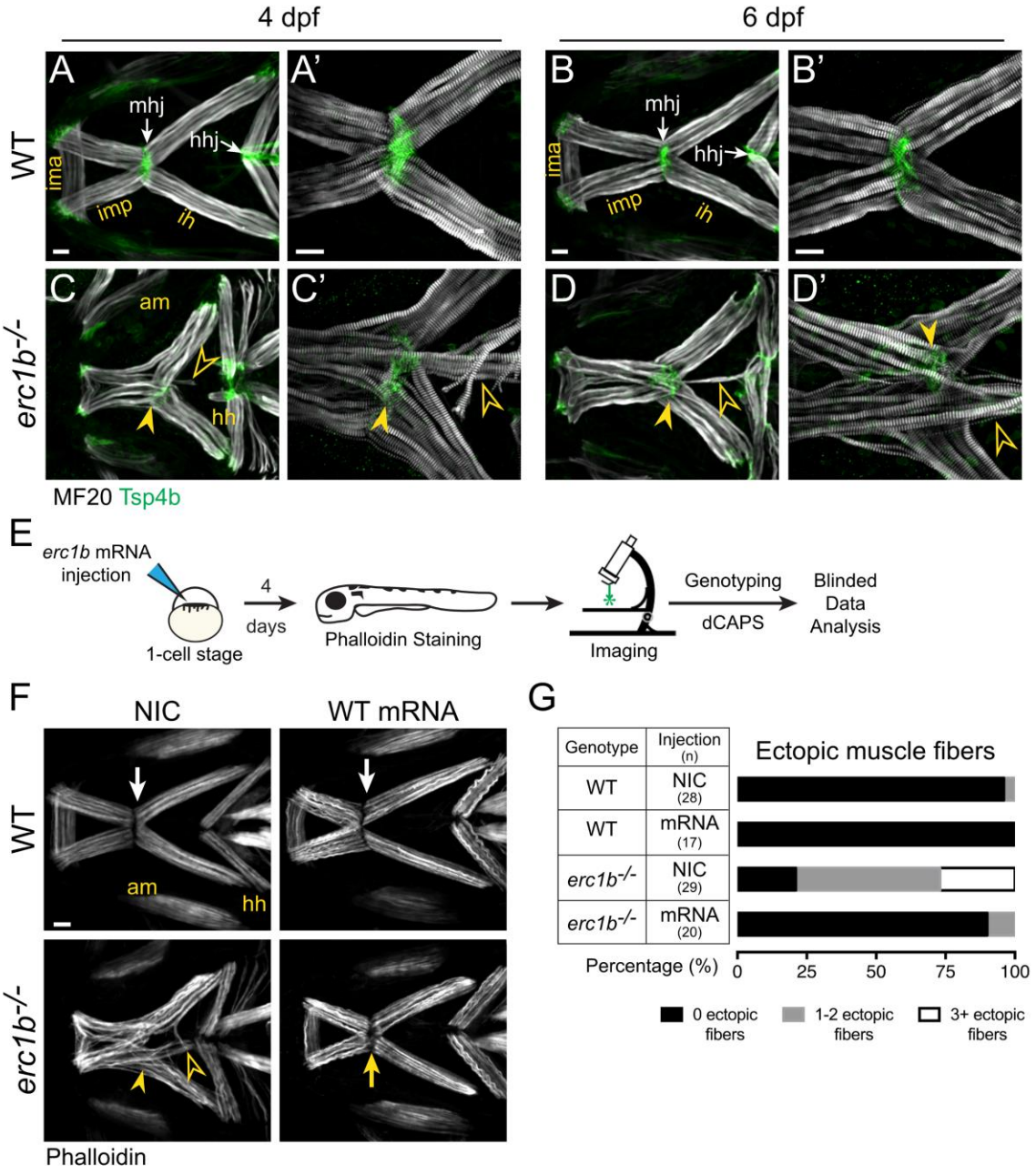

Figure 2.3. Overexpression of Erc1b rescues ectopic jaw muscle fiber phenotype in Erc1b deficient larvae.

Labeling of WT lower jaw muscle fibers with muscle myosin antibody (MF20, white) and myotendinous junction marker (Tsp4b, green, arrows) at 4 dpf (**A** (n=6)) and 6 dpf (**B** WT (n=10)). *erc1b*$^{-/-}$ larvae at 4 dpf (C (n=5)) and 6 dpf (D (n=10)) display partially disorganized lower jaw musculature, including disorganized mhj (closed arrowheads) and 1-2 ectopic muscle fibers extending towards the hhj (open arrowheads). **(A'-D')** Higher magnification images of mhj in individual larvae show severe (3+) ectopic fibers in *erc1b*$^{-/-}$ larvae **(C'-D')**. **(E)** Experimental design for zebrafish WT *erc1b* mRNA injections into single-cell embryos and subsequent analysis of muscle fiber phenotype.

(F) Representative images of phalloidin-stained muscles in WT (top) and *erc1b*$^{-/-}$ (bottom). Arrows indicate organized mhj, arrowhead indicate disorganized mhj, open arrowheads indicate ectopic muscle fibers. **(G)** Quantification of percent of larvae displaying ectopic muscle fibers. Sample sizes (n) for each genotype and injection denoted in the table. All images are maximum intensity projections; ventral view, anterior to the left. Scale bars = 25 μm. ima: intermandibularis anterior; imp: intermandibularis posterior; ih: interhyal; am: adductor mandibulae; hh: hyohyal; mhj: mandibulohyoid junction; hhj: hyohyal junction.

Erc1b deficiency perturbs trigeminal nerve growth and branching.

The motor branch of the trigeminal nerve innervates the muscles responsible for jaw movement (Chandrasekhar, 2004; Guthrie, 2007). It was previously shown that zebrafish mutations in a gene causing defects in facial (VIIth cranial) nerve cell body migration can cause altered jaw movements in zebrafish (Asante et al., 2021). During development, cell bodies of cranial nerves are specified in the hindbrain and migrate to their respective rhombomeres (Chandrasekhar et al., 1997; Moens and Prince, 2002). Axonal projections from posterior cluster of trigeminal cell bodies (Vth cranial nerve posterior nucleus, Vp), located in 2nd rhombomere, exit the hindbrain and extend laterally and ventrally into the first and second branchial arches of the zebrafish head (Chandrasekhar, 2004; Tanaka et al., 2007) (Fig. 2.4A). To visualize cranial motor nerves in live embryos, we crossed the heterozygous *erc1b*^{m533} mutant line to a transgenic zebrafish line that expresses cytosolic GFP under the *isl1* promoter (Tg(*isl1:GFP*)) (Higashijima et al., 2000). We first evaluated cranial nerve cell body localization post-migration at 48 hpf in the dorsal hindbrain of WT and *erc1b*$^{-/-}$ Tg(*isl1:GFP)* embryos. We did not observe any significant differences in localization of cranial nerve cell bodies between WT and *erc1b*$^{-/-}$ embryos (Fig. 2.4B). We next examined trigeminal motor axon growth by performing time-lapse imaging of live Tg(*isl1:GFP)* animals from 46 hpf to 66 hpf (Fig. 2.4C, Movie 3A-B). At

46 hpf, the bilateral trigeminal nerves have projected to the ventral craniofacial surface and into the first branchial arch of both WT and *erc1b*$^{-/-}$ embryos (Fig. 2.4D-F). By 48 hpf in WT embryos, the left and right trigeminal nerves made contact at the midline (Fig. 2.4E, white arrows), which persists throughout the time-lapse as the axon tips grew in a posterior direction towards the second branchial arch. In *erc1b*$^{-/-}$ embryos, trigeminal nerve growth was delayed for several hours, with the bilateral nerves failing to make midline contact throughout the time-lapse (Fig. 2.4F, yellow arrowheads). Although the tips of the nerves in *erc1b*$^{-/-}$ stalled when growing towards the midline, axonal growth in the mutants still occurred as we observed small axons ectopically branching off the anterior side of the trigeminal nerves (Fig. 2.4E, open arrowheads).

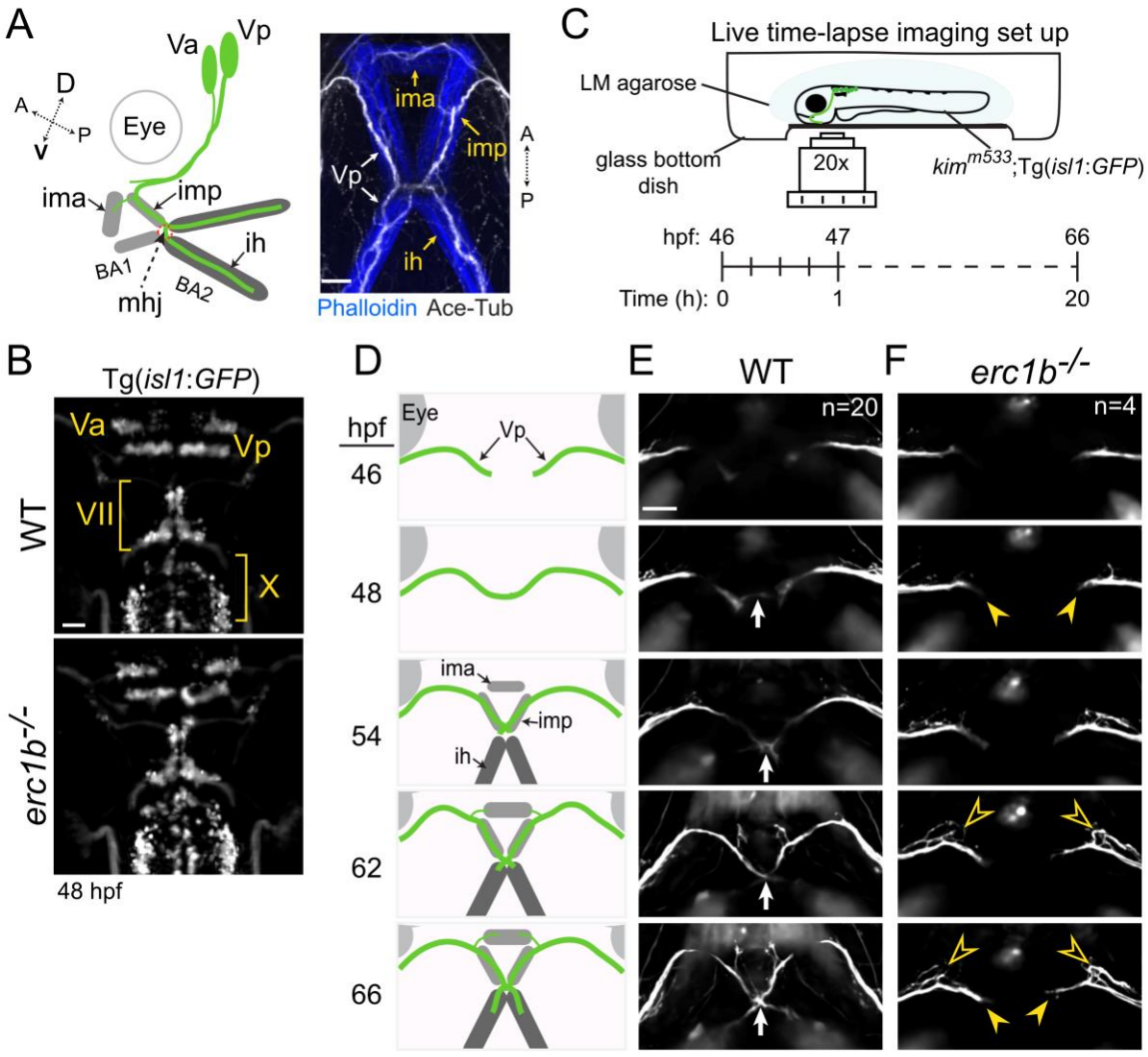

Figure 2.4. Erc1b deficiency perturbs trigeminal nerve growth.
(A) Left: schematic of trigeminal motor nerve (Va: anterior trigeminal cluster; Vp: posterior trigeminal cluster) projections into the first (BA1) and second branchial arches (BA2) of zebrafish larvae; ima: intermandibularis anterior; imp: intermandibularis posterior; ih: interhyal; mhj: mandibulohyoid junction. Right: Whole-mount IF of cranial motor nerves (Ace-Tub: acetylated tubulin, white) and lower jaw muscles (phalloidin, blue). Orientation (dorsal (D), ventral (V), anterior (A), posterior (P)) indicated. **(B)** Clusters of cranial motor neurons (Va, Vp: trigeminal; VII: facial; X: vagus) in hindbrain of 48 hours post-fertilization (hpf) WT and *erc1b*$^{-/-}$ Tg(isl1:eGFP) embryos (dorsal view). **(C)** Experimental design for time-lapse imaging of growing trigeminal nerves in transgenic WT and *erc1b*$^{-/-}$ embryos. **(D)** Schematic of WT trigeminal nerve growth and appearance of lower jaw muscles. Stills from time-lapse of trigeminal nerve growth in a WT embryo **(E)** and **(F)** *erc1b*$^{-/-}$ embryo (ventral view). Arrows indicate midline contact, arrowheads indicate axonal growth delay, open arrowheads indicate ectopic branching. Number of examined animals (n) listed in the first time-lapse images. All images are maximum intensity projections, anterior on top. Scale bars = 25 μm..

We independently verified the axonal growth defect findings from the live imaging experiment through whole-mount IF co-labeling of the trigeminal nerves with antibodies against acetylated tubulin (Ace-Tub) and SV2, a synaptic vesicle protein. At 48 hpf, the trigeminal nerves in WT embryos contact each other at the midline (Fig. 2.5A, white arrow), whereas *erc1b*$^{-/-}$ embryos displayed axonal growth delays (yellow arrowheads), replicating what was observed by live imaging. As the trigeminal nerves extend towards the posterior craniofacial region at 62 and 68 hpf, we observed increased filament branching in *erc1b*$^{-/-}$ (Fig. 2.5A, open arrowheads). We next assessed trigeminal nerve branching at 4 dpf, after the nerve has innervated the jaw muscles (Higashijima et al., 2000; Schilling and Kimmel, 1997). At this developmental timepoint, *erc1b*$^{-/-}$ larvae displayed numerous thin fibers across the midline between thicker nerve filaments (Fig. 2.5B, open arrowheads). The trigeminal nerve branching architecture was semi-automatically traced from images of live transgenic animals using Imaris 3D rendering software. Branching analysis revealed two main characteristics of *erc1b*$^{-/-}$ mutants: trigeminal nerve filaments were thinner in diameter compared to WT (Fig. 2.5C) and displayed more branching fibers (Fig. 2.5D). We further assessed the branching morphology of the trigeminal nerves by analyzing Sholl intersections (Bird and Cuntz, 2019; Sholl, 1953) (the number of branch contacts occurring on concentric rings at the midline of each animal), and found that *erc1b*$^{-/-}$ had a higher number of intersections than WT (Fig. 2.5E). The observed increase in nerve branching lead to an increase in the total length of the trigeminal nerve filaments in *erc1b*$^{-/-}$ (Fig. 2.5F). Abnormal trigeminal nerve

growth and branching of *erc1b*$^{-/-}$ could alter innervation of the jaw movement muscles, which might ultimately lead to jaw dysfunction.

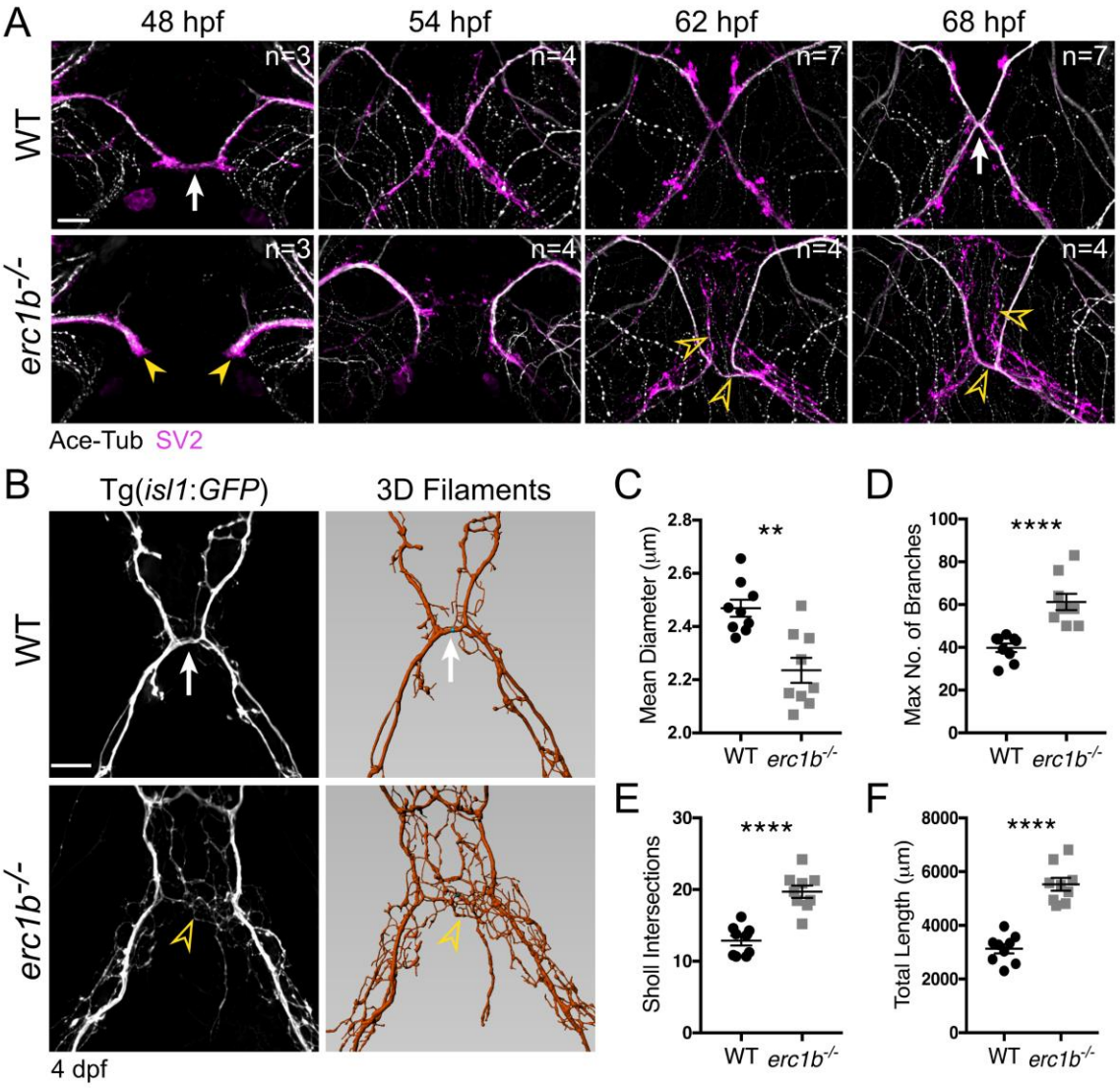

Figure 2.5. Trigeminal nerve outgrowth and branching are significantly altered in Erc1b deficient zebrafish.
(**A**) Whole-mount IF with antibody labeling acetylated tubulin (white) and SV2 (magenta) in WT and *erc1b*$^{-/-}$ embryos. White arrow indicates midline contact in WT. Yellow arrowheads indicate delayed trigeminal outgrowth in *erc1b*$^{-/-}$ embryos. Open yellow arrowheads indicate increased trigeminal nerve branching in *erc1b*$^{-/-}$ embryos (62-68 hpf). Number of examined animals (n) listed in top right of each image. (**B**) Left: images of live 4 dpf transgenic (Tg(*isl1*:GFP)) WT and *erc1b*$^{-/-}$ larvae. White arrow indicates nerve branching in WT. Open yellow arrowhead indicates ectopic branching in

erc1b$^{-/-}$ larvae. Right: Imaris 3D filament tracing of the trigeminal nerve from images on the left. Quantification of mean diameter of trigeminal filaments (**C**), number of filament branches (**D**), Sholl intersections (**E**), and total trigeminal nerve length (**F**) in *erc1b*$^{-/-}$ and WT larvae. Symbols indicate number of animals (WT n=9, *erc1b*$^{-/-}$ n=9), lines indicate mean with SEM. Mann-Whitney U t-test (two-tailed) was used for statistical analysis, 95% confidence interval, **p<0.01, ****p<0.0001. All images are maximum intensity projections, ventral view with anterior on top. Scale bars = 25 μm.

Neuromuscular junctions in erc1b*$^{-/-}$ *mutants are small and diffusely distributed in muscle tissue.

NMJ formation and clustering is well established, especially for spinal motor neurons in zebrafish (Jing et al., 2010; Panzer et al., 2006; Panzer et al., 2005; Zhang et al., 2004); however, innervation of the lower jaw muscles by cranial nerves has received considerably less attention. We evaluated trigeminal nerve innervation of jaw muscles by whole-mount IF staining of NMJs with an antibody against SV2, which labels presynaptic terminals in the trigeminal nerve, and a fluorescently conjugated alpha-bungarotoxin (αBTX), which labels postsynaptic acetylcholine receptors on jaw muscles. NMJs appear in large clusters in WT larvae, while in *erc1b*$^{-/-}$ mutants, clusters were smaller and more diffuse (Fig. 2.6A). To evaluate the number and size of NMJs, we used Imaris 3D rendering software to automatically generate surfaces representing SV2 and αBTX staining (Movie 4A-B). A single NMJ was defined as closely opposing SV2 and αBTX surfaces, and the size of a NMJ was defined by the combined volume of both surfaces. Mutant larvae have significantly more, yet smaller, NMJs than WT at 4 dpf (Fig. 2.6B-C). We did not observe major differences in colocalization of SV2 and αBTX (Fig. 2.6D), or in the overlapped volume ratio of NMJ 3D surfaces (Fig. 2.6E), suggesting that these pre- and postsynaptic NMJ markers are aligned in both WT and *erc1b*$^{-/-}$ larvae.

Despite not seeing significant defects in the co-localization of NMJ markers, the overall spatial distribution of NMJs in *erc1b*$^{-/-}$ larvae appeared more diffuse and disorganized compared to WT (Fig. 2.6A, yellow brackets). We evaluated distribution of stained NMJ clusters in 4 dpf larvae in relation to the mandibulohyoid junction (mhj) using phalloidin (muscle) and SV2/αBTX (NMJ) co-staining. Plotting of NMJ XY coordinates showed more organized of clusters in WT (Fig. 2.6F) compared to a dense, dispersed distribution of NMJ clusters in *erc1b*$^{-/-}$ larvae (Fig. 2.6F'). The NMJs in WT larvae were more symmetrically dispersed from the mhj compared to *erc1b*$^{-/-}$ (Fig. 2.6G), and *erc1b*$^{-/-}$ NMJs were located closer to the mhj than in WT (Fig. 2.6H). In summary, these results indicate that at 4 dpf, when the trigeminal nerves have innervated jaw muscles and begin controlling jaw movements, *erc1b*-deficient larvae display abnormal number, size, and spatial distribution of NMJs.

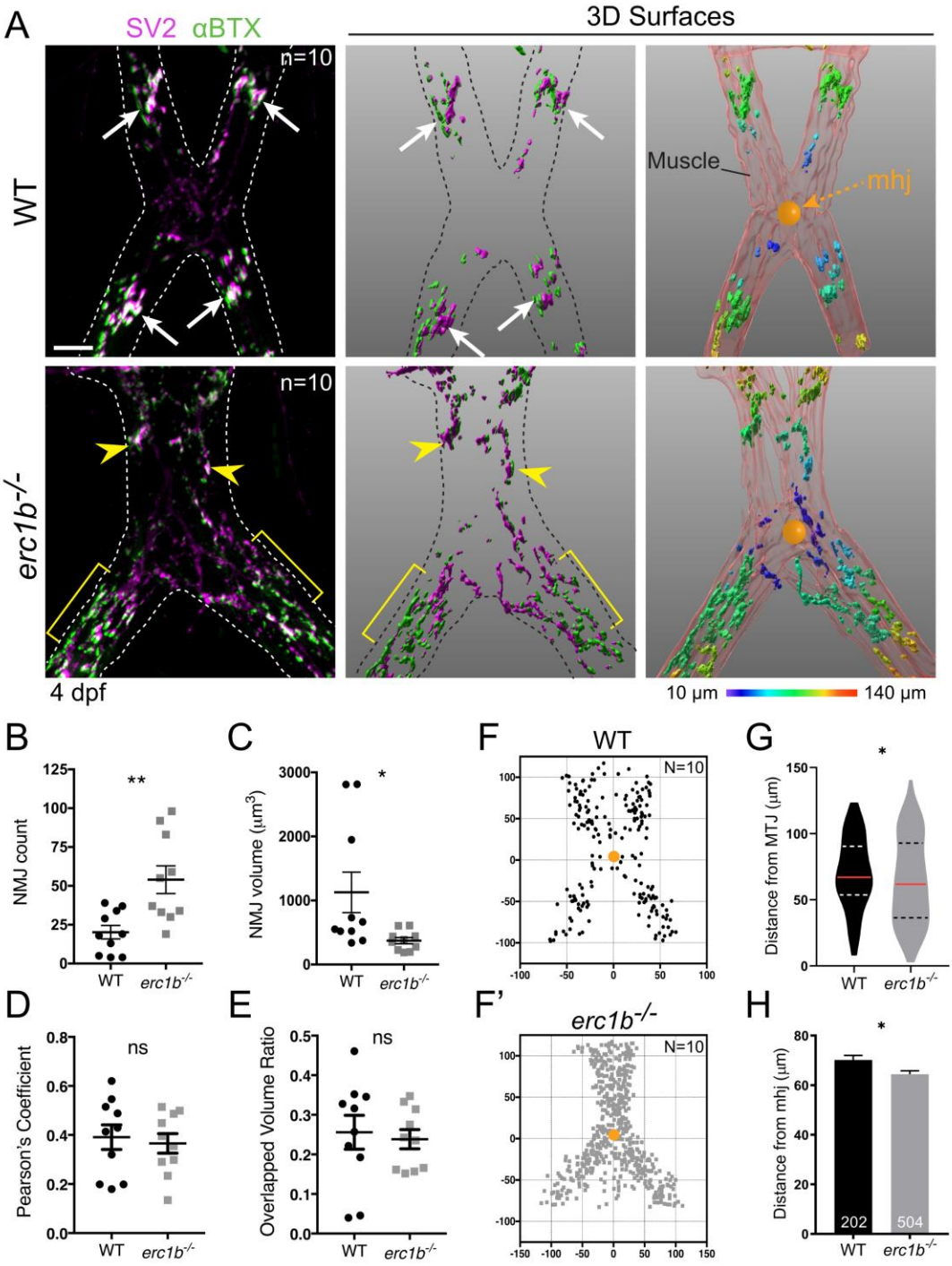

Figure 2.6. Small, diffusely distributed NMJs appear in Erc1b deficient larvae. (**A**) Left: IF labeling with SV2 (magenta) and αBTX (green) at 4 dpf *erc1b*$^{-/-}$ and WT; dotted line outlines jaw muscles. Large clusters of NMJs (white arrows) form in WT, *erc1b*$^{-/-}$ larvae clusters (yellow arrowheads) dispersed throughout the tissue (yellow brackets). Middle: Imaris 3D renderings of NMJs. Right: Pseudo-colored NMJs based on the distance from mandibulohyoid junction (mhj, orange ball) (see Methods for details).

Quantification of the number of NMJs (**B**), NMJ volume (**C**), SV2/αBTX colocalization Pearson's coefficient (**D**), and overlapped 3D volume ratio (**E**) in WT and *erc1b*$^{-/-}$ larvae. Symbols indicate individual embryos (WT N=10, *erc1b*$^{-/-}$ N=10), lines indicate mean with SEM. The location of each NMJ in WT (**F**) and *erc1b*$^{-/-}$ larvae (**F'**) plotted in XY in reference to the mhj (0,0; orange ball). (**G**) Violin plots of NMJ distance from the mhj (median = red line, upper and lower quartiles = dotted lines). (**H**) NMJ distance to the mhj; bars indicate mean with SEM, total number of NMJs noted at the bottom of each bar (WT n=202, *erc1b*$^{-/-}$ n=504). Mann-Whitney U t-test (two-tailed) was used for statistical analysis, 95% confidence interval, *p<0.05, **p<0.01. All images are maximum intensity projections, ventral views with anterior on top. Scale bars = 25 μm.

NMJs fail to organize in erc1b*$^{-/-}$ *mutants during development.

To clarify whether NMJ distribution defects in *erc1b*$^{-/-}$ larvae occurs during maturation of the synapse, or if there is a defect in NMJ distribution and organization over the course of development, we performed whole-mount SV2/αBTX IF at consecutive developmental timepoints and assessed NMJ distribution in 62-80 hpf embryos as was done in 4 dpf larvae (Fig. 2.6). In WT embryos at 48 hpf, the trigeminal nerves are labeled by SV2 staining (Fig. 2.7A, white arrowheads), consistent with coordinated trafficking of synaptic components along axons occurring prior to innervation (Bury and Sabo, 2011; Sabo et al., 2006). As development progressed, SV2 clusters concentrated at presumptive presynaptic terminals and colocalized with clusters acetylcholine receptors, labelled with αBTX, on jaw muscle surfaces in WT embryos (Fig. 2.7A, white arrows). While the number and volume of colocalized NMJ markers in WT embryos did not drastically change from 62-80 hpf (Fig. 2.7C-D), NMJs staining appeared further away from the mhj, which coincides with jaw growth during these time periods (Fig. 2.7E). On the contrary, in *erc1b*$^{-/-}$ embryos at 48 hpf, SV2 was found throughout the entire length of the trigeminal nerve, but was delayed in concentrating into clusters with αBTX, as observed in WT (Fig. 2.6B, yellow arrowheads). The number of colocalized NMJ clusters in

erc1b$^{-/-}$ embryos increased from 62 to 80 hpf (Fig. 2.7C), but they remained smaller than age-matched WT embryos (Fig. 2.7D). Colocalized SV2/αBTX staining in *erc1b*$^{-/-}$ embryos also dispersed away from the mhj over time, but they were positioned closer to the mhj than in age-matched WT embryos (Fig. 2.7E). These data show that NMJ distribution in *erc1b*$^{-/-}$ zebrafish is abnormal throughout the course of development.

We hypothesized that the increased number of NMJs observed at 4 dpf (Fig. 2.6) is associated with the increased trigeminal nerve branching in Erc1b deficient zebrafish (Fig. 2.5). To address this possibility, we imaged live Tg(*isl1*:GFP) animals that had been incubated in fluorescently conjugated αBTX to visualize acetylcholine receptors on jaw muscles. During the periods of trigeminal nerve growth delay observed in *erc1b*$^{-/-}$ embryos at 2 dpf (Fig. 2.7F, yellow arrowheads)), there appears to be reduced αBTX staining. However, at later developmental stages (3 and 4 dpf), we observed increased branching in *erc1b*$^{-/-}$ (Fig. 2.7F, open arrowheads) as well as increased αBTX staining. To quantify the number of αBTX surfaces in 4 dpf larvae, we used Imaris 3D software. We found that *erc1b*$^{-/-}$ larvae had a higher number of trigeminal nerve branches and αBTX surfaces compared to WT. However, WT larvae exhibit a more linear relationship between the number of αBTX surfaces and trigeminal nerve branches (R^2=0.6896) than *erc1b*$^{-/-}$ larvae (R^2=0.02046) (Fig. 2.7F'), which indicates a well-organized process in WT that is lost in Erc1b deficient larvae.

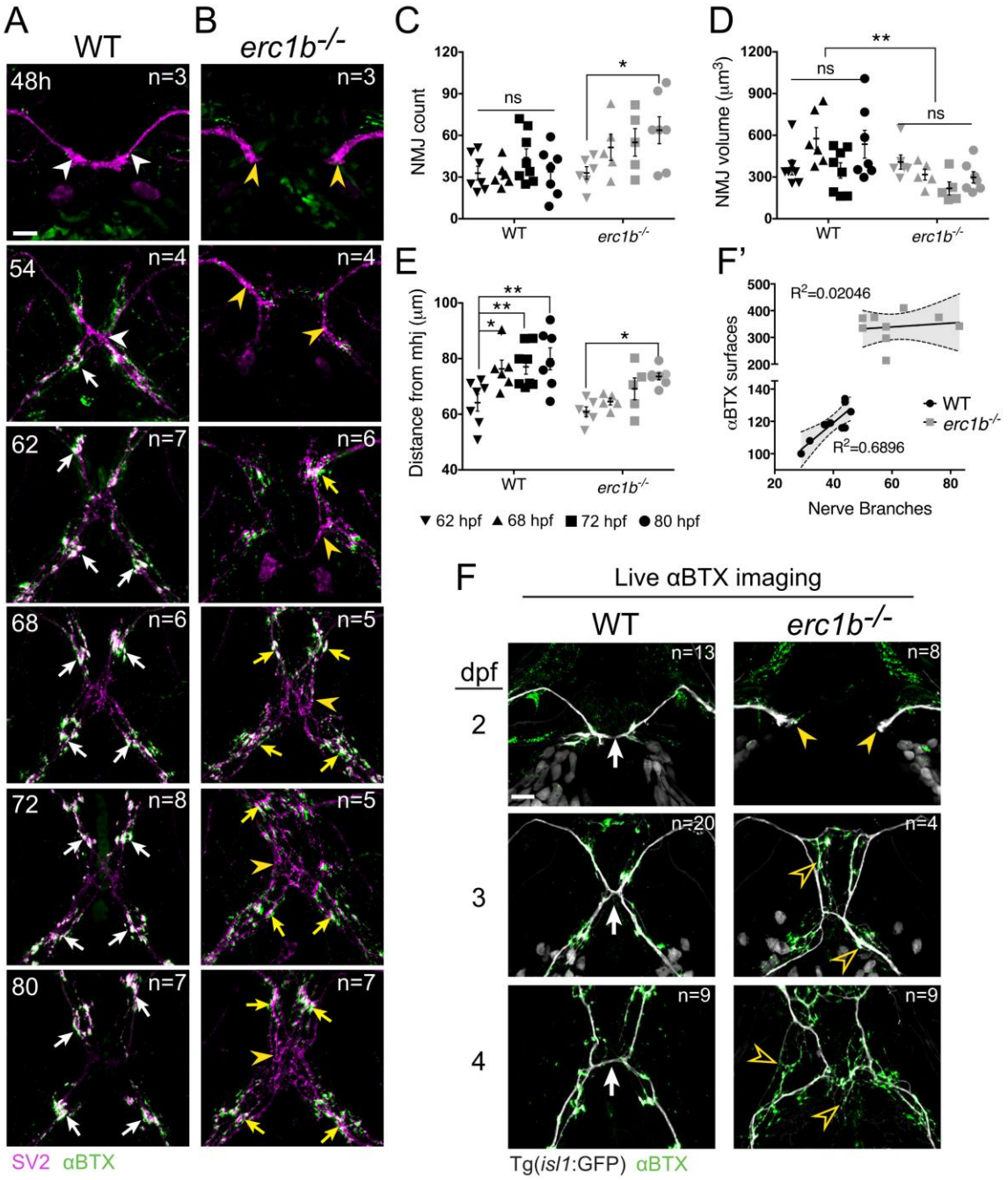

Figure 2.7. NMJs in Erc1b deficient zebrafish fail to organize during development. (**A**) Sequential NMJ staining of fixed tissue (SV2, magenta; αBTX, green) in WT embryos. White arrowheads indicate SV2 staining throughout the trigeminal nerve (48 hpf), and white arrows indicate coalescence of SV2/αBTX staining. (**B**) In *erc1b*$^{-/-}$ embryos, SV2 signal localizes within trigeminal nerve branches (yellow arrowheads) in addition to coalescence around αBTX (yellow arrows). (**C-E**) Quantification of 3D NMJ renderings in 62-80 hpf animals. Symbols indicate individual animals, lines indicate mean with SEM. Two-way ANOVA with Sidak's multiple comparison was used for

statistical significance, **p<0.01, *p<0.05. (**F**) Representative images of live WT (left) and erc1b$^{-/-}$/Tg(*isl1*:GFP) larvae (right) following αBTX incubation. White arrows indicate trigeminal nerve midline in WT. Yellow arrowheads indicate trigeminal nerve growth tips, and open yellow arrowheads indicate ectopic trigeminal nerve branching in *erc1b*$^{-/-}$ larvae. (**F'**) Linear regression of trigeminal nerve branches and αBTX surfaces in 4 dpf larvae (WT n=9, *erc1b*$^{-/-}$ n=9). Symbols indicate individual animals, with best fit line, R^2 values and 95% confidence interval (shaded area). All images are maximum intensity projections, ventral views with anterior on top. Number of examined animals (n) listed in top right of each image. Scale bars = 25 μm.

Erc1b Rab-binding domain activity contributes to nerve branching, but not NMJ organization and muscle attachment.

ERC1, also known as Rab6IP2 (Monier et al., 2002), contains a Rab-binding domain located near its C-terminus, which was shown to be required for ERC1 function in protein trafficking[46-48]. To test whether the functionality of Erc1b depends on its role as a Rab GTPase interactor, we constructed a truncated *erc1b* mRNA transcript (*erc1b*$^{\Delta 960}$) by inserting a stop codon at the beginning of the Rab-binding domain (Fig. 2.8A). We injected full-length *erc1b* (WT) mRNA or *erc1b*$^{\Delta 960}$ mRNA into single-cell embryos from *kim*^{m533}/Tg(*isl1*:GFP) heterozygous crosses (Fig. 2.8B) and grew to 4 dpf for genotyping and data analysis. To test Erc1b requirement for trigeminal nerve branching, GFP+ larvae were collected for live imaging. Overexpression of WT *erc1b* mRNA was sufficient to reduce trigeminal nerve branching in injected *erc1b*$^{-/-}$ larvae (Fig. 2.8C, yellow arrow) compared to non-injected *erc1b* mutant controls (Fig. 2.8C, open yellow arrowhead), while having no effect on WT larvae. In contrast to injection of the full-length WT *erc1b* transcript, overexpression of an *erc1b*$^{\Delta 960}$ mRNA did not reduce trigeminal nerve branching in *erc1b*$^{-/-}$ larvae (Fig. 2.8D, open yellow arrowheads). To test whether the Rab-binding domain of Erc1b is required for NMJ organization, we stained injected

embryos with NMJ markers, SV2 and αBTX. Surprisingly, we observed that NMJs were organized into clusters in *erc1b*$^{-/-}$ larvae injected with either WT or *erc1b*$^{\Delta 960}$ mRNA, suggesting that the Rab-binding domain is not necessary for the role of Erc1b in NMJ clustering (Fig. 2.8E). We found a significant reduction in the trigeminal nerve branching index of *erc1b*$^{-/-}$ larvae injected with full-length WT *erc1b* mRNA compared to NIC and *erc1b*$^{\Delta 960}$ injected larvae (Fig. 2.8F), while the number of NMJs in *erc1b*$^{-/-}$ was significantly reduced following injection of either WT or *erc1b*$^{\Delta 960}$ mRNA (Fig. 2.8G). We also found that injection of *erc1b*$^{\Delta 960}$ mRNA reduced the percent of *erc1b*$^{-/-}$ larvae that display ectopic muscle fibers compared to NIC *erc1b*$^{-/-}$ (Fig. 2.8H-I). These results indicate that the Erc1b Rab-binding domain is required for rescue of the trigeminal nerve branching, but not for NMJ organization or muscle attachment.

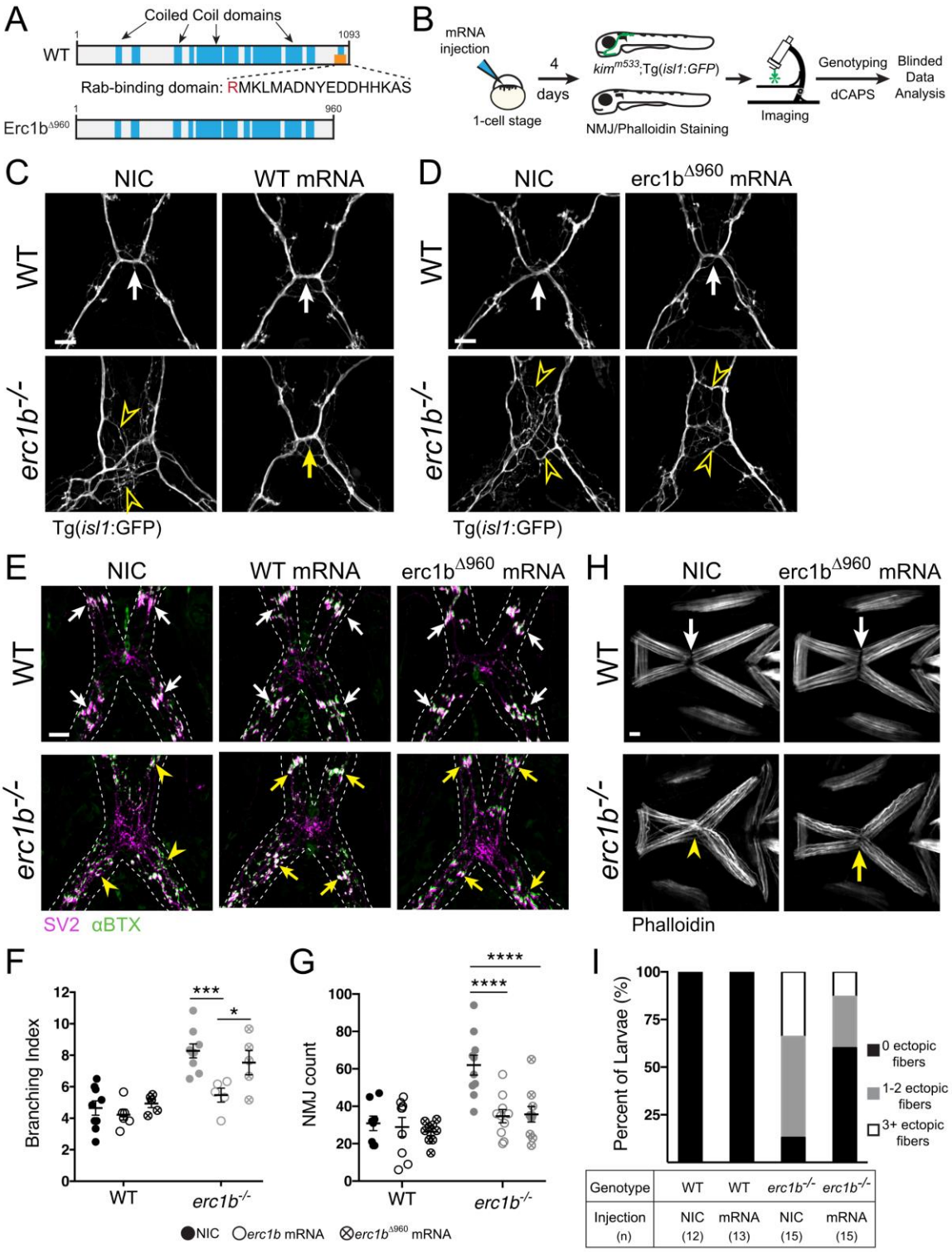

Figure 2.8. Erc1b Rab-binding domain is required for trigeminal nerve branching, not NMJ organization or muscle attachment

(A) Schematic of WT zebrafish Erc1b and truncated Erc1b$^{\Delta 960}$ constructs, stop codon replaced R960 of the Rab-binding domain. **(B)** Experimental design of mRNA

overexpression and imaging of live transgenic or stained larvae for phenotypic analysis. Representative images of live **(C)** NIC and WT mRNA injected and **(D)** *erc1b*$^{\Delta 960}$ mRNA injected WT (top) and *erc1b*$^{-/-}$/Tg(*isl1*:GFP) larvae (bottom). Arrows indicate WT trigeminal nerve midline crossing; open arrowheads indicate ectopic trigeminal branching. **(E)** Representative images of NMJ (SV2, magenta; αBTX, green) stained NIC, WT mRNA, *erc1b*$^{\Delta 960}$ mRNA injected larvae. Arrows indicate NMJ clusters, arrowheads indicate small, dispersed NMJs. **(F)** Quantification of trigeminal nerve branching index and **(G)** NMJ count of NIC, WT *erc1b* mRNA injected, and *erc1b*$^{\Delta 960}$ mRNA injected larvae. Symbols indicate individual animals, lines indicate mean with SEM. Two-way ANOVA with Sidak's multiple comparison was used for statistical significance, *p<0.05, ***p<0.001, ****p<0.0001. **(H)** Representative images of phalloidin-stained muscles in NIC and *erc1b*$^{\Delta 960}$ mRNA injected larvae. Arrows indicate organized mhj (mandibulohyoid junction), arrowhead indicate disorganized mhj. **(I)** Quantification of percent of larvae displaying ectopic muscle fibers. Sample sizes (n) for each genotype and injection denoted in the table. All images are maximum intensity projections, ventral views with anterior on top. Scale bar = 25 μm.

Discussion

Jaw movement is a common behavior that links most vertebrates together, and yet, the cellular mechanisms contributing to its physiology are not well described. In this study, we examined the process of trigeminal motor innervation of the ventral craniofacial muscles that control jaw movement. We discovered Erc1b as a novel molecular component involved in jaw movement as *erc1b* mutant zebrafish have disrupted jaw muscle organization, trigeminal nerve branching, and NMJ organization. Zebrafish Erc1b is homologous to mammalian ERC1 (also known as ELKS1, RAB6IP2, and CAST2), a scaffolding protein found to be expressed in both nonneuronal (Astro et al., 2014) and neuronal cells types (Held and Kaeser, 2018). A zebrafish single-cell transcriptome atlas shows *erc1b* appears to be broadly expressed throughout different cell types, including muscle and neural cell populations (Farnsworth et al., 2020). Functionally, ERC1 modulates vesicle trafficking in a variety of cell types specifically through its Rab-binding domain (Grigoriev et al., 2007; Nyitrai et al., 2020). ERC1 has been reported to

localize at the presynaptic active zone (Sudhof, 2012) of NMJs in both vertebrates (Tokoro et al., 2007) and invertebrates (Wagh et al., 2006), and has been shown to associate with structures important for NMJ postsynaptic maturation (Proszynski and Sanes, 2013). However, the role of ERC1 at the NMJ has not been evaluated in vertebrates *in vivo*, as a global mouse knockout model to study ERC1 function is not viable (Liu et al., 2014). Thus, the *kimble*^{m533}/*erc1b* zebrafish mutant is the first vertebrate model that offers the possibility to investigate the global loss of ERC1 function *in vivo*. Furthermore, the availability of transparent zebrafish transgenic lines and genetic manipulation techniques are powerful tools to examine cellular mechanisms of jaw movement.

Defects in skeletal muscle organization can have significant impact on muscle contraction. Previous studies of mutant zebrafish reported that defects in jaw muscle attachment affect jaw closure (McGurk et al., 2017), similar to what we observed in *erc1b*$^{-/-}$ larvae. One of our main findings from examination of lower jaw movement muscles and tendons is that a large portion of *erc1b*$^{-/-}$ larvae display only 1-2 ectopic muscle fibers that extend past the mandibulohyoid junction (mhj) towards the hyohyal junction (hhj). The observed muscular phenotypes appear to mainly affect the lower jaw muscle groups while the upper jaw muscles (adductor manidbulae) and trunk muscles (data not shown) are not affected. These few ectopic fibers are unlikely to be the only cause of the jaw movement defects observed in *erc1b*$^{-/-}$ larvae, especially given that we did not observe any fiber detachment in Erc1b mutants that are present in other craniofacial zebrafish mutants (Unlu et al., 2020). Therefore, we conclude that while the tendons are stable, there is a defect in tendon organization in *erc1b*$^{-/-}$ larvae, as indicated

by Tsp4b staining. Because the antibody recognizes both intracellular and extracellular Tsp4b, we cannot rule out that this defect stems from mislocalized tenocytes. Previous studies in the zebrafish model found that cranial tendon condensation and jaw muscle fiber attachment requires muscle contraction (Subramanian et al., 2018), which is controlled by the signals sent by motor nerves to the muscle fibers. These findings suggest that the lower jaw musculature defects observed in *erc1b*$^{-/-}$ may be in addition to alterations in trigeminal nerve outgrowth and innervation.

Surprisingly, we observed two distinct trigeminal defect phenotypes in Erc1b deficient zebrafish: an initial growth delay followed by excessive nerve branching and innervation. The initial pathfinding of the trigeminal nerves appears normal in *erc1b*$^{-/-}$ mutants as we did not observe any significant defects between WT and mutant embryos at 46 hpf when the nerve projects into the first branchial arch. Instead, mutant embryos have a delay in trigeminal nerve outgrowth, which might be due to disruptions in cell adhesion that is necessary during axon outgrowth. Previous studies in zebrafish found that a mutation in a cell adhesion molecule, MDGA2A, resulted in defects in cranial motoneuron axon growth during development (Ingold et al., 2015). In addition to its role in vesicle trafficking, ERC1 has also been shown to play a role in cell migration through focal cell adhesion turnover (Astro et al., 2016; Sala et al., 2019; Sala et al., 2018). In primary interneuron cell cultures, ERC1 was shown to be part of an adhesion complex at the tips of growing neurites, and siRNA knockdown of ERC1 reduced outgrowth (Franchi et al., 2016). However, the previous in vitro experiments do not explain why Erc1b deficiency also results in increased trigeminal nerve branching in the zebrafish model. This specific phenotype can only be observed in an *in vivo* model because of the

need for extracellular growth cues that are absent in a Petri dish environment. Whether the trigeminal nerve growth phenotype observed in *erc1b*$^{-/-}$ zebrafish is due to loss of Erc1b function in cell adhesions at the trigeminal nerve growth cones will need to be addressed by future studies.

We found there is a robust NMJ disorganization phenotype that is unique to this genetic *erc1b* mutant. Vertebrate mutations in the Agrin-LRP4-MuSK pathway, believed to be the predominant pathway for NMJ formation, are characterized by phenotypes of reduced innervation (Lin et al., 2001), or complete absence of NMJs (Jing et al., 2010; Kim et al., 2008; Ono et al., 2001). In the *erc1b* mutant, we did not observe defects in colocalization, or volume overlap of SV2/αBTX markers, suggesting the mutant phenotype is not likely related to defects in NMJ formation. Instead, the distinct innervation defects in *erc1b*$^{-/-}$ mutants, compared to those of the Agrin-LRP4-MuSK pathway, suggests that Erc1b is involved in a novel genetic pathway that is required for distribution and organization of NMJs in the lower jaw muscles. It is currently unclear what mechanisms are involved in the organization of NMJs during development, although the organized distribution of synapses has been shown to be specific for each muscle type (Yin et al., 2019). One possible mechanism for NMJ organization involves pre-patterning of acetylcholine receptors on the muscle surface prior to arrival of growing motor axons (Flanagan-Steet et al., 2005; Jing et al., 2010; Panzer et al., 2006). Pre-patterned acetylcholine receptors are observed in zebrafish trunk (Panzer et al., 2005) and mouse skeletal muscles (Yang et al., 2001); however, in our analysis of NMJ development in the craniofacial muscles, we did not observe pre-patterned acetylcholine receptors. This finding may relate to the arrival of trigeminal motor neurons into the first

branchial arch before the appearance of muscles (Higashijima et al., 2000; Schilling and Kimmel, 1997). Organization of NMJs is also controlled by synaptic activity, which is important for synaptic competition and elimination (Walsh and Lichtman, 2003), spatial distribution of NMJs into synaptic "refractory zones" (Skorpen et al., 1999), and NMJ size (Balice-Gordon and Lichtman, 1993). Whether the observed NMJ phenotype in Erc1b deficient zebrafish is due to alterations in synaptic activity remains an open question. Given that nerve branching and NMJ defects in *erc1b*$^{-/-}$ mutants occur much earlier than jaw muscle activity commences, changes in synaptic activity are unlikely to be causal. However, further investigation is needed to define the molecular mechanisms by which Erc1b/ERC1 regulates NMJ formation.

Lastly, we examined the role of the Rab GTPase-binding domain of Erc1b in cranial nerve branching, muscle attachment, and NMJ organization. While full-length Erc1b rescues trigeminal nerve branching, the Rab-binding domain appears to be dispensable for both muscle organization and NMJ clustering. Rab-mediated membrane trafficking is important for neuronal development, including axon outgrowth, as shown in both cell culture and animal models (Mori et al., 2013; Ponomareva et al., 2016; Schlager et al., 2010). Studies examining the role of Rab proteins in axon outgrowth found that loss of Rab-mediated trafficking results in decreased axon outgrowth, likely due to a reduction in the supply of membrane to the tips of growing axons (Villarroel-Campos et al., 2016). However, we observed the opposite effect in our Erc1b deficient zebrafish model: *erc1b*$^{-/-}$ displayed increased number of trigeminal nerve branches and overall trigeminal nerve length. Therefore, we conclude that this is an unlikely mechanism. This conclusion is in agreement with other studies on the role of ERC1's C-terminal Rab-

binding domain in vesicle exocytosis, suggesting that C-terminal truncated ERC1 does not inhibit membrane-bound vesicles secretion, instead, it affects synchrony, or timing, of vesicle release (Grigoriev et al., 2007). Future studies will unravel how Rab-mediated trafficking controls cranial nerve branching and innervation of jaw muscles, and whether unique ERC1 protein interactions mediate NMJ organization and muscle attachment.

In summary, we utilized a global vertebrate knockout model to further understand the development of the multiple cellular components that contribute to jaw movements. By doing so, we discovered novel *in vivo* roles for ERC1 in craniofacial muscle organization, trigeminal nerve outgrowth and innervation, thus expanding upon previous in vitro studies on ERC1 function.

CHAPTER III

INVESTIGATING THE TISSUE-SPECIFIC FUNCTIONS OF ERC1B IN CRANIOFACIAL MUSCLES AND CRANIAL MOTOR NERVES

Introduction

The neuromuscular junction (NMJ) is a tripartite synapse, consisting of a presynaptic motor nerve and a postsynaptic muscle fiber that are surrounded by a terminal/perisynaptic Schwann cell (Darabid et al., 2014; Sanes and Lichtman, 1999). However, the identity of which cell type (motor neuron, muscle fiber, or Schwann cell) functions as the main driver NMJ synaptogenesis mains a puzzle. The two prevailing theories are that NMJ synaptogenesis is driven by either the motor neuron (neurocentric) or the muscle (myocentric) (Lin et al., 2008). The neurocentric model of NMJ synaptogenesis suggests that release of neuron-derived agrin specifically drives accumulation of acetylcholine receptors (AChRs) on the muscle fiber surface following activation of the Lrp4-MuSK signaling cascade (Kim and Burden, 2007; Zhang et al., 2004). However, the neurocentric model is challenged by observations that cultured myotubes express clusters of AChRs even in the absence of motor neurons, suggesting there is some intrinsic function in muscles that drives AChR clustering (Lin et al., 2008). A similar finding was observed in vivo: AChR clusters are present on muscle fibers prior to the arrival of nerves and may function to guide axon growth and pattern innervation (Flanagan-Steet et al., 2005; Lin et al., 2001; Yang et al., 2001). This suggests that initial AChR clustering on muscle fibers is nerve independent, however, subsequent NMJ

maturation and stabilization does require agrin release from neurons (Lin et al., 2001). Together, these findings indicate that NMJ formation and maturation relies on coordinated muscle-specific and neuron-specific processes. While most NMJ synaptogenesis studies have examined skeletal muscle groups such as trunk (Flanagan-Steet et al., 2005; Panzer et al., 2005) and limb muscles (Walker et al., 2021), significantly less is known about the roles of cranial motor nerves and masticatory muscles in formation of NMJs to control jaw movement.

It was previously shown that loss of Erc1b in zebrafish results in defects in craniofacial muscle organization, trigeminal nerve outgrowth, and NMJ patterning (Luderman, et al., In Revisions). Zebrafish *erc1b* is homologous to ERC1 in humans and other vertebrate species. ERC1 has been shown to localize at the NMJ in both embryonic and adult vertebrate animals, but its direct function in organizing the vertebrate NMJ has not been investigated (Juranek et al., 2006; Nishimune, 2012; Tokoro et al., 2007). ERC1 has been shown to function in neurons at presynaptic active zones of NMJs (Held et al., 2016; Nishimune, 2012; Sudhof, 2012), and has been shown to surround clusters of mature AChRs in cultured myotubes (Proszynski and Sanes, 2013). Additionally, loss of ERC1 expression in patients is associated with a number of muscle defects including axial hypotonia and peripheral hypertonia (Rooryck et al., 2009), and myopathic facies (Thevenon et al., 2013). Antibodies against ERC1 were recently identified in serum from a Lambert-Eaton myasthenic syndrome patient, an autoimmune disorder targeting neuromuscular transmission (Huijbers et al., 2013).

Prior to our work in the zebrafish model, the specific function of ERC1 at the NMJ had not been evaluated in a vertebrate species. In global *erc1b* knockout larvae, we

showed that there is no major defect in pre- and postsynaptic marker alignment; however, there is a defect in the patterning of NMJs in *erc1b*$^{-/-}$ mutants compared to wild type (WT) larvae. Given the reported ERC1 expression on either side of the NMJ synapse and the known neuronal and muscle-specific roles in NMJ synaptogenesis, we sought to establish cell specific roles for Erc1b in the cranial motor nerves and craniofacial muscles. We first examined expression of endogenous Erc1 paralogs in WT craniofacial tissue to determine whether zebrafish Erc1 is expressed in both cranial nerves and in craniofacial muscles. We next used molecular cloning to develop Tol2kit constructs to overexpress fluorescent Erc1b fusion proteins specifically in either craniofacial muscles or in the cranial motor neurons (Kwan et al., 2007) (Figure 3.1). Tol2 constructs were injected into single-cell staged *erc1b*$^{-/-}$ and WT embryos to examine expression and localization of Erc1b fusion proteins in either the cranial motor nerves or in craniofacial muscles and were found to have similar expression as endogenous Erc proteins. Future work will use these constructs to develop stable overexpression lines to examine the cell-specific function of Erc1b in the craniofacial muscles or the cranial motor nerves.

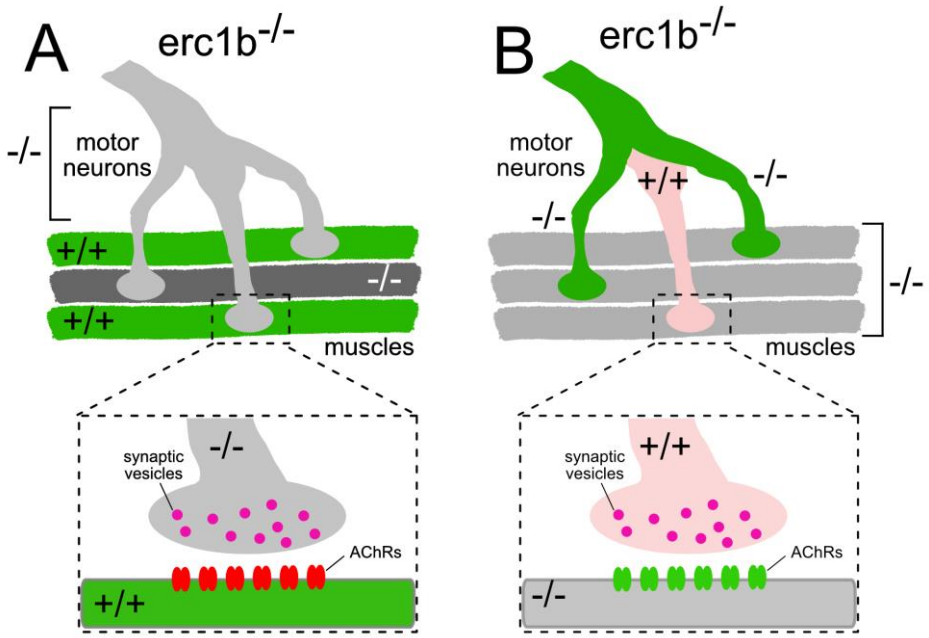

Figure 3.1. Assessing Erc1b cell autonomous function in cranial motor neurons and craniofacial muscles
(A) Experimental design for mosaic overexpression of Erc1b in muscles of *erc1b*$^{-/-}$ zebrafish. Green muscles express the Tol2 construct, gray muscles and motor neurons do not. (**B)** Experimental design for mosaic overexpression of Erc1b in cranial motor neurons of *erc1b*$^{-/-}$ zebrafish. Pink neurons express the Tol2 construct, green neurons and gray muscles do not.

Methods

Zebrafish maintenance and breeding

Zebrafish were raised under standard laboratory conditions as previously described (Liu et al., 2011; Unlu et al., 2020; Westerfield, 2000). All experiments were conducted according to the guidelines established by the Institutional Animal Care and Use Committee at Vanderbilt University Medical Center (protocol number M1700020-00). The *erc1b/kimble* line was previously described (Luderman, et al., In Revisions;(Neuhauss et al., 1996). Adult zebrafish lines were kept in the AB or Tg(*isl1*:GFP)^{rw0} (Higashijima et al., 2000) background for phenotypic analysis. Zebrafish were imaged live or were fixed at indicated developmental stages (hours or days post-fertilization). Embryos used for subsequent live imaging were grown in 0.003% 1-phenyl-2-thiourea (PTU, Sigma-Aldrich, P7629) to prevent pigmentation, otherwise fish were raised to indicated stages in embryo medium (Müller et al., 2013; Westerfield, 2000).

Cryosectioning and Immunofluorescence (IF)

Processing for IF was performed as previously described (Sarmah et al., 2010) with modifications. Embryos were fixed in freshly prepared 2% PFA for 20 minutes at room temperature, washed off with multiple rinses of PBS-0.1% Tween-20 (PBT), followed by incubation in 30% sucrose/PBS. Embryos were embedded in Cryomatrix™ (ThermoFisher Scientific) and frozen at -80ºC for 15 minutes. Sections (12 µm-thick) were collected with a Leica CM-1900 cryostat (Leica CM1900) and collected onto Fisherbrand™ Superfrost™ Plus slides. Sample slides were dried for 30 minutes and rehydrated in PBS before staining. Permeabilization was performed with ice-cold acetone

for 2 minutes at -20ºC. Slides were incubated in a 2% BSA, PBS-0.1% Triton-X 100 primary blocking solution for 30 minutes at room temperature, followed by overnight primary antibody incubation [1:200 ERC1 (mouse monoclonal, ELKS-30, Abcam, ab50312); 1:500 GFP antibody (chicken polyclonal, Vanderbilt Antibody and Protein Resource); 1:500 acetylated tubulin (mouse monoclonal, Sigma, T7451); 1:250 (mouse monoclonal, DSHB)] in primary blocking solution at 4ºC. Secondary antibodies were diluted in a 2% BSA, 2% goat, PBS-0.1% Triton-X 100 blocking solution (1:500 anti-Mouse Alexa Fluor-488, Thermo Fisher, A21141; anti-Mouse Alexa Fluor-633, Thermo Fisher Scientific, A21126; anti-Chicken-Alexa Fluor-488, Thermo Fisher, A11039; anti-Mouse DyLight-550, Thermo Fisher, 84540) and co-incubated with 1:250 Alexa Fluor 488 conjugated alpha-bungarotoxin (αBTX, Thermo Fisher, B13422) and Alexa Fluor 405 conjugated phalloidin (Thermo Fisher, A30104) for one hour at room temperature. Following antibody incubations, slides were rinsed multiple times in PBS-0.1% Triton X-100 before being were cover-slipped with ProlongGold® anti-fading agent (Thermo Fisher).

Slides were imaged on a Nikon Spinning Disk confocal microscope with an Apo TIRF 100x oil objective (1.49 NA, 0.2 µm slice depth) using Nikon Elements software. Images were deconvolved using Nikon Elements software and presented as maximum intensity Z-projections.

Construction of Gateway Vectors for Tol2kit System

Zebrafish *zCREST1* enhancer sequence (NCBI accession AB158303.1) was amplified from WT genomic DNA and cloned into pGEM-T Easy vector (Promega) by T-A cloning. The enhancer region was subsequently subcloned into pDONRp4-p1R following

PCR with primers containing attB4 (forward) and attB1 (reverse) recombination sites using Gateway® BP clonase II enzyme mix (Thermo Fisher, 11789020). A minimum promoter (*hsp70l*) was amplified and inserted downstream of the zCREST1 enhancer in the pDONR construct using HiFi DNA Assembly Cloning (NEB, E5520S). This construct served as a 5' promotor entry vector (p5E_zCREST1) for Tol2kit Multistep Gateway Cloning system (Kwan et al., 2007). p5E_unc503 was a gift from Joachim Berger & Peter Currie (Addgene plasmid # 64020; http://n2t.net/addgene:64020; RRID:Addgene_64020). Other Tol2kit constructs, including destination vectors containing Tol2 transposition sequences (pDestTol2CG2, pDestTol2pA2), middle entry vectors (pME_TagRFP, pME_mCherry) and 3' entry vectors were (p3E_mCherrypA, p3E_v2a-EGFP) were previously provided to the lab. A middle entry vector containing the coding sequence for zebrafish *erc1b* was provided by previous lab members (Levic, et al., unpublished). Cell-specific expression Tol2 constructs were created by incubating a 5' promotor vector, middle entry vector, 3' entry vector, and the destination vector with Gateway® LR Clonase II Plus enzyme mix (Thermo Fisher, 12538120) overnight at room temperature. After transformation, recombined Tol2 expression constructs were screened by restriction enzyme digestion and confirmed by Sanger sequencing. See Table 3.1 for primers, Tol2kit constructs, and reagents used to create cell specific Tol2 constructs.

Microinjection of Tol2kit constructs

100 pg medaka transposase mRNA and 150-175 pg of Tol2 constructs were injected into 1-cell stage zebrafish embryos collected from *kimble*^{m533}/AB or *kimble*/Tg(*isl1*:GFP)

heterozygous crosses. Injected embryos were grown at 27°C in 0.003% PTU in embryo media and were screened at 2 dpf for GFP+ hearts, indicating construct integration.

Live Imaging and Fluorescent αBTX staining

4 dpf larvae with GFP+ hearts were collected for subsequent live imaging of Erc1b overexpression in either cranial motor nerves or craniofacial muscles. Live labeling of AChRs was performed by incubating embryos injected with craniofacial muscle specific Erc1b constructs in Alexa Fluor 488 or 555 conjugated αBTX for 1.5 hours at room temperature as previously described (Luderman, et al., In Revisions). Live embryos were lightly anesthetized, embedded in 0.9% low-melt agarose on glass-bottom confocal dishes overlaid with embryo media containing Tricaine. Imaging was performed on a Nikon Spinning Disk confocal microscope equipped with a motorized, multipoint stage and a Photometrics Prime 95B sCMOS monochrome camera. Z-stack images were acquired under a Plan Apo Lambda 40x oil objective (1.3 NA, 0.3 µm slice depth) using Nikon Elements software. Images were deconvolved using Nikon Elements and presented as maximum intensity Z-projections.

Table 3.1. Primers, constructs, and reagents used in this study

Primer name	**Primer Sequence (5′→3′)**
zCREST1_Fwd_1	ctgagtggacctggccacag
zCREST1_Rev_2	gaaaaccctgattgctggaa
zCREST1_BP Fwd_1	GGGGACAACTTTGTATAGAAAAGTTGctgagtggacctggccacag
zCREST1_BP Rev_2	GGGGACTGCTTTTTTGTACAAACTTGgaaaaccctgattgctggaa
p5e_zcrest1_SDM FWD	gcctCAAGTTTGTACAAAAAAGTTGAAC
p5e_zcrest1_SDM REV	ctgtcTTGGAATGAAACAGACCATTTTG
p5e_hsp70lins Fwd	ctgtttcattccaagacaggtcaggggtgtcgcttggttatttc
p5e_hsp70lins Rev	ttttttgtacaaacttgaggcaggaaaaaaaaacaattagaattaattttatatttatacaa tttatggtgc
Tol2kit Component	**Function**
pDONRp4-p1R	Donor vector for making 5′ entry clones
pDestTol2pA2	Destination vector with Tol2 inverted transposons
pDestTol2CG2	Destination vector with Tol2 inverted transposons *and cmlc2*:*eGFP* transgenesis marker
p5E_zCREST1	5′ entry clone for cranial motor neuron specific expression
p5E_unc503	5′entry clone for muscle fiber specific expression
p5E_hsp70l	5′ entry clone used to subclone *hsp70l*
pME_tagRFP	Middle entry clone with coding sequence for tagRFP
pME_mCherry	Middle entry clone with coding sequence for mCherry
pME_erc1b	Middle entry clone with coding sequence for *erc1b*
p3E_mCherrypA	3′ entry clone for C-terminal fusions
p3E_v2a_EGFP	3′ entry clone containing a self-cleaving viral 2a peptide
pCS2FA-transposase	For in vitro transcription of capped medaka Tol2 transposase mRNA
Restriction Enzyme	**Function**
StuI (NEB)	Linearizes pDONR-zCREST1 for HiFi DNA Cloning
NotI-HF (NEB)	Linearize pCS2_transposase for mRNA in vitro transcription

Results

Endogenous zebrafish Erc1 paralogs are expressed in cranial neurons and craniofacial muscles

ERC1 has been shown to be expressed in axon terminals of neurons and surrounding AChRs in cultured myotubes (Franchi et al., 2016; Held and Kaeser, 2018; Proszynski and Sanes, 2013). To determine where Erc1b is expressed endogenously in zebrafish craniofacial tissues, immunofluorescence was performed using a commercially available monoclonal antibody against human ERC1, which recognizes the entire Erc family of proteins in zebrafish (Erc1a, Erc1b, and Erc2). In 4 days post-fertilization (dpf) WT larvae, ERC1 positive staining was observed within both the cell bodies and the axons of cranial nerves labeled with anti-GFP or acetylated tubulin, respectively (Figure 3.2). Additionally, ERC1 staining was concentrated highest in areas that are positively labeled with SV2, a presynaptic vesicle marker, in cranial nerves. This finding of a close association between zebrafish Erc proteins and presynaptic vesicles in the cranial nerves is corroborated by previous studies that have shown ERC1 localizes with presynaptic vesicles in neurons (Held et al., 2016; Nyitrai et al., 2020).

Based on previous findings that ERC1 associates with AChRs in muscles, zebrafish Erc localization in relation to AChRs in craniofacial muscles was assessed in 4 dpf WT larvae. ERC1 puncta were found in craniofacial muscles labeled with phalloidin, with highest concentration surrounding AChRs labeled with αBTX (Figure 3.2B). These findings indicate that zebrafish Erc family of proteins are endogenously expressed in both cranial nerves and craniofacial muscles and are associated with pre- and postsynaptic NMJ markers.

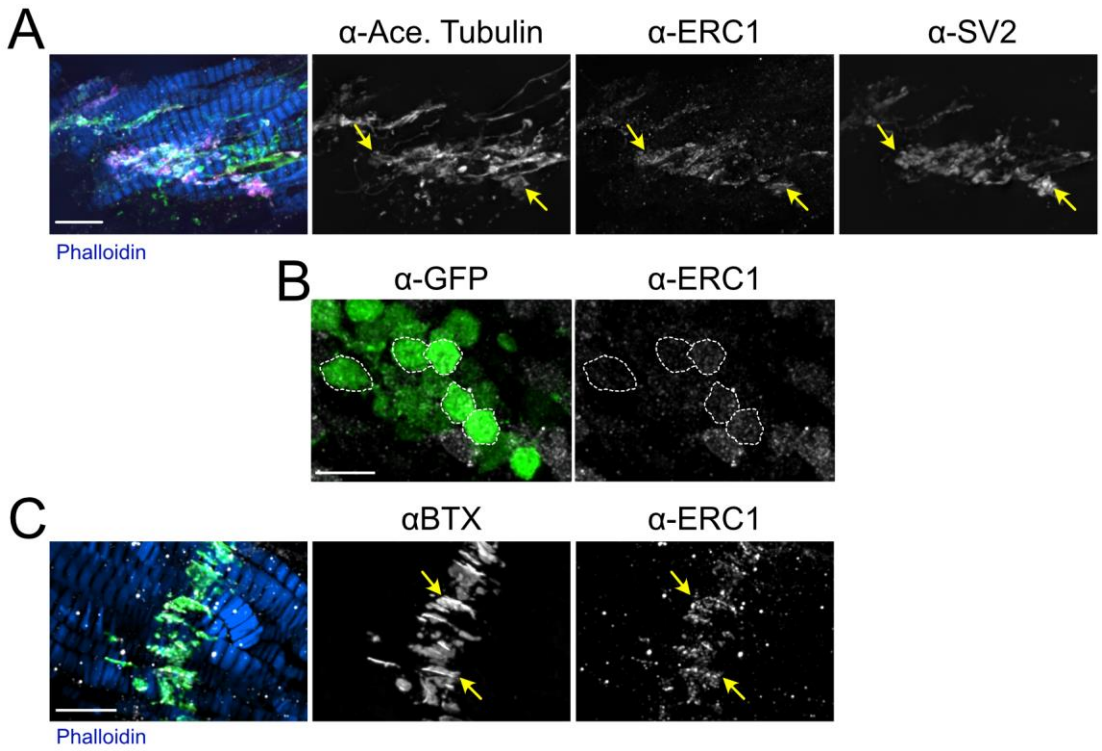

Figure 3.2. Zebrafish Erc proteins are associated with NMJ markers in cranial nerves and craniofacial muscles

Immunofluorescence on sectioned craniofacial tissue from 4 dpf WT larvae. **(A)** Yellow arrows indicate high areas of co-expression of zebrafish Erc paralogs within cranial neuronal axons co-labeled with antibodies against acetylated tubulin and SV2. **(B)** Erc paralogs are expressed within GFP labeled cranial nerve cell bodies from Tg(*isl1:GFP*) larvae (dashed lines encircle individual cells). **(C)** Erc is associated with acetylcholine receptors (αBTX) in craniofacial muscles; yellow arrows indicate areas of high co-expression. Scale bars = 10 μm.

Designing cell-specific constructs to assess Erc1b function and localization in craniofacial muscles

Given the observations that zebrafish Erc proteins are localized on either side of the craniofacial NMJ, we next sought to determine the cell-specific function of Erc1b in the cranial motor nerves or craniofacial muscles. Cell-specific gene function can be assessed in zebrafish by the transposon-based Tol2kit system (Kwan et al., 2007). This system employs multisite Gateway cloning to create an expression construct that is randomly integrated into the zebrafish genome to drive expression of a fluorescent protein or a fusion protein of a gene-of-interest within a specific cell or tissue type. The utility of this transgenesis approach is highlighted by the extensive library of entry clones, or construct 'building blocks', that are available from various plasmid repositories, and the ease in which new entry clones can be made to customize expression.

Loss of *erc1b* in zebrafish causes craniofacial muscle organization defects. To assess the function of Erc1b in the craniofacial muscles, we used a muscle-specific promoter to drive overexpression of an Erc1b fusion protein. The promoter vector (p5E_503unc) used to drive expression contains a 503 bp region upstream of the zebrafish *unc45b* gene, which acts a myosin chaperone in striated muscle (Berger and Currie, 2013). We confirmed the 503unc promoter is sufficient to drive mosaic expression of tagRFP in craniofacial muscles by injecting a Tol2 construct into single-cell embryos from a *erc1b*/Tg(*isl1:GFP*) heterozygous cross (Figure 3.3). Individual tagRFP-labelled muscle fibers were observed in craniofacial muscles as well as trunk muscles of 4 dpf injected embryos, confirming this promoter construct can be used in to examine Erc1b expression and function within craniofacial muscles.

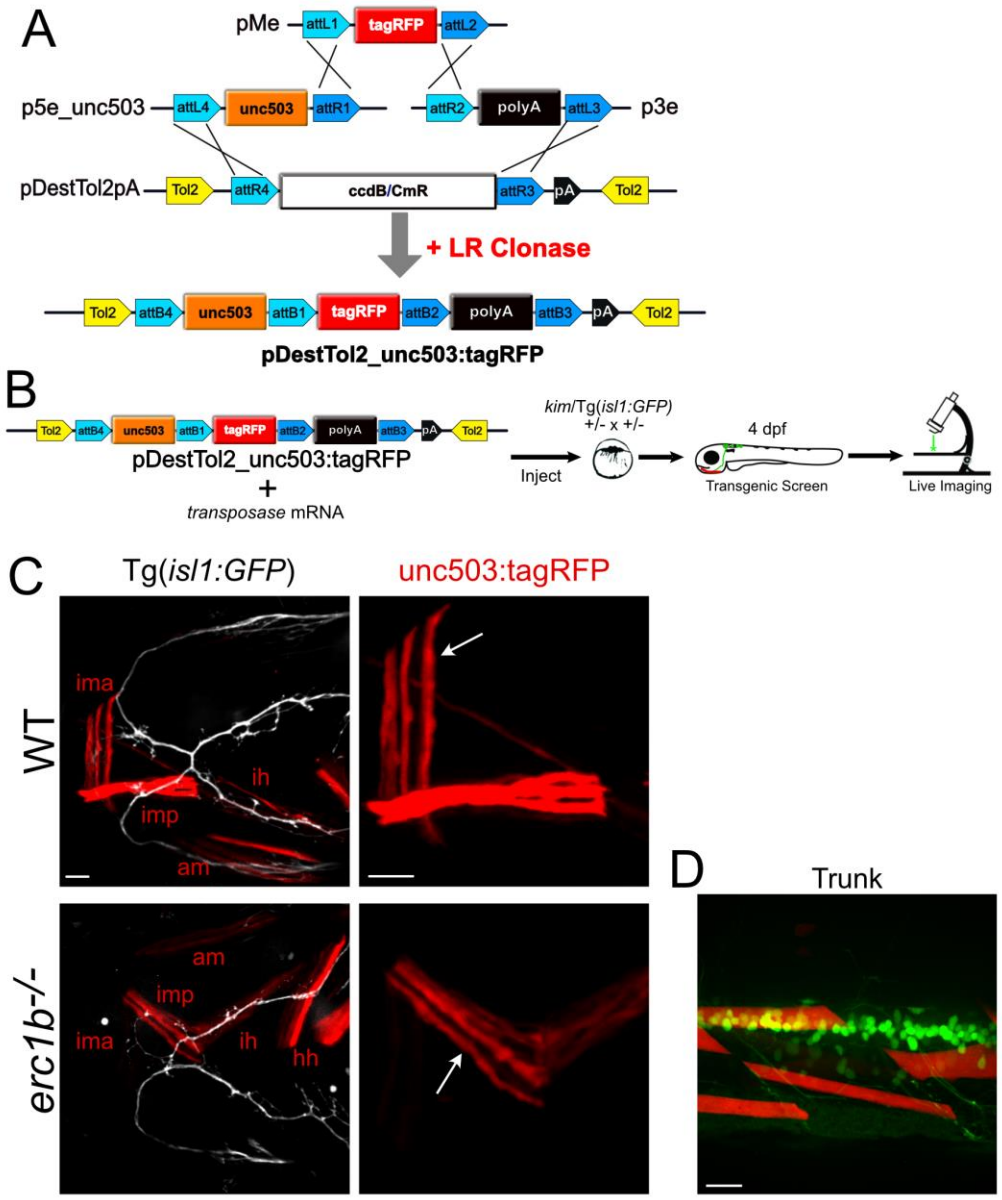

Figure 3.3. Muscle-specific promotor drives mosaic expression in craniofacial muscles

(A) Design of a Tol2 expression construct driving tagRFP overexpression in muscles using the p5e_unc503 promoter. **(B)** Injection of unc503:tagRFP Tol2 construct into *kim*/Tg(*isl1*:GFP) embryos with transgenic screen and live imaging at 4 dpf. **(C)** Representative images of WT and *erc1b*$^{-/-}$ larvae mosaically expressing tagRFP in individual craniofacial muscle fibers (arrows). **(D)** tagRFP+ muscle fibers are also observed in trunk muscle fibers. Scale bar = 25 μm. Intermandibularis anterior (ima); intermandibularis posterior (imp); adductor mandibularis (am); interhyal (ih); hyohyal (hh).

Endogenous localization of zebrafish proteins previously assessed by a pan-ERC1 antibody identified the presence of Erc proteins around AChRs in craniofacial muscles. To determine whether Erc1b specifically localizes around AChRs, we cloned a Tol2 construct to drive expression of a C-terminus tagged Erc1b-mCherry fusion protein under the 503unc promoter (Figure 3.4). To simplify our screening method to identify which embryos had integration of the Tol2 construct, we utilized a destination vector that contains a secondary transgenesis marker (*cmlc2*:*eGFP*) that drives eGFP expression in the heart. The Tol2 construct was injected into single-cell embryos collected from an *erc1b*/AB heterozygous cross, and were screened at 4 dpf for the transgenesis marker. The genomic integration rate of the expression construct was approximately 50% of injected embryos (data not shown). To assess where the Erc1b-mCherry fusion protein localized in craniofacial muscles, live mosaic transgenic embryos were imaged following incubation in fluorescently conjugated αBTX to visualize AChRs on the craniofacial muscles. Erc1b-mCherry puncta were associated with αBTX-labelled AChRs, similar to what was observed in the endogenously labelled tissue. This finding suggests that Erc1b associated with AChRs in craniofacial muscles.

Our previous analysis revealed that loss of Erc1b resulted in disorganized craniofacial muscle fibers, including ectopic fibers extending beyond their tendon attachment points. To further assess the function of Erc1b in organization of craniofacial muscle fibers, we replaced the C-terminal mCherry protein with a self-cleaving V2A-EGFP reporter in the unc503 Tol2 expression construct (Figure 3.5). In this manner, individual muscle fibers that overexpress Erc1b are labeled with GFP. This mosaic labeling of muscle fibers that overexpress Erc1b will be used in future analyses to assess

organization of muscle fibers as well as volume and patterning measurements of AChRs following incubation of fluorescently conjugated αBTX.

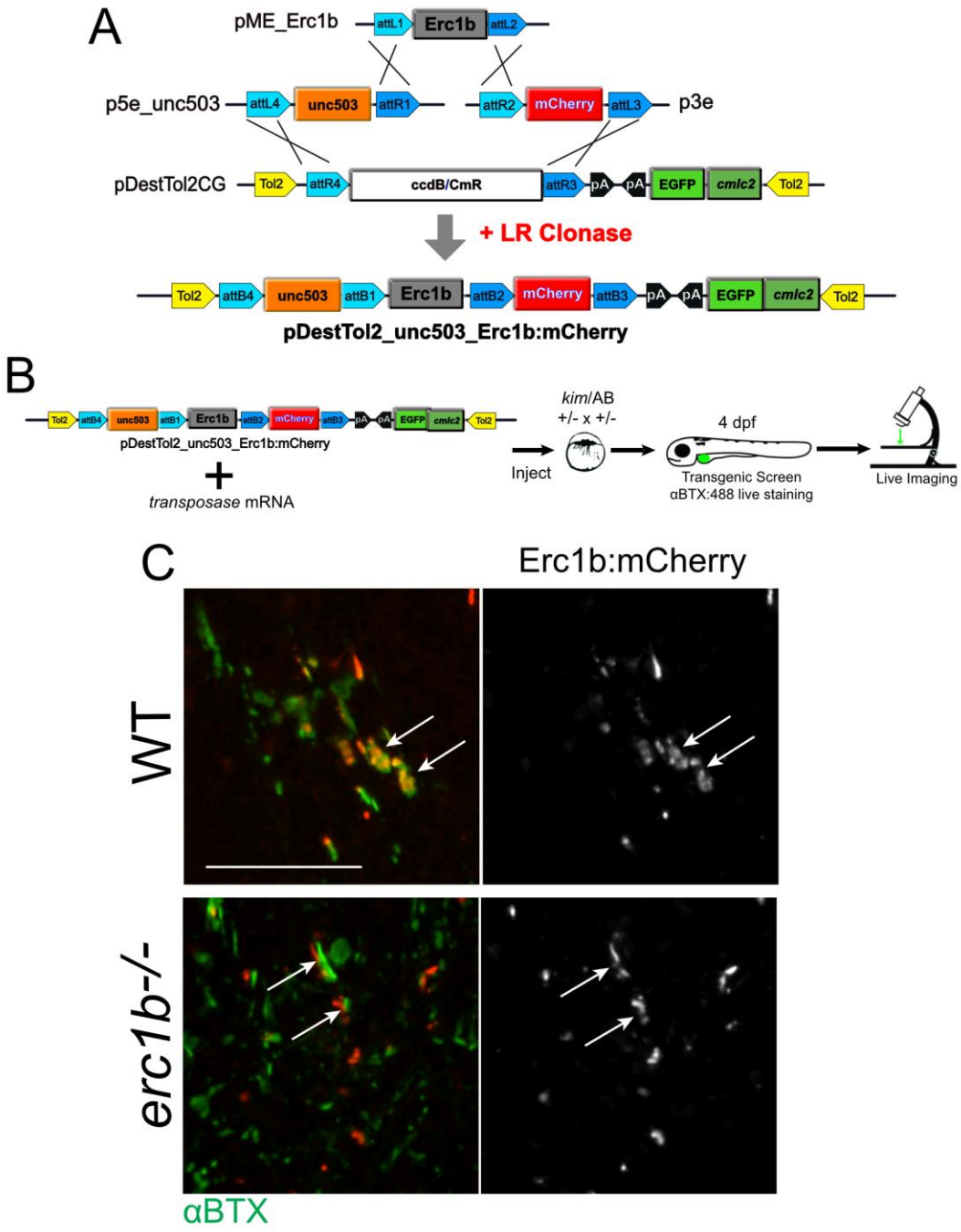

Figure 3.4. Erc1b fusion proteins localize around acetylcholine receptors in craniofacial muscles

(A) Design of a Tol2 expression construct driving Erc1b:mCherry fusion protein overexpression in muscles. **(B)** Injection of Erc1b:mCherry fusion construct into *kim*/AB single-cell embryos with transgenic screening and live imaging at 4 dpf following incubation in αBTX:488. **(C)** Erc1b:mCherry localizes around αBTX-stained acetylcholine receptors (arrows) in representative images of WT and *erc1b*$^{-/-}$ larva. All images are maximum intensity projections, scale bar = 25 μm.

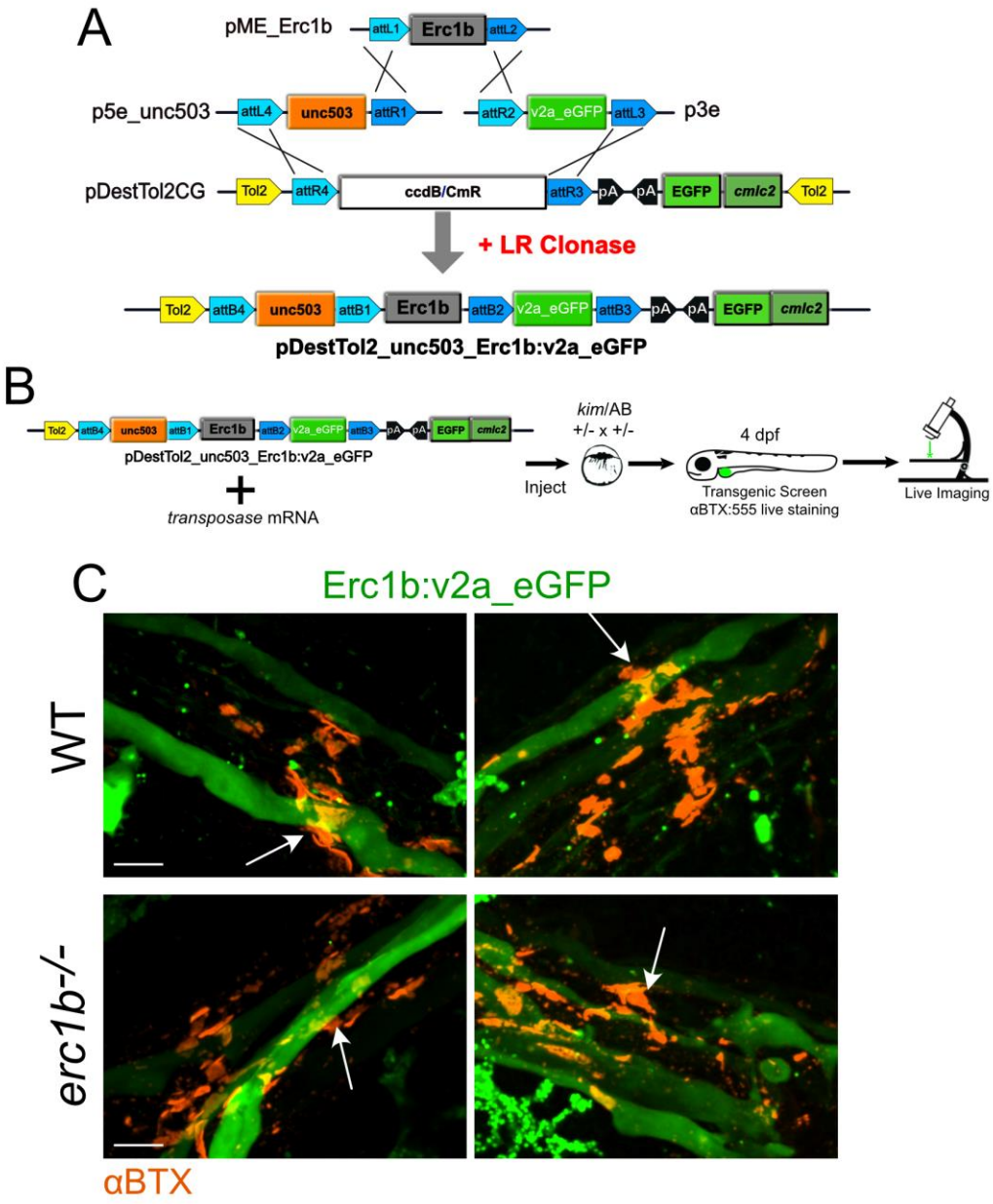

Figure 3.5. Overexpression of Erc1b in muscle fibers can be used to assess acetylcholine receptor size

(A) Design of a Tol2 expression construct driving Erc1b:v2a_eGFP self-cleavable fusion protein overexpression in muscles. **(B)** Injection of Erc1b:v2a_eGFP construct into *kim*/AB single cell embryos with transgenic screening and live imaging at 4 dpf following incubation in αBTX:555. **(C)** Self-cleavable eGFP labels individual muscle fibers in both WT and *erc1b*$^{-/-}$ larva. Incubation in αBTX labels acetylcholine receptors (arrows). All images are maximum intensity projections, scale bar = 25 µm.

Designing cell-specific constructs to assess Erc1b function and localization in cranial motor nerves

We previously used a transgenic fish line (Tg(*isl1:*GFP)) that expresses GFP in the cranial motor neurons to discover that loss of Erc1b results in defects in trigeminal motor nerve outgrowth and innervation of the craniofacial muscles. Therefore, we wanted to use the same promoter region that was used to create the Tg(*isl1*:GFP)^{rw0} line to assess the function of Erc1b within the same cranial motor nerves that exhibited the axonal growth defect. The Tg(*isl1*:GFP) line was created by injecting a plasmid containing a 4.1 kb *Isl1* promoter and a 15-kb fragment enhancer region that was found 10 kb downstream of the *isl1* locus to drive expression specifically in cranial motor neurons (Higashijima et al., 2000). However, this 15-kb enhancer fragment is unwieldly to clone and use for cell-specific analysis as large expression constructs lowers construct genomic integration efficiency. Fortunately, a more manageable 800-bp regulatory region, termed zCREST1 (zebrafish conserved regulatory element for *islet-1* 1), was isolated from 15-kb cranial motor neuron enhancer fragment, and when inserted just upstream of a minimal promoter (*heat shock protein 70l*, *hsp70l*), drives expression in the same cranial motor neurons as the original Tg(*isl1*:GFP) line (Uemura et al., 2005). Pairing the zCREST1 region with a minimal promoter is sufficient for efficient production of both transient, mosaic expression and stable transgenic zebrafish lines (Grant and Moens, 2010; Mapp et al., 2010; Mapp et al., 2011).

To assess cell-specific function of Erc1b in cranial motor neurons, we engineered a Tol2kit promoter vector containing zCREST1, cloned from genomic DNA, upstream of *hsp70l* (p5E_zCREST1) (Figure 3.6). We confirmed that our zCREST1 promoter vector

can be used for mosaic expression in the cranial motor neurons by injecting a Tol2kit expression construct for expression of mCherry into Tg(*isl1*:GFP) embryos. We observed mosaic mCherry expression in cranial nerve cell bodies and axons, similar to GFP expression in the same embryos. This finding suggested that the zCREST promoter can be used in conjunction with other Tol2kit vectors to drive expression in the cranial motor neurons.

We mosaically overexpressed a C-terminal tagged Erc1b-mCherry fusion protein to examine localization of Erc1b within cranial motor axons (Figure 3.7). Our Tol2kit expression vector contained the *cmlc2*:eGFP transgenesis marker to identify which injected embryos had integration of the fusion protein. Injection of the Tol2 expression construct into *erc1b*/Tg(*isl1*:GFP) heterozygous crosses resulted in a 40% genome integration rate (data not shown). mCherry signal was observed within the cranial motor axons of live 4 dpf injected embryos, supporting our previous observation of endogenous zebrafish Erc proteins localize within cranial motor axons.

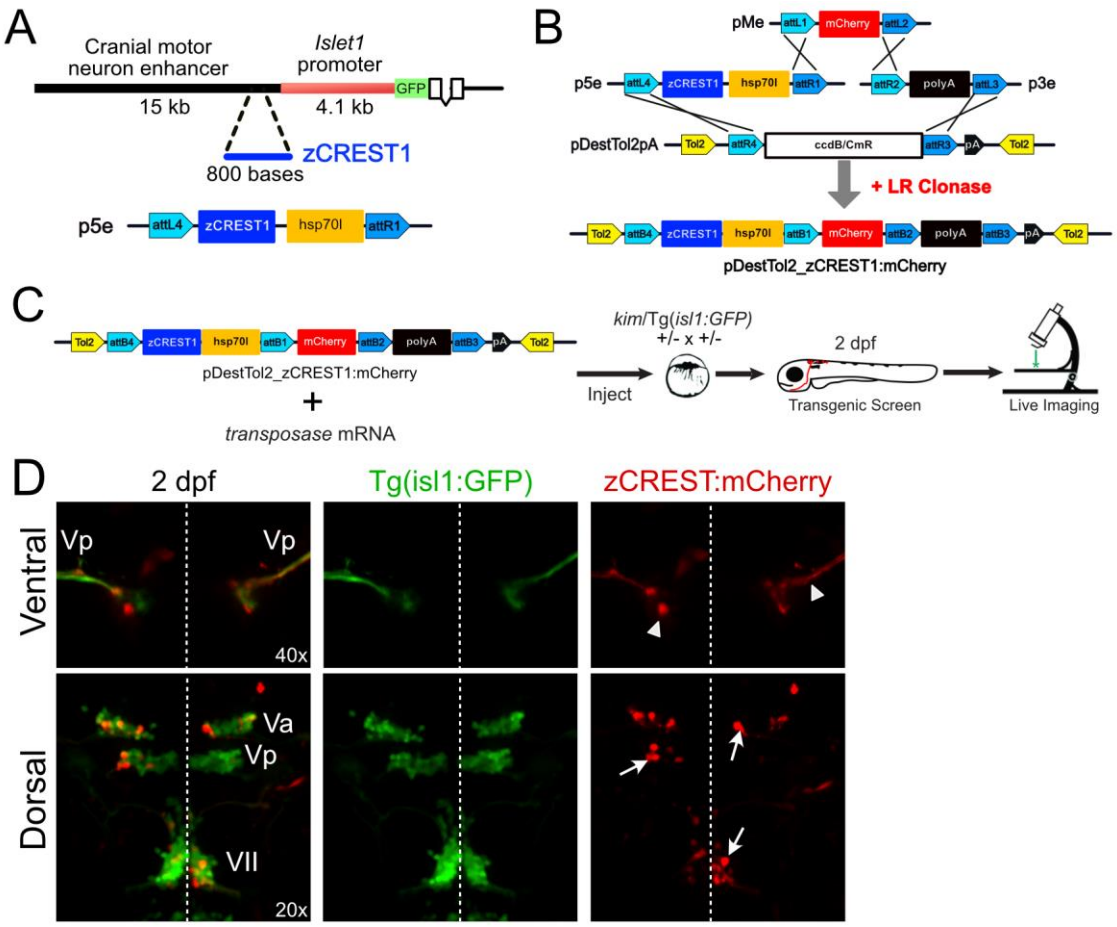

Figure 3.6. The zCREST1 promoter drives mosaic overexpression in cranial motor nerves

(A) The 800-bp zCREST1 enhancer region was cloned out of the cranial motor neuron enhancer and inserted into a 5' promoter construct for Tol2kit overexpression. (**B)** Design of a Tol2 expression construct driving mCherry overexpression in cranial motor neurons. (**C)** Injection of zCREST1:mCherry Tol2 construct into *kim*/Tg(*isl1*:GFP) embryos. (**D)** Representative images of 2 dpf embryos displaying mosaic mCherry expression within Tg(*isl1*:GFP)+ trigeminal cranial motor axons (Vp; top) and cranial nerve cell bodies (Vp, Va, VII; bottom). Dashed line signifies midline, white triangles indicate Vp growth cone and axons, white arrows indicate single cell bodies expressing mCherry. All images maximum intensity projections.

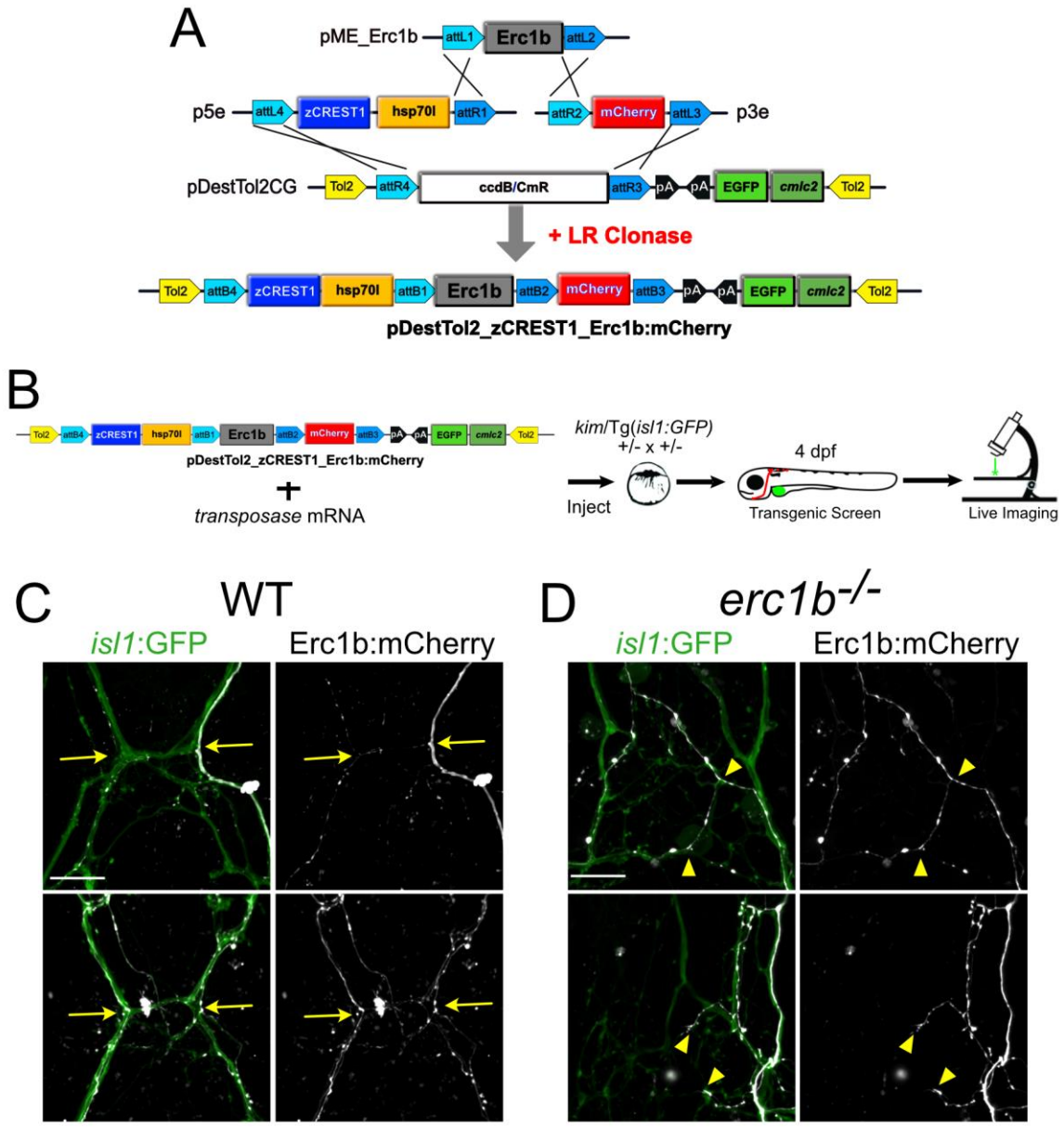

Figure 3.7. Mosaic overexpression of Erc1b in cranial motor neurons
(A) Design of a Tol2 expression construct driving Erc1b:mCherry fusion protein overexpression in cranial motor neurons. **(B)** Injection of Erc1b:mCherry fusion construct into *kim*/Tg(*isl1:GFP*) single cell embryos with transgenic screening and live imaging at 4 dpf. **(C)** Representative images of WT larvae expressing mCherry within cranial motor nerves. Yellow arrows signify midline crossing. **(D)** Representative images of *erc1b*$^{-/-}$ larvae expressing mCherry within cranial motor nerves. Yellow arrowheads signify ectopic midline crossing. All images maximum intensity projections. Scale bar = 20 µm.

Discussion

While historically, the roles of motor neurons and muscle fibers in the initiation and maintenance of NMJs have been often thought of as a "chicken-and-egg problem", more recent studies have established that NMJ synaptogenesis requires collaboration between the neurons and muscles. We previously discovered loss of Erc1b results in NMJ patterning defects on the muscles that control jaw movements in zebrafish larvae (Luderman, et al. In Revisions). However, dissecting the function of Erc1b in NMJ patterning is complicated by the fact that *erc1b*$^{-/-}$ larvae also exhibit defects in cranial nerve outgrowth and craniofacial muscle organization. Here, we designed cranial nerve and craniofacial muscle cell-specific expression constructs that can be further used to address the question of the function of Erc1b in NMJ patterning.

Previous studies have identified ERC1 expression at NMJs in mouse tissues and surrounding AChR plaques in cultured myotubules (Nishimune, 2012; Proszynski and Sanes, 2013). Our analysis identified zebrafish Erc paralog positive staining in the axons of cranial nerves and in association with AChRs in craniofacial muscles in wild-type larvae. The commercially available ERC1 antibody used recognizes all members of the Erc family of proteins in zebrafish: Erc1a, Erc1b, and Erc2. For that reason, this current immunofluorescence technique is unable to distinguish between Erc paralogs. Additionally, we observed Erc positive staining in tissue from *erc1b*$^{-/-}$ larvae (data not shown). It was previously shown that the nonsense *erc1b* mutation (Q253X) results in loss of Erc1b protein observed via Western blot analysis using the same pan-Erc antibody (Levic et al, unpublished). Therefore, the Erc antibody staining observed in *erc1b*$^{-/-}$ larvae may be other Erc paralogs, Erc1a or Erc2. Interestingly, even though these other Erc

paralogs are still present in *erc1b*$^{-/-}$ tissue, we previously have shown that the mutant larvae phenotypes are specific to loss of Erc1b function (Luderman, et al. In Revisions). therefore, the functions of the other Erc paralogs may not be redundant of Erc1b in craniofacial muscles and cranial motor nerves. Future analysis would be needed to fully assess specific Erc paralog expression and function in craniofacial tissue.

In zebrafish trunk muscles, AChR clusters prepatterned on the muscle fiber surface prior to the arrival of the motor neuron growth cone function as guideposts for axonal growth and initial NMJ synaptogenesis (Panzer et al., 2006). However in craniofacial tissue, the cranial motor neurons differentiate and send their projections out of the hindbrain to the target ventral tissues prior to craniofacial muscle differentiation (Schilling and Kimmel, 1997) (Figure 3.8). Therefore, it is unlikely that muscle-specific cues are providing guidance for cranial nerve growth, at least during growth into the first pharyngeal arch. We previously found that *erc1b*$^{-/-}$ embryos displayed trigeminal nerve growth defects prior to the appearance of ventral craniofacial muscles, thus representing a nerve-specific phenotype (Luderman, et al., In Revisions). For this reason and others, we felt it was important to assess cell-specific function for Erc1b in the cranial nerves and in the craniofacial muscles. So far, we have developed and validated cell-specific expression constructs to drive mosaic overexpression of Erc1b. However, our preliminary analysis has not shown any rescue or relief of the *erc1b*$^{-/-}$ phenotype following mosaic overexpression. This result may be explained by the mosaicism of the Tol2 system. In our experience, large Tol2kit plasmids have difficulty integrating into the genome for expression, which could be the case in this situation as the expression vectors driving expression of the Erc1b fusion proteins are over 10 kb in size. As such, even though we

were observing a 40-50% integration efficiency of the secondary transgenesis marker, we observed few muscle fibers or axons that expressed the fusion protein in the craniofacial tissue. It is unlikely that these few cells overexpressing Erc1b in mutant larvae are sufficient to rescue the tissue phenotype we had observed. Therefore, future work may require establishment of stable, non-mosaic overexpression lines to assess Erc1b function in the cranial nerves and craniofacial muscles.

Our hope is that these cell-specific constructs would help elucidate the function of ERC1 at vertebrate NMJs, which has not been evaluated in an *in vivo* model as of yet. Although this work has focused on the roles of motor neurons and muscles in NMJ synaptogenesis, more recent evidence has also implicated terminal/perisynaptic Schwann cells in NMJ maturation and maintenance (Barik et al., 2016; Feng and Ko, 2008). Therefore, additional experiments may be needed to assess the function of ERC1 in other cell types that also contribute to NMJs.

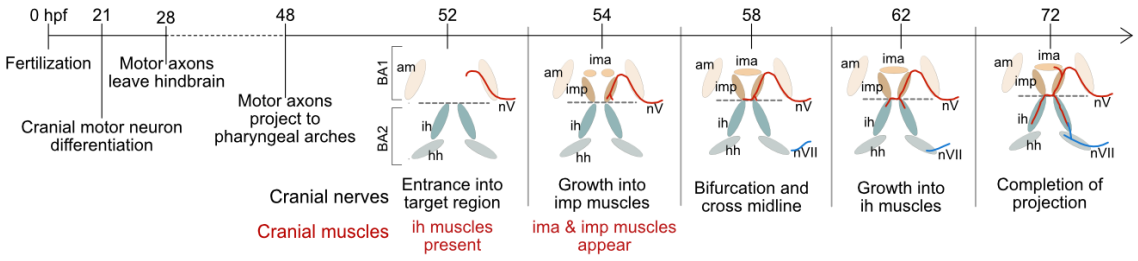

Figure 3.8. Timeline of muscle appearance and cranial nerve innervation
The cranial nerves differentiate and begin growing towards the ventral craniofacial region prior to the appearance of some target muscles in branchial arches 1 and 2 (BA1, BA2). The trigeminal motor nerve (nV) grows into BA1 by 52 hours post-fertilization (hpf) and bifurcates at the BA1/BA2 midline by 58 hpf. The facial motor nerve (nVII) enters BA2 by 62 hpf. nV motor neurons innervates muscles of both BA1 and BA2, while nVII motor neurons innervate muscles of BA2. Based on data by (Tanaka et al., 2007). adductor mandibulae (am); intermandibularis anterior (ima); intermandibularis posterior (imp); interhyal (ih); hyohyal (hh); trigerminal motor nerve (nV); facial motor nerve (nVII).

CHAPTER IV

DISTINGUISHING THE ROLES OF ZEBRAFISH *ERC1* PARALOGS IN CRANIOFACIAL DEVELOPMENT

Introduction

Developmental delay and intellectual disabilities are key features in patients with subtelomeric chromosomal deletions (Han and Park, 2021). Microdeletions within the distal arm of chromosome 12 (12p13.33-p13.32) have been identified in 28 different patients (Han and Park, 2021; Leyser et al., 2016; Mio et al., 2020). Patients share developmental disorder diagnoses including autism spectrum disorder (ASD) (Silva et al., 2014), oculoauriculovertebral spectrum (OAVS) (Rooryck et al., 2009), and developmental verbal dyspraxia (DVD) (Thevenon et al., 2013). Additionally, patients exhibit abnormal physical features including facial dysmorphia, hypertelorism, micrognathia, microcephaly, and abnormal behaviors including attention deficit disorder (ADD), attention deficit hyperactivity disorder (ADHD), and anxiety (Abdelmoity et al., 2011; Baker et al., 2002; Macdonald et al., 2010; Silva et al., 2014). Variable patient phenotypes appear to be associated with the size of the microdeletion, indicating that haploinsufficiency of several genes within the deleted region could be responsible for the observed phenotypes (Table 4.1). While chromosome 12 deletions vary between 1.3Mb and 6.0Mb in size, a candidate gene to evaluate for its role in patient phenotypes is *ERC1*, as it falls within the smallest region of overlap among most deletions (Figure 4.1).

ERC1 (also known as ELKS, CAST2, Rab6IP2) is a coiled-coil cytoplasmic protein with multiple alternatively spliced isoforms differentially expressed in both neuronal and non-neuronal cells of vertebrates (Wang et al., 2002). Originally cloned as a random fusion gene from papillary thyroid carcinoma cells, ERC1 was subsequently identified as a Rab6 interacting protein (Rab6IP2), containing a C-terminal Rab-binding domain (RBD), that has been shown to function in post-Golgi trafficking and vesicle capture at the cell cortex of cells (Grigoriev et al., 2007; Monier et al., 2002; Nakata et al., 1999). Beyond Rab-vesicle capture, ERC1 has also been implicated in focal adhesion turnover for cell motility in non-neuronal cells (Astro et al., 2014; Astro et al., 2016; Sala et al., 2019). In neurons, ERC1 functions in modulating vesicle release as a member of the presynaptic active zone (PAZ) cytomatrix, as conditional knockout (KO) of *ERC1* in mice *ex vivo* brain slices alters synaptic vesicle release probability (Held et al., 2016; Liu et al., 2014; Ohtsuka et al., 2002; Wang et al., 2002). While not explicitly examined, RNAi knockdown in immature interneurons suggest ERC1 may function in axonal outgrowth through interactions with focal adhesion complexes (Franchi et al., 2016).

Alternative splicing generates C-terminal ERC1 isoforms expressed in humans: a shorter isoform ending in -IWA that is primarily expressed in the brain, and a longer isoform, ending in -EESS, that is widely expressed in nonneural tissues (Deguchi-Tawarada et al., 2004; Inoue et al., 2006; Liu et al., 2014; Nomura et al., 2009; Ohara-Imaizumi et al., 2005). Subsequent analysis has also identified alternative start sites in murine ERC1 isoforms (Liu et al., 2014; Nyitrai et al., 2020). *In vitro* studies have attempted to distinguish ERC1 isoform specific functions. For example, it was originally thought that only the longer ERC1 isoform interacts with Rab6 through its C-terminal

Rab-binding domain, whereas the C-terminal PDZ domain of the brain-specific, shorter ERC1 isoform interacts with other presynaptic active zone components in neurons, such as RIMs (Wang et al., 2002). However, recent studies have shown that the brain specific ERC1 isoform also functions in capturing Rab6 vesicles in presynaptic terminals (Nyitrai et al., 2020). This suggests that there may be more functionality crossover between neuronal and nonneuronal ERC1 isoforms. To our knowledge, ERC1 isoform function has not been evaluated in an *in vivo* vertebrate model to explain both neurological and morphological phenotypes associated with 12p13 microdeletions.

While other vertebrates, including rodents and *Xenopus*, have a single *ERC1* gene that produces multiple protein isoforms, zebrafish have two paralogous *erc1* genes found on separate chromosomes in the zebrafish genome: *erc1a* (chr. 25) and *erc1b* (chr. 4). These paralogous genes are likely to be a product of a teleost-specific genome duplication event that occurred in zebrafish ancestral species (Glasauer and Neuhauss, 2014; Lu et al., 2012). Interestingly, the zebrafish *erc1* paralogs are homologous to the major human ERC1 (hERC1) isoforms: Erc1a is homologous to the brain-specific -IWA hERC1 isoform, and the longer Erc1b paralog is homologous to the longer -EESS hERC1 isoform that is widely expressed, including a C-terminal RBD (Figure 4.2). Since the zebrafish *erc1* paralogs are encoded on separate chromosomes, we can use genetic approaches to investigate the function of each Erc1 paralog to ascertain the function of homologous hERC1 isoforms.

Using an unbiased forward genetics approach in zebrafish, we previously identified a mutant zebrafish line that carries a nonsense mutation in zebrafish paralog *erc1b* (*kimble*^{m533}) and recapitulates some of the craniofacial phenotypes observed in

12p13.33 deletion patients (Neuhauss et al., 1996)(Levic, et al. unpublished). In the *erc1b* global knockout model, we observed not only craniofacial dysmorphology, but also neuronal defects. We used a reverse genetics approach to assess the biological role of *erc1a* using CRISPR/Cas9 genome editing. We used *in situ* hybridization techniques to determine *erc1a* expression appears to be neuronal specific, whereas *erc1b* expression maybe more globally expressed in craniofacial tissues. Lastly, we determined that zebrafish *erc1* paralogs have nonredundant functions as overexpression of *erc1a* does not rescue *erc1b* mutant phenotypes.

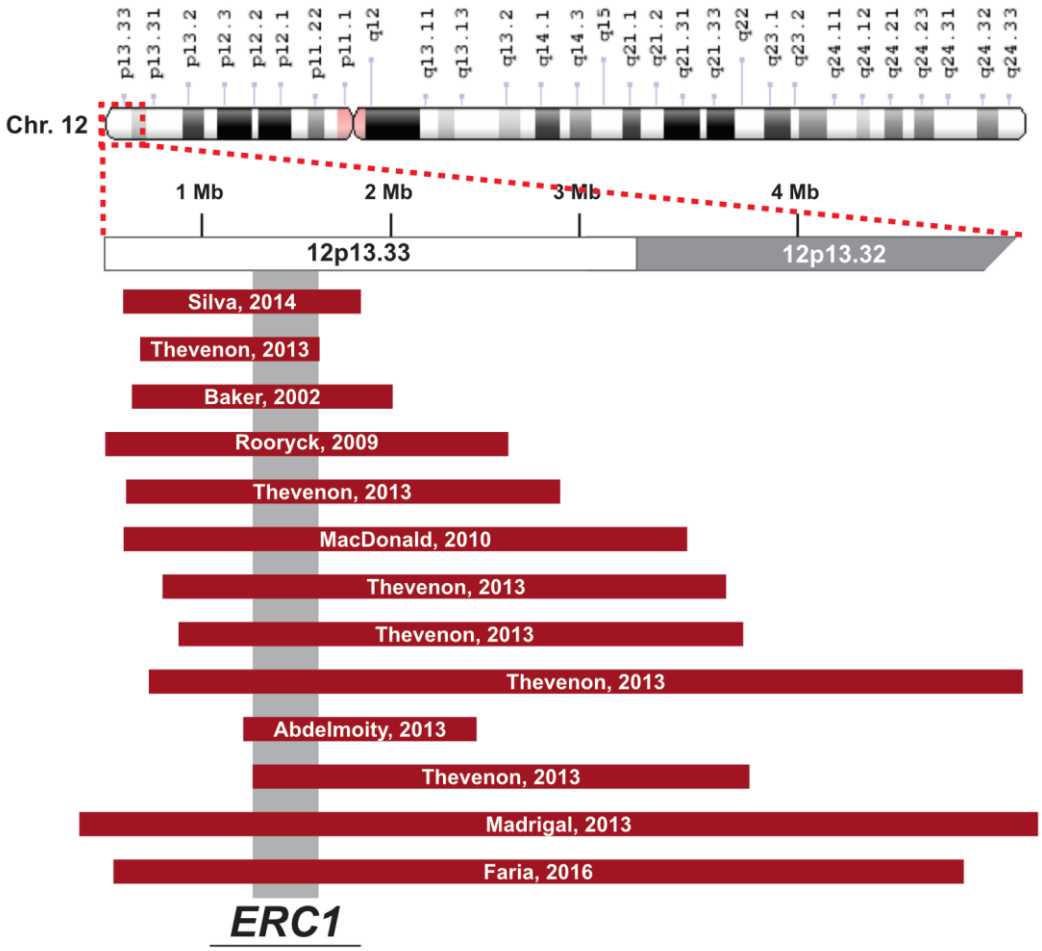

Figure 4.1. *ERC1* is found within the smallest region of overlap of 12p13.33 deletion patients.
Full idiogram of chromosome 12 is across the top, with a partial idiogram of chromosome band 12p13.33-p13.32 below. Red bars represent the minimum deletion sizes of patients identified in the literature. Gray vertical bar represents the location of *ERC1* within the deleted regions. Adapted from (Silva et al., 2014).

Table 4.1. Summary of clinical features and deletion size of patients with 12p13 microdeletions.
Adapted from (Faria et al., 2016). Developmental delay (DD); intellectual disability (ID); attention deficit disorder (ADD); attention deficit hyperactivity disorder (ADHD); Oculo-auriculo-vertebral spectrum (OAVS); childhood apraxia of speech (CAS).

First author, year	Baker, 2002	Rooryck, 2009	MacDonald 2010	Abdelmoity, 2011	Vargas, 2012	Madrigal, 2012	Thevenon, 2013					Silva, 2014	Faria, 2016
							patient 1	patient 6	patient 7	patient 8	patient 9		
12p13 Del (Mb)	1.65	2.3	2.95	1.39	4.5	6.0	3.2	3.1	2.76	2.5	4.76	1.5	4.2
Feature													
DD/ID	+	+	+	+	+	+	+	+	+	+	+	+	+
Behavioral problems	+	+	+	-	+	-	-	+	-	-	+	-	+
ADD/ADHD	-	-	-	-	-	+	+	+	+	+	+	+	-
Speech delay	+	+	+	+	+	-	+	+	+	+	+	+	+
Microcephaly	+	+	+	-	-	-	-	-	-	+	+	-	-
Micro/ retrognathia	-	+	-	-	-	-	-	-	-	+	-	-	+
Eye anomalies	+	+	-	+	-	+	+	-	+	-	+	-	+
Ear anomalies	+	+	+	-	-	+	+	+	+	+	+	-	+
Nose anomalies	-	+	+	+	-	+	+	-	-	-	+	-	+
Malocclusions	+	+	+	+	+	+	+	+	+	+	+	+	+
Other diagnoses		OAVS					CAS, macro-celphaly	CAS, myopathic facies			CAS	spina bifida occulata	Feeding problems

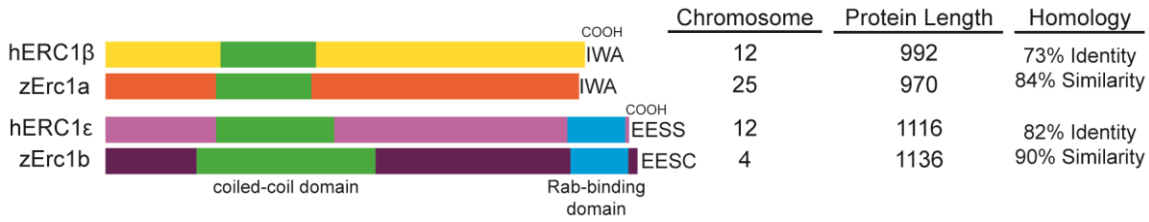

Figure 4.2. Homology, domain structures of Zebrafish Erc1 paralogs and human ERC1 isoforms

Methods

Fish maintenance and breeding

Zebrafish were raised under standard laboratory conditions at 28.5°C as previously described (Barrallo-Gimeno et al., 2004; Montero-Balaguer et al., 2006). All experiments were conducted following the guidelines established by the IACUC at Vanderbilt University Medical Center under the protocol number ID: #M1700020-00. The *erc1b/kimble*^{m533} line was previously described were kept in AB genetic background for phenotypic analysis (Luderman, et al., In Revisions;(Neuhauss et al., 1996). Embryos were staged and fixed at indicated stages, i.e. hours post-fertilization (hpf) and days post-fertilization (dpf) as described previously (Kimmel et al., 1995a).

Live imaging of embryos & head size index analysis

4 dpf embryos were anesthetized in Tricaine (Sigma), mounted in 3% methylcellulose (Sigma) and imaged using Zeiss Stemi 2000-C with HRc camera. Using dorsal views in ImageJ, head length was measured from jaw protrusion to the pectoral fins, and head width was measured between the ear capsules. Inner canthal distance was measured between the closest edges of the retinas. Craniofacial morphology was determined by

evaluating the head length to width ratio. Statistical analysis was performed using Student's t-test (two-tailed), 95% confidence interval.

Cartilage staining

4 dpf embryos were stained for cartilage with Alcian blue as described previously with modifications (Melville et al., 2011; Walker and Kimmel, 2007). In brief, larvae were fixed for 1 hour in 4% paraformaldehyde (PFA) at room temperature, and then stained overnight in 0.2% Alcian blue and 60 mM $MgCl_2$ in 70% ethanol at room temperature. Stained larvae were bleached in 1.5% H_2O_2, 1% KOH solution for 20 minutes at room temperature, followed by subsequent de-staining and clearing with multiple rinses of KOH/glycerol solutions and stored in 0.1% KOH, 50% glycerol. Stained larvae were imaged with Zeiss Axioimager Z1 scope equipped with Axiocam HRc camera. ImageJ was used to measure Meckel's cartilage length and ethmoid plate area. Statistical analysis was performed using Student's t-test (two-tailed), 95% confidence interval.

Cloning of erc1a cDNA

Zebrafish *erc1a* (NM_001015065.1) coding sequence was cloned from cDNA acquired from AB genomic background larvae using TOPO™ XL-2 Complete PCR Cloning Kit (Thermo Fisher, K8050-10) and primers listed in Table 4.1. The 2.9 kb coding sequence was subsequently excised out of the TOPO XL-2 vector and ligated into pCS2+ using EcoRI restriction digest and T4 DNA ligase. Insertion of the *erc1a* coding sequence was confirmed by Sanger sequencing and the pCS2+_*erc1a* plasmid was used for in vitro transcription.

mRNA overexpression

Zebrafish *erc1b* and *erc1a* cDNA vectors were linearized by NotI digestion and synthesized capped mRNA transcripts were produced via in vitro transcription with mMESSAGE mMACHINE SP6 transcription kit (Thermo Fisher Scientific). 1200 pg of mRNA diluted in 0.3x Danieau buffer was micro-injected into single cell-stage embryos. Embryos were grown to 4 dpf for live imaging, and post-imaging genotyping. Embryos were automatically imaged on a VAST Bioimager in both the dorsal and lateral orientations. Live images were analyzed for craniofacial morphology and inner canthal distance in ImageJ as discussed previously.

Whole-mount in situ hybridization probe construction and RNAscope

To create an RNA probe targeting *erc1a*, a region 100-bp upstream of the stop codon to 300-bp within the 3' UTR of *erc1a* was cloned into cloned into pGEM-T Easy vector (Promega) by T-A cloning. Following linearization and purification of the plasmid, in vitro transcription using a DIG RNA labeling mix and either T7 RNA polymerase or SP6 RNA polymerase to create antisense and sense probes, respectively. RNA probes were purified and validated on a gel before being used for in situ hybridization. Embryos to be used for whole-mount in situ hybridization were raised in 0.2 mM 1-phenyl-2-thiourea (Sigma) to block pigmentation, and were fixed at appropriately stages in 4% PFA overnight at 4˚C. Whole-mount in situ hybridization was performed as previously described (Barrallo-Gimeno et al., 2004; Thisse and Thisse, 2014).

Custom fluorescent *erc1a* and *erc1b* RNAscope® probes were ordered from Advanced Cell Diagnostics, Inc. (ACD, Bio-Techne, Haywood, CA). RNAscope® Multiplex Fluorescent v2 Assay was performed as previously described and using

technical notes published on the RNAscope website (https://acdbio.com/rnascope-multiplex-fluorescent-v2-assay) (Gross-Thebing, 2020).

Whole mount immunofluorescence (IF) and fluorescence microscopy

NMJ (SV2 & αBTX) and phalloidin staining. 4 dpf zebrafish were fixed in 4% PFA overnight at 4˚C. PFA was washed off with multiple rinses of PBS-0.1% Tween-20 (PBT). Under a dissecting microscope, the tip of the tail was removed from each animal. Next, samples were bleached in 1.5% H_2O_2/1% KOH, rinsed multiple times in PBT, and then permeabilized in ice-cold acetone for 7 minutes at -20˚C. Samples were blocked in 2% normal goat serum, 1% BSA in PBS-0.5% Triton X-100. Primary antibodies were diluted in the blocking solution (1:100 anti-SV2, DSHB; 1:300 anti-acetylated tubulin, Sigma, no. T7451) and incubated overnight at 4˚C with gentle rocking. Alexa Fluor 488 conjugated αBTX (1:250, 1 mg/mL, Thermo Fisher Scientific, no. B13422), rhodamine phalloidin (1:250, Thermo Fisher Scientific, no. R415), and secondary antibodies (1:1000 anti-Mouse Alexa Fluor 555; anti-Mouse Alexa Flour 633, Thermo Fisher Scientific, no. A21126) were diluted in blocking solution and incubated overnight at 4˚C with gentle rocking. Following incubation, antibodies were rinsed several times in PBS-0.5% Triton X-100 before clearing and storage in 90% glycerol until imaging.

Acetylated Tubulin, WGA, HuC/D & SV2 staining. 4 dpf zebrafish were fixed in Prefer fixative (Anatech) at room temperature overnight-2 days as previously described (Taylor et al., 2011). After washing off fixative, larvae were post-fixed in 4% PFA at room temperature and rinsed in PBT. Samples were bleached in 1.5% H_2O_2/1% KOH as above, and then permeabilized in PBS-0.5% Triton X-100 for 10 minutes at room temperature. Samples were blocked in 5% normal goat serum, 1% BSA, 1% DMSO in PBS-0.1%

Triton X-100 for 1 hour at room temperature. Primary antibodies were diluted in blocking solution (1:100 anti-SV2, DSHB; 1:300 anti-acetylated tubulin, Sigma, no. T7451; 1:250 anti-HuC/D, Thermo Fisher 16A11) and incubated overnight at 4˚C with gentle rocking. Alexa Fluor 555 conjugated wheat germ agglutinin (WGA, 1:300, Thermo Fisher W32464) and secondary antibodies (1:1000 anti-Mouse Alexa Fluor 555, Thermo Fisher, no. A21147; anti-Mouse Alexa Flour 633, Thermo Fisher, no. A21126) were diluted in blocking solution and incubated overnight at 4˚C with gentle rocking. Following incubation and rinsing in PBS-0.1% Triton-X 100, antibodies were post-fixed in 4% PFA for 20 minutes at room temperature before being cleared in 50% glycerol and stored in 90% glycerol prior to imaging.

For imaging of whole-mount IF samples, zebrafish were embedded in 0.9% low-melt agarose on glass-bottom confocal dishes and imaged on a Nikon Spinning Disk confocal microscope with Plan Apo Lambda 20x (0.75 NA, 0.9 μm slice depth) or 10x (0.45 NA, 2.5 μm slice depth) objective. Images were deconvolved using Nikon Elements software and presented as maximum intensity Z-projections.

CRISPR/Cas9 genome editing of erc1a

CRISPR/Cas9 target sites within zebrafish *erc1a* gene (GRCz10 assembly) were identified using the CHOPCHOP (Montague et al., 2014) web tool. Target oligos and guide RNA scaffold oligo are listed in Table 4.2. A cloning-free method to generate sgRNA templates was performed as previously described (Varshney et al., 2015). Upon annealing two oligos, gaps were filled with T4 DNA polymerase (NEB), yielding a double stranded linear template for in vitro transcription. Guide RNAs were synthesized with MEGAshortscript™ T7 transcription kit (ThermoFisher Scientific).

To generate mutations with CRISPR/Cas9 system, a mixture of 500pg purified Cas9 protein (PNA Bio Inc, # CP01) and 150 pg gRNA was injected into one-cell stage embryos. Injected embryos were grown to 4 dpf stage for phenotypic analysis. Mutations generated in injected embryos were detected using a heteroduplex mobility shift assay using PCR primers that amplify the CRISPR target region. PCR products were subjected to denaturation and rehybridization in a thermocycler before being run on a 10% acrylamide gel to resolve multiple banding patterns, which indicates the presence of CRISPR-induced indels. PCR-amplified products were cloned into pGEM-T Easy vector (Promega) by T-A cloning and sequenced using SP6 primers to individually detect various indel mutations created by CRISPR/Cas9 system.

Stable CRISPR-generated mutant lines were established by growing gRNA/Cas9 injected embryos to adulthood to generate founders (G_0). To screen for germline transmission, potential founders were crossed to wild-type (AB) fish, and their progeny (F1) was assessed for mutations in *erc1a* by heteroduplex assay. Subsequent lines were made by outcrossing heterozygote carriers to AB fish, or incrossing siblings to establish a homozygous mutant line.

Acknowledgements

Daniel Levic previously cloned *erc1b* transcripts from wild-type cDNA that were used for subsequent sub-cloning and mRNA in vitro transcription, and provided images of *erc1b in situ* hybridization expression.

Table 4.2. Primers used in this study

Primer name	**Primer Sequence (5′→3′)**
sgRNAscaff	ttttgcaccgactcggtgccacttttcaagtTgataaCggactagccttattttaacttgctatttctagctctaaaac
erc1aE5_02 gRNA	AATTAATACGACTCACTATAGGTCTGCAAGCCAAGAAGCTgttttagagctagaaatagc
erc1aE5_01F2	TGGACCAAGTTAAGCAAGACCT
erc1aE5_02R1	AGCACTTCAATATGCTGTTTGC
erc1a RACE GSP3	GTCCATGAAGGCCAAGATGT
erc1a UTR1	acgtttgcaggctctttgag

Results

Mosaic erc1a CRISPR mutations cause dorsal cartilage defects that are subsequently lost in stable lines

To test the biological role of *erc1a*, I designed several guide RNAs (gRNAs) targeting exons within a predicted coiled-coil domain of the zebrafish Erc1a protein using CRISPR/Cas9 genome editing (Figure 4.3). This target structural domain site was chosen to hopefully cause misfolding and subsequent protein degradation. Of the gRNAs tested, the gRNA against a location within exon 5 showed the greatest efficiency in generating indels in transient assays. Co-injection of the exon 5 target gRNA and Cas9 protein into WT embryos produced mutant phenotypes in over 90% of injected embryos. Live imaging analysis of *erc1a* mosaic mutants revealed distinct craniofacial dysmorphology and decreased inner canthal distance (ICD). Alcian blue staining revealed *erc1a* mosaic mutants have smaller ethmoid plate areas, suggesting transient *erc1a* depletion causes defects in dorsal/neurocranium cartilage morphology. Transient CRISPR embryos carry multiple indels within the target *erc1a* exon, suggesting the observed craniofacial phenotypes are due to mutation mosaicism.

These observed mosaic *erc1a* mutant phenotypes are distinctly different from the craniofacial and head skeleton phenotypes observed in *erc1b*$^{-/-}$ mutants (Figure 4.4). Mutations within both zebrafish *erc1* paralogs results in craniofacial dysmorphia, evident as a decrease in head length to width ratio. However, whereas *erc1a* mosaic mutants display defects in the dorsal/neurocranium cartilage, including reduced area of the ethmoid plate, *erc1b*$^{-/-}$ mutants exhibit defects in the ventral/visceral cartilage with reduced Meckel's cartilage length. Additionally, ICD varies between the two paralogs:

erc1b$^{-/-}$ mutants exhibit increased distance between the retina (hypertelorism), whereas *erc1a* mosaic mutants display a significant decrease in retinal distance (hypotelorism). These differing mutant phenotypes indicate that *erc1a* and *erc1b* may play different roles in craniofacial development.

Once we verified that targeting exon 5 of *erc1a* efficiently produced indels and a mutant phenotype, we proceeded to establish a stable *erc1a* mutant zebrafish line by injecting diluted amounts of gRNA and Cas9 protein into one-cell stage wild-type embryos, which were then grown to adulthood to establish founder (F0) *erc1a* zebrafish lines. Individual F0 fish, identified to pass *erc1a* mutations to their progeny, were outcrossed to wild-type AB lines to establish F1 generations. F1 adult fish were genotyped and sequenced to identify multiple *erc1a* mutant alleles, all of which are predicted to result in a frameshift mutation and early truncation of Erc1a (Figure 4.5). Successive outcrosses with wild-type lines helped to clean potential non-specific mutations out of the background. Live imaging of an F1 incross revealed no significant difference in body length, craniofacial morphology, or ICD between wild type, heterozygous, or homozygous *erc1a* mutants. Lack of a gross morphology in homozygous *erc1a* mutants was observed for each of the observed *erc1a* alleles. Therefore, we grew an F1 incross to adulthood to determine if homozygous *erc1a* mutants would survive and be viable. Within this F2 generation, multiple homozygous *erc1a* adults were identified and could produce viable progeny from a sibling incross. We confirmed that the homozygous *erc1a* mutant lines carry their mutant allele through transcription by sequencing cDNA. Homozygous *erc1a* mutant larvae did not exhibit any gross neurological defects observed by whole-mount immunofluorescence of a pan-

neuronal marker (Figure 4.6). Homozygous *erc1a* mutant larvae also did not exhibit ventral craniofacial muscle organization or neuromuscular junction defects that are observed in *erc1b*$^{-/-}$ larvae at 4 dpf. These results suggest that, at least to this level of assessment, homozygous *erc1a* do no present observable defects, and that *erc1b*$^{-/-}$ present a much more severe, observable phenotype.

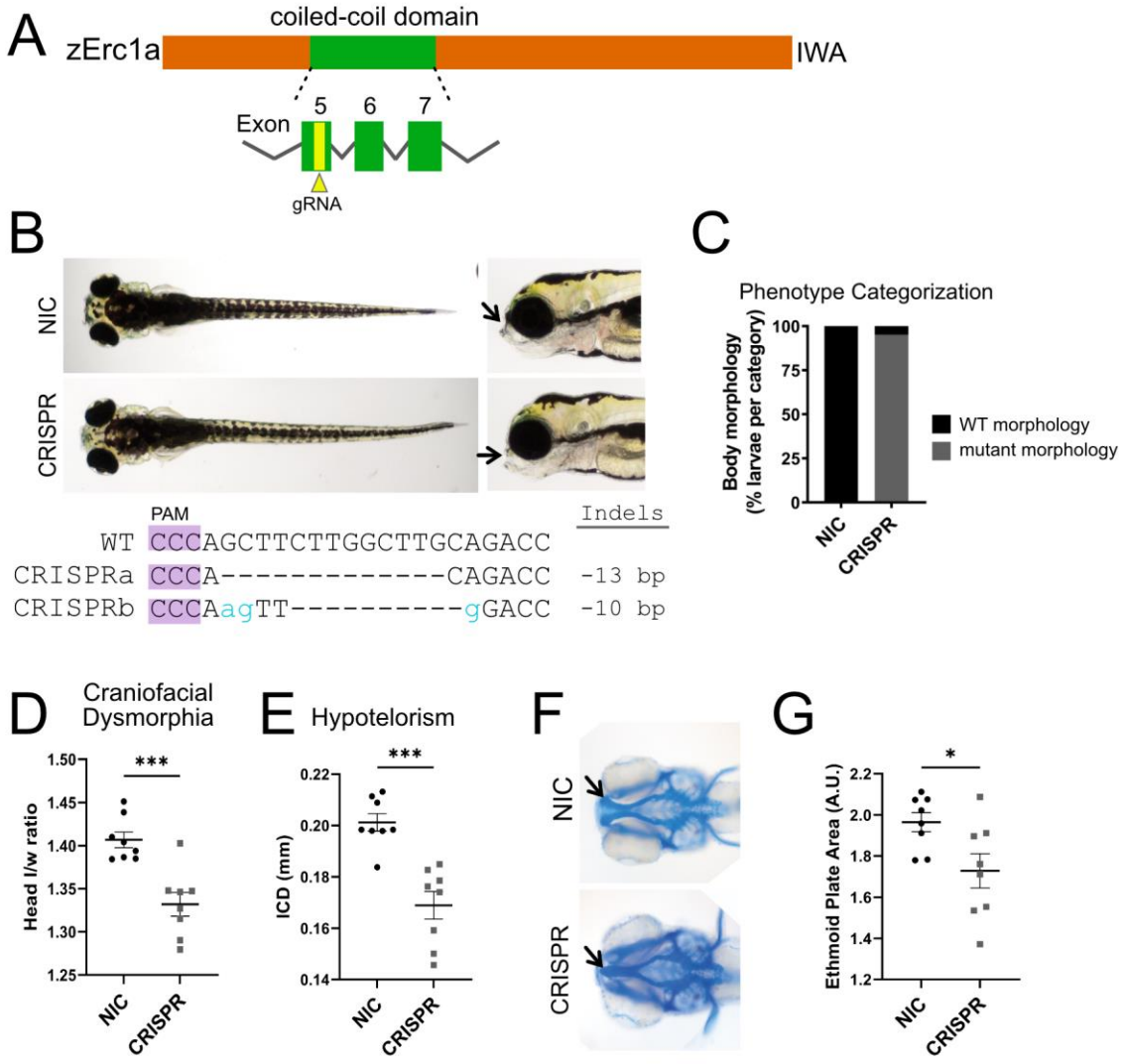

Figure 4.3. Mosaic *erc1a* CRISPR mutants display neurocranium cartilage defects **(A)** CRISPR design targeting exon 5 of *erc1a*. **(B)** Representative live images of 4 dpf non-injected control (NIC) and CRISPR injected larva with altered jaw angle (arrow). WT *erc1a* target sequence and mosaic indels produced in CRISPR inject larva. PAM sequence highlighted in purple. **(C)** Phenotype categorization of WT or mutant morphology following CRISPR injection. Quantification of live images including **(D)** head length/width ratio and **(E)** inner canthal distance (ICD). **(F)** Representative images of Alcian blue stained 4 dpf NIC and CRISPR injected larva; arrows indicate ethmoid plate. **(G)** Quantification of ethmoid plate area. Symbols signify individual larvae. Mann-Whitney U t-test (two-tailed) was used for statistical analysis, 95% confidence interval, *p<0.05, ***p<0.001.

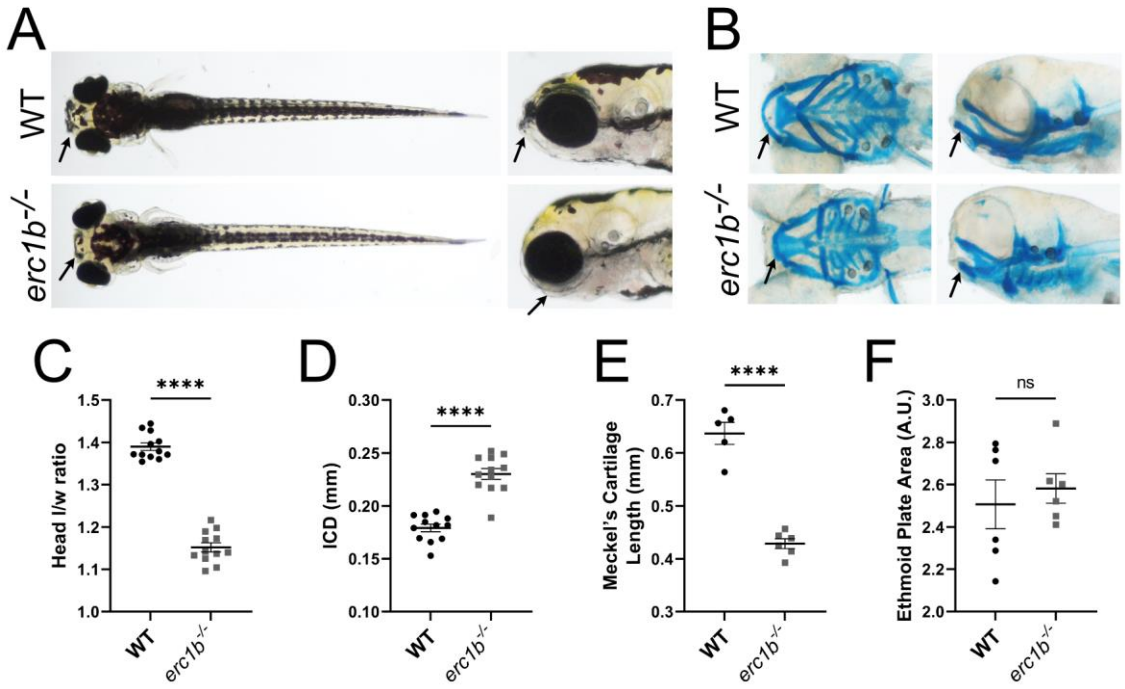

Figure 4.4. Stable *erc1b* mutant line presents with defects in ventral cartilage and hypertelorism

(A) Representative images of live 4 dpf WT and *erc1b*$^{-/-}$ larvae, dorsal and lateral views. Jaws indicated by arrows. (**B)** Representative images of 4 dpf Alcian blue stained WT and *erc1b*$^{-/-}$ larvae, ventral and lateral views. Meckel's cartilage indicated by arrows. Quantification of live images including **(C)** head length/width ratio and **(D)** inner canthal distance (ICD). Quantification of Alcian blue images including **(E)** Meckel's cartilage length and **(F)** ethmoid plate area. Symbols signify individual animals. Mann-Whitney U t-test (two-tailed) was used for statistical analysis, 95% confidence interval, ****p<0.0001.

Zebrafish erc1 paralogs are differentially expressed in neurological, craniofacial tissue

Previous studies have indicated that ERC1 isoforms are differentially expressed: the shorter, -IWA isoform is brain-specific, whereas the longer, -EESS isoform is expressed in nonneuronal tissues (Liu et al., 2014; Wang et al., 2002). Based on the literature, and our previous findings that mosaic *erc1a* and homozygous *erc1b* mutations lead to differential phenotypes in craniofacial cartilage, we sought to determine expression patterns of the zebrafish *erc1* paralogs. We synthesized an antisense and sense RNA probe targeting a ~400-bp region of *erc1a* that encompasses both the stop codon and portion of the 3' UTR for whole mount *in situ* hybridization (Figure 4.7). Expression of *erc1a* was restricted to the brain and retina in 4 dpf wild-type larvae. In contrast, expression of *erc1b* was enriched in developing cartilage and pharyngeal arches (D. Levic data, unpublished). However, this method of *in situ* hybridization does not provide high spatial resolution of the expression patterns, and we are not able to detect both genes simultaneously.

To further investigate expression of *erc1a* and *erc1a*, we purchased custom designed RNA probes specific to each *erc1* paralog to be used with the RNAscope® Multiplex technology, which boasts the ability to detect lowly expressed transcripts at a sub-cellular level (Gross-Thebing et al., 2014). Expression of *erc1a* and *erc1b* was evaluated in 1-4 dpf wild-type tissue (Figure 4.8). In dorsal/neuronal tissues, both *erc1a* and *erc1b* are expressed, with little expression of *erc1a* at 1 dpf observed. In ventral/pharyngeal arch tissues, only expression of *erc1b* was observed. These results agree with our previous results from traditional whole-mount *in situ* hybridization that *erc1a* is expressed primarily in neuronal tissue. Additionally, we discovered that *erc1b*

appears to be expressed not only in ventral craniofacial tissue, but also neuronal tissues, overlapping the *erc1a* expression pattern. However, we were unable to determine tissue or cell-specific expression with our RNAscope probes, nor were we able to independently validate the specificity of the probes we received as we found *erc1b* expression in both the neuronal and ventral tissues of *erc1b*$^{-/-}$ larvae (Figure 4.9).

Overexpression of erc1a does not rescue erc1b mutant phenotypes

Analysis of zebrafish *erc1* paralog expression patterns suggest there may be overlap in expression of *erc1a* and *erc1b* in neuronal tissues. Therefore, we sought to examine whether the zebrafish *erc1* paralogs have redundant function by performing genetic replacement experiments. Full-length *erc1a* and *erc1b* coding sequences were cloned from wild-type embryos and *in vitro* transcribed into mRNA for injections into single-cell embryos from an *erc1b* heterozygous cross (Figure 4.10). Following injection, embryos were grown to 4 dpf for phenotypic analysis and live imaging. Overexpression of wild-type *erc1b* mRNA significantly rescued the body morphology of *erc1b*$^{-/-}$ larvae, including the presence of the protruding jaw, compared to overexpression of *erc1a* mRNA, which did not rescue *erc1b*$^{-/-}$ compared to non-injected control (NIC) larvae. Injection of *erc1b* mRNA but not *erc1a* mRNA was able to rescue both ICD and craniofacial morphology in *erc1b*$^{-/-}$ larvae to a similar level as WT siblings. This finding suggests that the zebrafish *erc1* paralogs have nonredundant functions in craniofacial tissue development.

Interestingly, multiple full-length *erc1b* transcripts were cloned from wild type tissue: a short isoform that ends in -IWA, and a long isoform that ends in -EESC (Figure 4.11). The short Erc1b isoform shares 77% homology with Erc1a, which is similar to the

homology observed between the long and short isoforms of Erc1b. Genetic replacement with either *erc1b* transcripts rescue the body morphology of *erc1b*$^{-/-}$ mutants, such as jaw protrusion. Additionally, overexpression of either *erc1b* transcript significantly rescues cellular phenotypes observed in *erc1b*$^{-/-}$ mutants, including craniofacial muscle organization and cranial motor nerve fasciculation and midline crossing, which were previously observed in *erc1b*$^{-/-}$ mutants (Luderman, et al. In Revision). These findings suggest that although *erc1* paralogs are unable to functionally replace one another, the multiple Erc1b isoforms are functionally redundant.

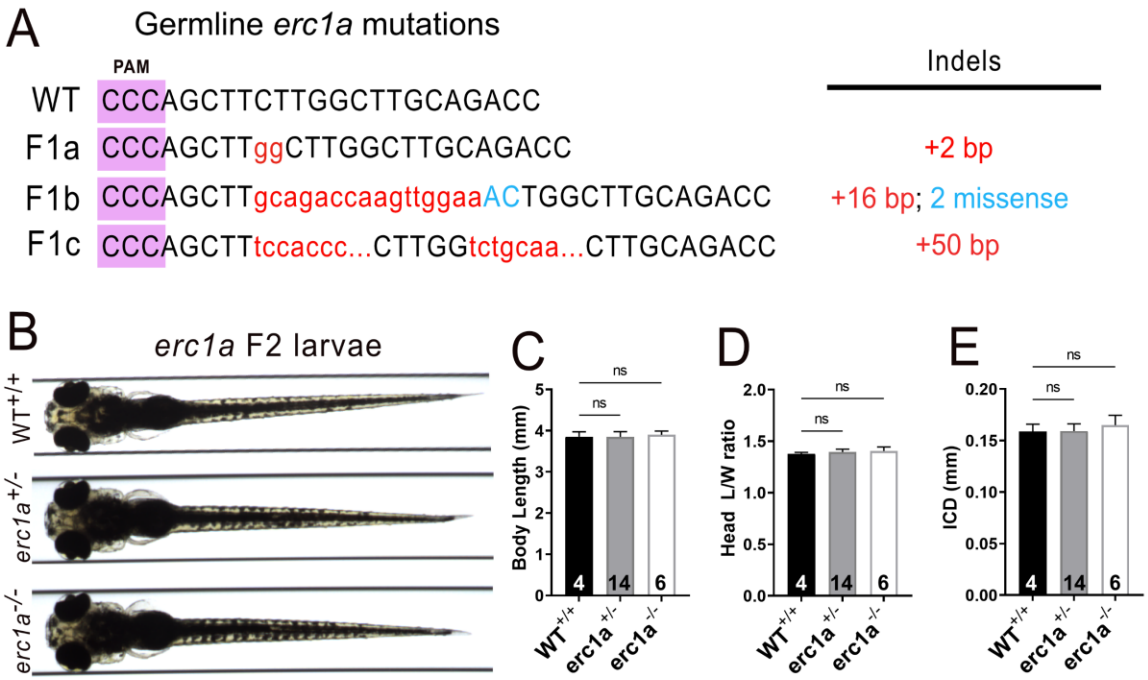

Figure 4.5. Stable *erc1a* homozygous mutants do not have distinguishable craniofacial morphological phenotypes
(A) Three independent germline *erc1a* mutant alleles. PAM sequence indicated by purple box; indels listed on the right (inserted nucleotides in red, missense nucleotides in blue). **(B)** Live images of 4 dpf wild type, heterozygous, and homozygous *erc1a* mutant larvae from a heterozygous cross of F1c mutant line. Quantification of **(C)** body length, **(D)** craniofacial morphology (head length/width ratio), and **(E)** inner canthal distance (ICD) from live images. Sample sizes indicated at the bottom of each bar. Two-way ANOVA with Sidak's multiple comparison was used for statistical significance.

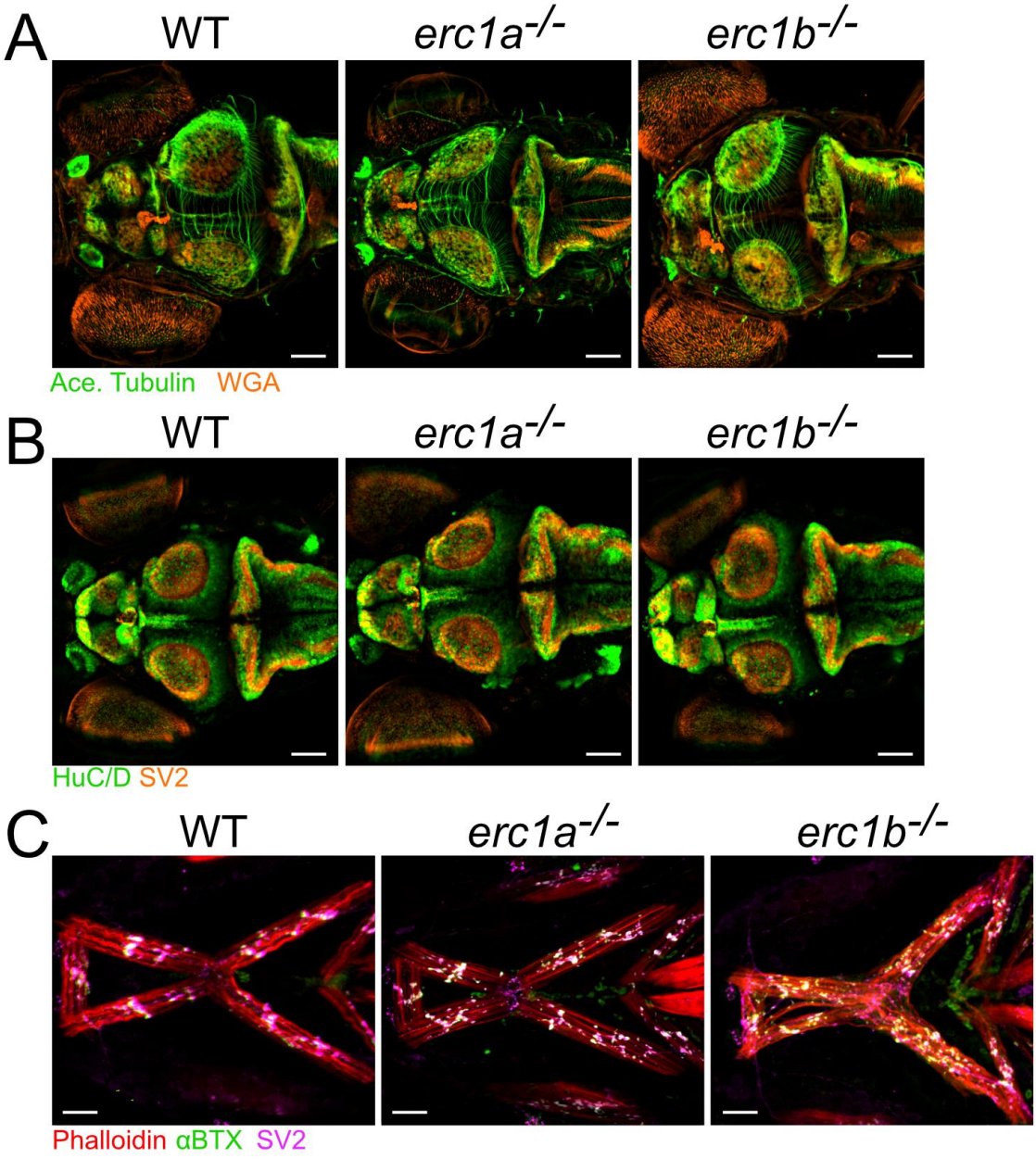

Figure 4.6. Homozygous *erc1a*$^{-/-}$ do not exhibit gross neurologic disruptions
Whole mount IF of 4 dpf WT, *erc1a*$^{-/-}$, and *erc1b*$^{-/-}$ larvae with antibodies against (**A)** acetylated tubulin (green) and wheat germ agglutinin (WGA, orange), (**B)** HuC/D (green) and SV2 (orange), and **(C)** ventral craniofacial neuromuscular junction (phalloidin, red; αBTX, green; SV2, magenta). All images are maximum intensity projections.

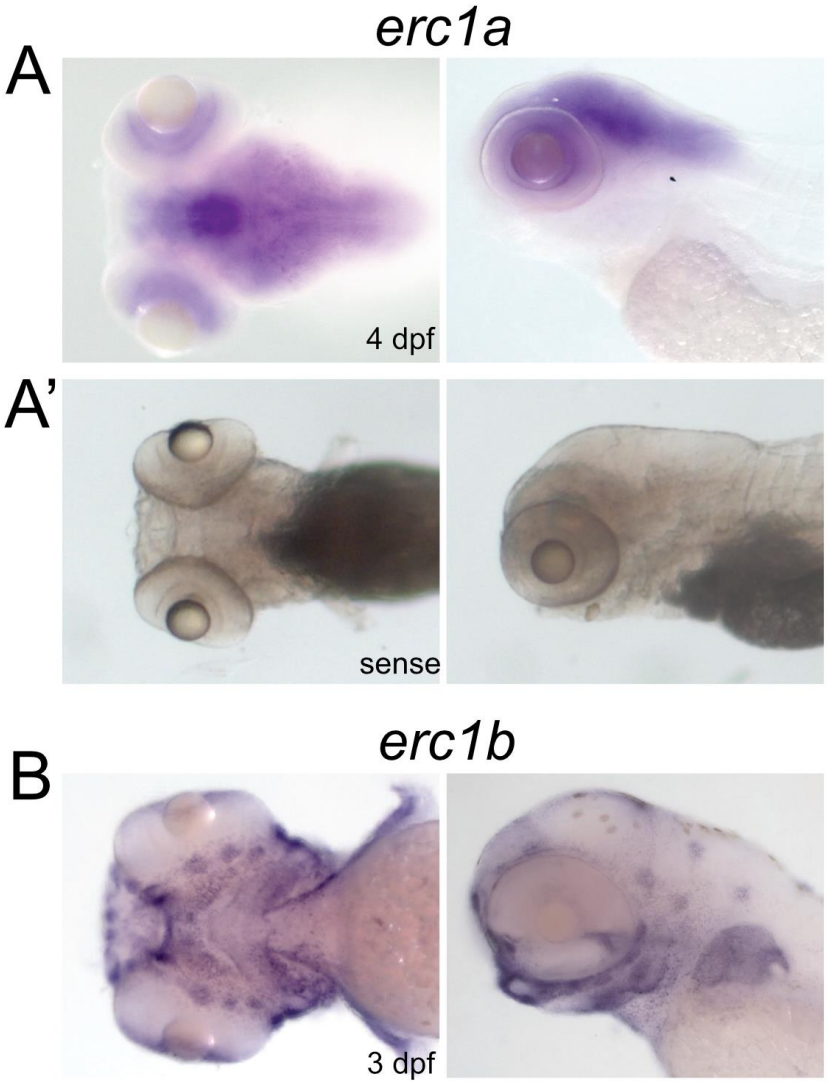

Figure 4.7. *erc1a* is expressed in the brain/retina, *erc1b* is expressed in ventral pharyngeal tissues using in-house made *in situ hybridization* probes
(A) 4 dpf wild type animals express *erc1a* in the brain and in the retina as indicated by anti-sense *erc1a* RNA probe. **(A')** Sense *erc1a* RNA probe. **(B)** 3 dpf wild type animals express *erc1b* in ventral pharyngeal arch tissues.

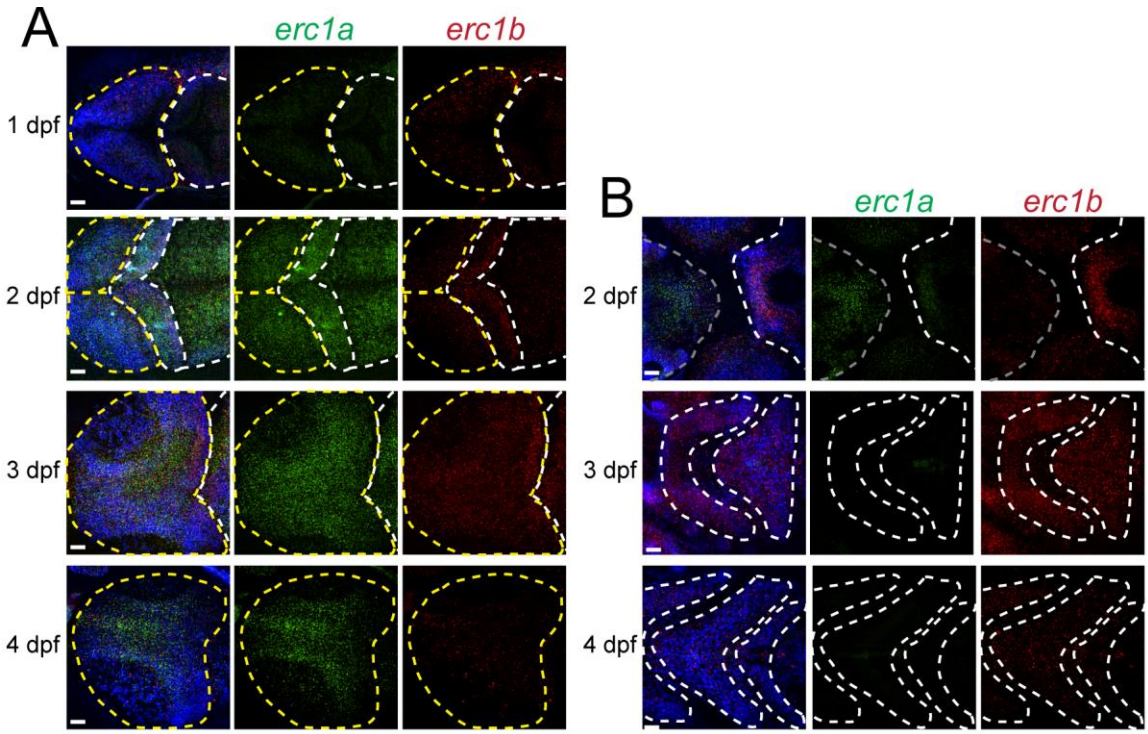

Figure 4.8. *erc1a* and *erc1b* RNAscope probes overlap expression in neuronal tissue, only *erc1b* is expressed in ventral craniofacial tissue.
(A) Dorsal views of RNAscope stained wild type tissues. Yellow dotted lines outline midbrain tissue; white dotted lines outline hindbrain tissue. (**B)** Ventral views of RNAscope stained wild type tissue. Gray outline in 2 dpf sample outlines neuronal tissue; white dotted lines outline pharyngeal cartilage tissue. All images are maximum intensity projections.

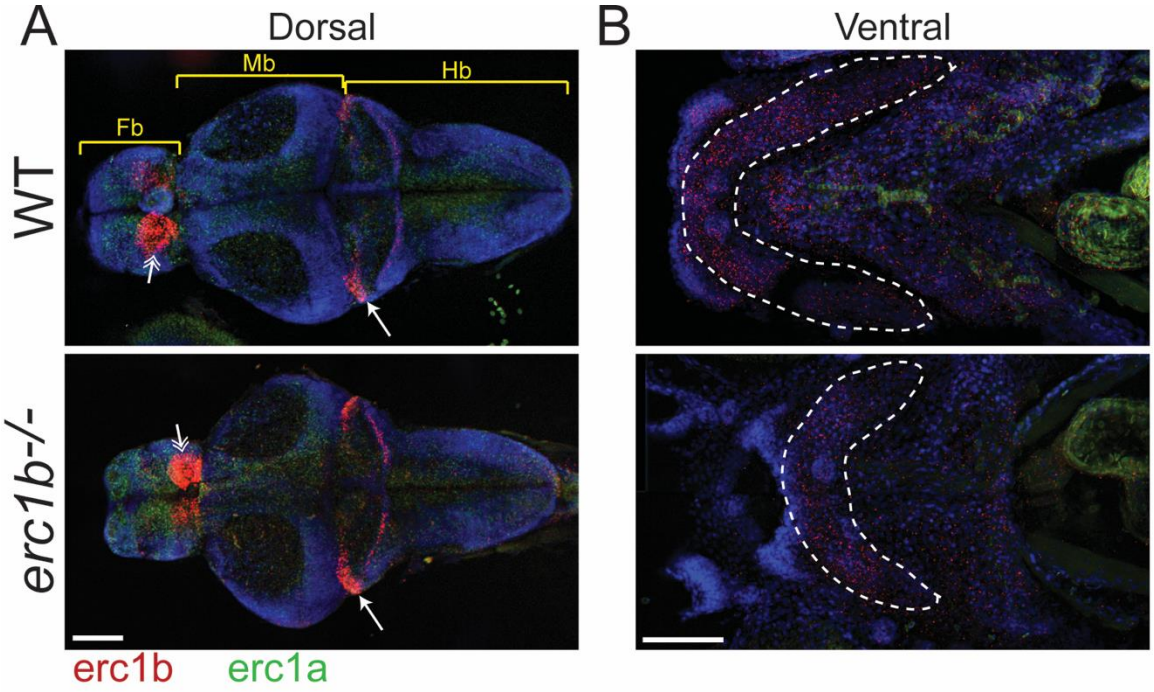

Figure 4.9. *erc1a* and *erc1b* are expressed in *erc1b*$^{-/-}$ larvae.
(A) Dorsal view of 4 dpf brains of RNAscope stained WT and *erc1b*$^{-/-}$ larvae. Yellow brackets signify zebrafish larva brain segments. Highest *erc1b* expression found in cerebellum (arrow) and habenula (double arrow). (**B)** Ventral view of 4 dpf WT and *erc1b*$^{-/-}$ larvae. White dotted lines outline Meckel's cartilage area. All images are maximum intensity projections. Scale bar = 100 μm.

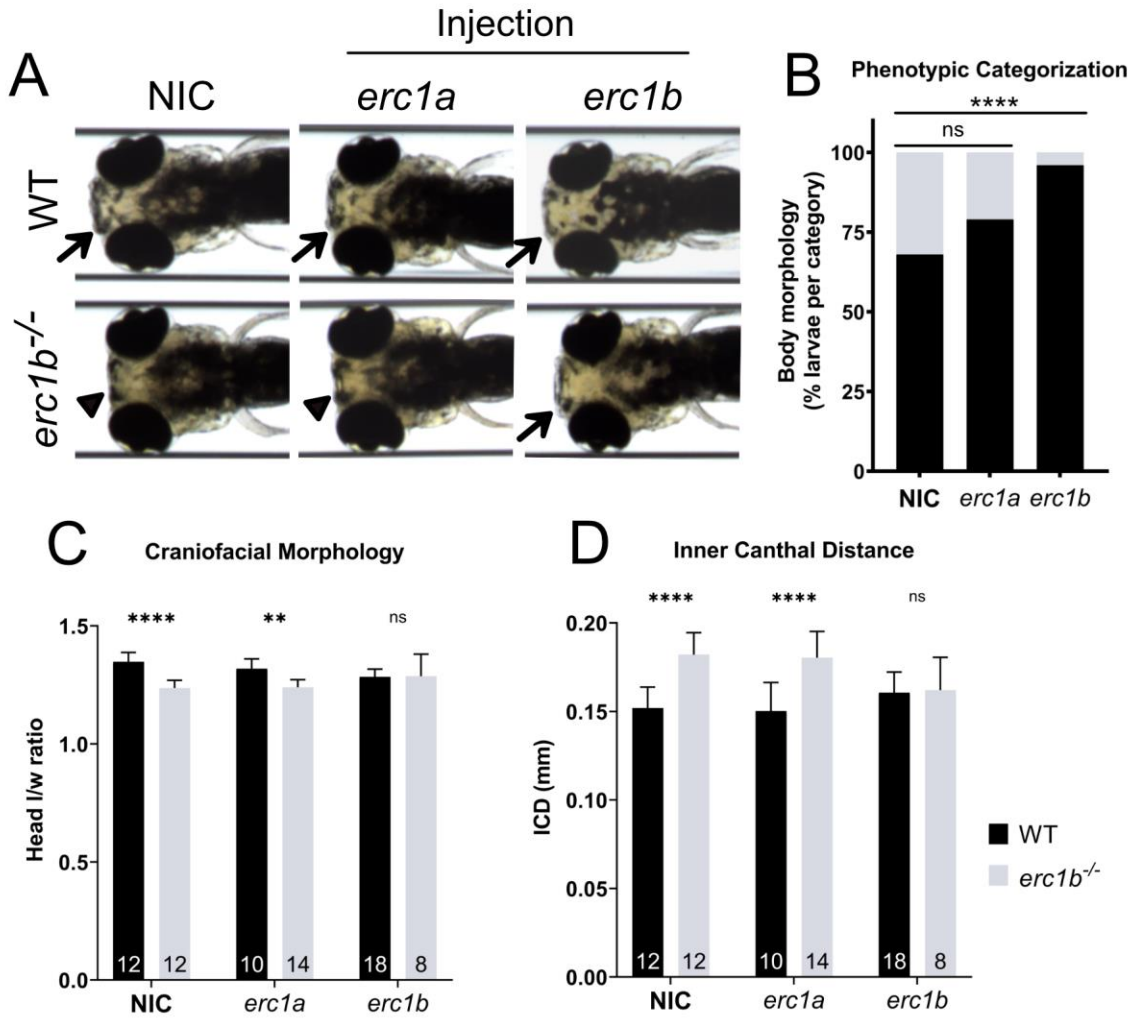

Figure 4.10. Overexpression of *erc1b* but not *erc1a* rescues *erc1b*$^{-/-}$ mutant phenotype

(A) Representative live images of 4 dpf WT and *erc1b*$^{-/-}$ larvae injected with full length *erc1a*, *erc1b* mRNA or non-injected controls (NIC). Arrows indicated protruding jaw, triangle indicate shortened jaw. (**B)** Phenotypic categorization of WT or *erc1b*$^{-/-}$ morphology in control or injected larvae. Chi-square was used for statistical analysis, ****p<0.0001. Quantification of live images including (**C)** head length/width ratio and (**D)** inner canthal distance (ICD). Sample sizes of each genotype/injection indicate at the bottom of each bar. Two-way ANOVA with Sidak's multiple comparison was used for statistical significance, ****p<0.0001, **p<0.01.

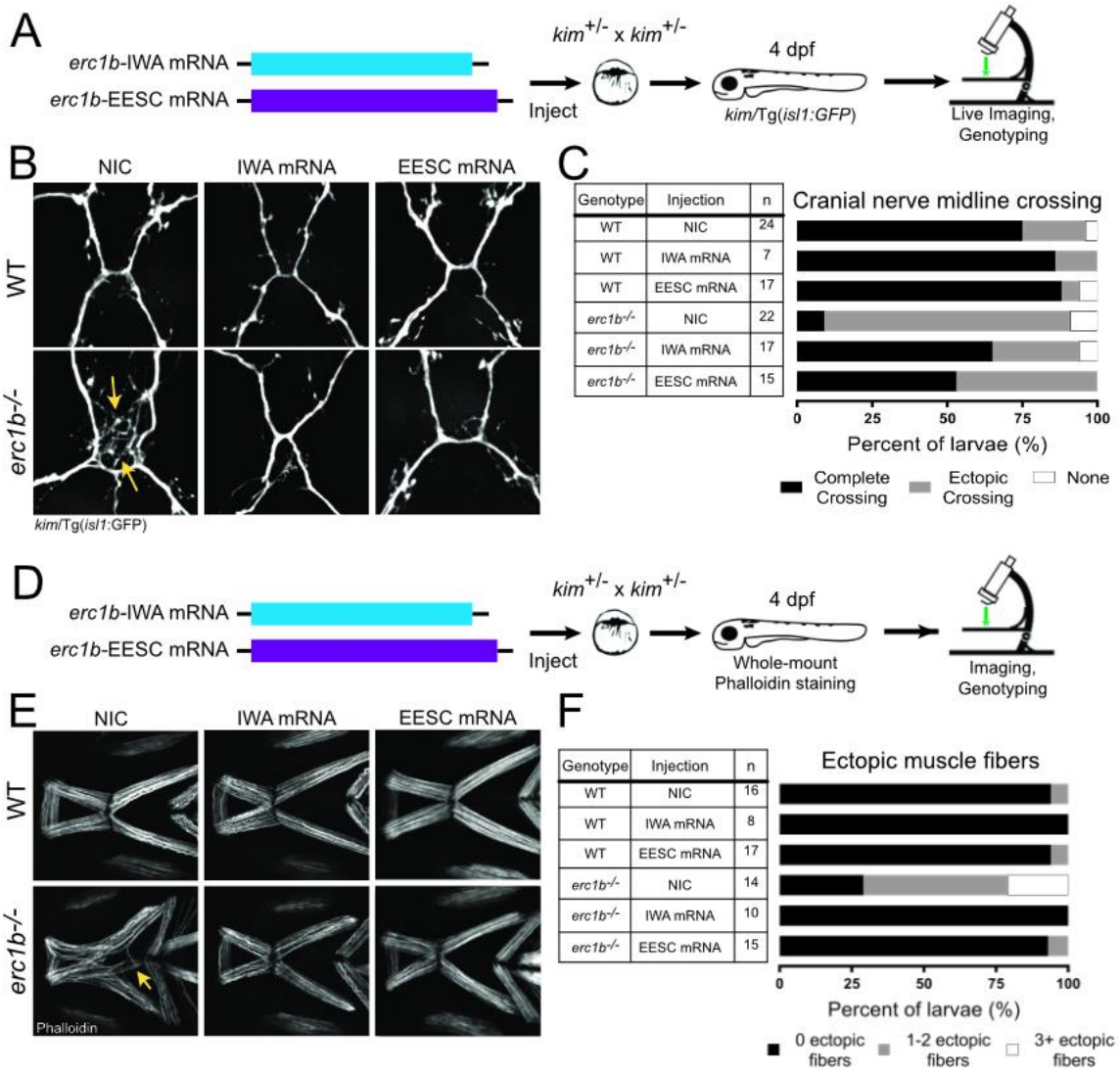

Figure 4.11. Both short and long Erc1b isoforms rescue *erc1b*$^{-/-}$ phenotypes
(**A**) Experimental design of *erc1b* isoform mRNA overexpression and live imaging of transgenic embryos for assessment of cranial nerve midline crossing. (**B**) Representative images of live NIC, *erc1b-IWA* and *erc1b-EESC* mRNA injected WT (top) and *erc1b*$^{-/-}$ /Tg(*isl1*:GFP) larvae (bottom). Yellow arrows indicate ectopic nerve midline crossing in NIC *erc1b*$^{-/-}$ larva. (**C**) Quantification of percent of larvae displaying ectopic cranial nerve midline crossing. Sample sizes (n) for each genotype and injection denoted in the table. (**D**) Experimental design for *erc1b* isoform mRNA injections into single-cell embryos and subsequent analysis of muscle fiber phenotype. (**E**) Representative images of phalloidin-stained muscles in WT (top) and erc1b$^{-/-}$ (bottom) (4 dpf). Yellow arrows indicate ectopic muscle fibers in NIC erc1b$^{-/-}$ larva. (**F**) Quantification of percent of larvae displaying ectopic muscle fibers. Sample sizes (n) for each genotype and injection denoted in the table. All images are maximum intensity projections of craniofacial ventral tissue.

Discussion

Whole-genome duplication events over the course of evolution have provided an immense amount of material for adaptation and diversification of species. The teleost-specific genome duplication event that occurred in a common ancestor millions of years ago resulted in a number of duplicated genes/orthologues in species, including zebrafish (*Danio rerio*). Zebrafish possess over 26,000 protein coding genes, with nearly 70% of those genes having at least one human orthologue (Collins et al., 2012; Howe et al., 2013). While less than half of human genes have a one-to-one relationship with a zebrafish orthologue, a large percentage of human genes are associated with multiple zebrafish genes (average 2.28 zebrafish genes for each human gene), which probably reflects genome duplication (Howe et al., 2013). Zebrafish has become a well-recognized model to understand the biological role of orthologous genes associated with complex and rare human disorders, including skeletal and neurological disorders (Bernier et al., 2014; Golzio et al., 2012; Luderman et al., 2017; Machado and Eames, 2017; Tropepe and Sive, 2003; Van Otterloo et al., 2016). Here, we present a study that takes advantage of genome duplication in zebrafish to investigate the contributions of individual isoforms of human ERC1 to craniofacial morphology and neurologic development to understand the facial and neurologic phenotypes observed in patients with chromosome 12p13.32-33 microdeletions.

The zebrafish genome can be easily manipulated by several gene depletion strategies to investigate gene function, including classical chemical mutagenesis by N-ethyl-N-nitrosourea (ENU), insertional mutagenesis, gene knockdown via morpholino-oligonucleotide injection, and newer techniques such as TALEN, zinc-finger nuclease

(ZFN) and CRISPR/Cas9 (Vacaru et al., 2014). We took a CRISPR/Cas9 targeting approach to produce mutations within *erc1a* to examine the role of the short hERC1 isoform during development. Generating CRISPR/Cas9 genetic mutants in zebrafish is both rapid and efficient (Li et al., 2016). While we initially observed a strong craniofacial phenotype following transient injections of the target gRNA and Cas9 protein, this phenotype was lost in subsequent outcrosses performed to establish stable mutant lines. In accordance with conventional CRISPR/Cas9 mutagenesis in the zebrafish field, we outcrossed three different *erc1a* mutation alleles and did not observe any gross morphological phenotypes in any of the *erc1a* mutant progenies. Observations from several model systems have revealed that reverse genetic mutagenesis techniques, such as TALEN, CRISPR/Cas9, can trigger genetic compensation pathways that result in lost phenotypes that are observed by other gene knockdown approaches (Buglo et al., 2020; De Souza et al., 2006; El-Brolosy and Stainier, 2017; Rossi et al., 2015). The exact mechanisms of genetic compensation are not fully understood, but one possibility is that the upregulation of a paralog gene, such as *erc1b* or another family gene, *erc2*, may compensate for the stable *erc1a* mutations. It is also not clear what triggers genetic compensation in the stable line, but not in the mosaic *erc1a* mutant. In comparison to the stable *erc1a* lines that carried a single mutant allele, the variation in size of the indels in mosaic CRISPR mutants may overwhelm the system, thus leading to an observable mutant phenotype. Another potential explanation is that transient CRISPR injections cause some off-target effects leading to the observed phenotypes that would be diluted in subsequent outcrossing when establishing the stable lines. Relying solely on transient, mosaic mutations is not ideal for investigating *erc1a* function, as we did not observe

consistent phenotypes with each gRNA/Cas9 injection, likely due to the number of and variation of indels that were produced. Future analysis of *erc1a* function in development will include other genetic knockdown approaches, such as morpholino targeting or CRISPR interference (CRISPRi), to try to bypass genetic compensation mechanisms.

For a paralog gene to functionally compensate for another, it would be expected that the tissue expression pattern of the two genes would overlap. Bulk tissue expression databases, such as GTex Portal (https://gtexportal.org/home/), indicate that human *ERC1* is broadly expressed with the highest expression being in the cerebellum and cerebellar hemisphere. Unfortunately, this online database does not encompass all tissues as expression data for bone or skeletal tissues are missing. Our analysis of zebrafish *erc1* paralogs using house-made RNA probes indicated that *erc1a* expression is restricted to the brain and retina, whereas *erc1b* is more broadly expressed in ventral craniofacial tissues. This appears to agree with rodent tissue expression: the long ERC1 isoform is expressed outside of the brain, whereas the shorter ERC1 isoform is expressed primarily within the brain (Liu et al., 2014; Wang et al., 2002). However, we discovered an overlap of expression of the *erc1* paralogs when we used commercially produced RNA probes. Although more work is needed to validate the specificity of these commercial probes, it was surprising to find this overlap in expression between *erc1a* and *erc1b* in neuronal tissue. This overlap in expression would also provide additional rationale to *erc1b* genetically compensating for *erc1a* in the stable CRISPR mutants.

Genetic replacement experiments in *erc1b*$^{-/-}$ mutants provide further evidence that *erc1b* may be functioning in a compensatory manner in *erc1a* CRISPR mutants. While overexpression of *erc1a* did not rescue *erc1b*$^{-/-}$ mutant phenotype, overexpression of

either a long -EESC or short -IWA *erc1b* transcript rescued not only gross morphology, but also the muscular and cranial nerve phenotypes that were previously found to be present in mutants (Luderman, et al. In Revision). These alternatively spliced *erc1b* transcripts were isolated simultaneously during cloning of the full-length *erc1b* coding sequence (D Levic, unpublished), and both transcripts carry the same nonsense mutation identified to cause the *erc1b*$^{-/-}$ mutant phenotype. It was originally thought that only the longer ERC1 transcript contained a C-terminal Rab-binding domain; however, a recent study revealed the shorter ERC1 isoform also has a Rab-binding domain near its C-terminus (Nyitrai et al., 2020). Homologous Rab-binding domains are found in both Erc1b alternatively spliced proteins. Interestingly, there is no identifiable Rab-binding domain found in Erc1a, regardless of having a high sequence homology with the short Erc1b isoform. Together, these findings suggest that not only do the *erc1 paralogs* in zebrafish have nonredundant functions, but also that the functional difference between the paralogs may be due to the Rab-binding function of the Erc1b isoforms. Furthermore, the Rab-binding function of Erc1b is likely critical for craniofacial development as *erc1b* $^{-/-}$ mutants exhibit morphological and cellular phenotypes whereas stable *erc1a* CRISPR mutants did not. Future studies will be needed to fully address the role of Erc1b Rab-binding during the development and morphology of craniofacial tissues.

CHAPTER V

CONCLUDING REMARKS & FUTURE DIRECTIONS

Summary

The research presented here illustrates the utility of animal model studies to identify a novel candidate gene involved in both craniofacial form and function during development. The zebrafish vertebrate model has the ability to combine forward and reverse genetics, *in vivo* imaging, genetic replacement and behavioral analysis to provide a system that is amendable to studying organogenesis at cellular and molecular levels. This principle is demonstrated by the studies detailed in Chapter II, where dysfunction of jaw movement was discovered in a global knockout zebrafish mutant. Further investigation revealed possible cellular phenotypes contributing to this behavior, including craniofacial muscle organization and cranial motor neuron innervation defects. Follow-up studies aimed to investigate the cell-autonomous function of craniofacial muscles and cranial motor nerves during nerve outgrowth, innervation, and neuromuscular junction synaptogenesis. Establishment of cell-specific promoters to drive expression in the craniofacial muscles or cranial motor nerves is detailed in Chapter III. Lastly, taking advantage of zebrafish genome evolution and reverse genetics, paralogous genes were found to perform nonredundant functions during craniofacial development in Chapter IV. The remainder of this chapter discusses the implications and significance of these findings and outlines future lines of investigation.

ERC1 is a candidate gene for human craniofacial dysmorphology and dysfunction

The work detailed in this thesis presents, for the first time, a global knockout of ERC1 in a vertebrate model. ERC1 has been an enigmatic protein of interest for cell and developmental biologists, neuroscientists, and geneticists for years. However, efforts to produce a global knockout in other vertebrate species, has been unfruitful in the past, resulting in embryonic lethality at early developmental stages (Liu et al., 2014; Nyitrai et al., 2020). For this reason, most studies on ERC1 function have relied heavily on conditional knockouts and ex vivo analysis of cells in culture. While these cell culture-based studies cannot be discounted for their efforts in investigating ERC1 subcellular localization and function, they are limited in their ability to determine the effect of ERC1 on gross morphology of a whole tissue or organism during development. This is particularly important because ERC1 is a candidate gene of interest in patients with 12p13.33-32 microdeletions. As such, I propose using the zebrafish *kimble*^{m533}*/erc1b* mutant line for future investigation of related human syndromes and phenotypes.

The *kimble*^{m533}*/erc1b* mutant was originally isolated from a chemical mutagenesis screen to identify mutations disrupting craniofacial development. One of the key distinguishing characteristics of the *kimble* mutant is a small jaw, or micrognathia, which is also a phenotype observed in many 12p13.33-32 microdeletion patients. In addition to the shortened jaw dysmorphology in mutants, we discovered that mutant larvae are unable to move their small jaws as well as wild-type larvae. As discussed in earlier sections, one mechanical contributor to craniofacial morphology is muscle contraction and activity. There are examples in both animal models and patients that provide evidence of muscular defects having significant impact on craniofacial morphology

(Brunt et al., 2015; Shwartz et al., 2013). Spontaneous craniofacial muscle contractions in zebrafish begin as early as 3 dpf, around the time that chondrocytes, which that make up craniofacial cartilage, begin intercalation (Shwartz et al., 2012). Therefore, it is plausible that the craniofacial muscular defects we observed in *erc1b*$^{-/-}$ mutants are directly related to the shortened jaw phenotype, but future experiments would be needed to test this hypothesis. Together, these findings in a zebrafish model of ERC1 function indicate that ERC1 is a candidate gene for both craniofacial morphology and function.

Neurologic deficits, neurodevelopment disorders, and intellectual disability are other hallmark phenotypes associated with 12p13 microdeletions. Investigation of brain size and gross morphology in *erc1b* zebrafish mutants did not reveal any significant defects. However, we did discover a significant defect in trigeminal motor nerve growth into the first pharyngeal arch as well as a fasciculation defect of the cranial motor nerves during muscle innervation. The function of ERC1 in axonal outgrowth has not been well established, apart from a lone study that observed decreased neurite length following ERC1 shRNA knockdown in cultured immature interneurons (Franchi et al., 2016). While most studies on ERC1 function in neurons have focused on neurotransmitter release, my studies and others suggest that ERC1 may play additional roles in neuronal axonal pathways and neuronal circuits. Future studies into possible ERC1 function in axonal growth and connectivity would need to be conducted in an *in vivo* animal model, such as the *erc1b* zebrafish mutant, or in neuronal organoids. These types of studies could provide further insight into the neurologic phenotypes associated with 12p13 microdeletions.

Establishing cell autonomous function of Erc1b in craniofacial tissue is not trivial

Beyond providing insight into the effect of a gene on gross morphology, studying gene function in an *in vivo* animal model allows researchers to examine the function of gene in the context of tissues or multiple cells. However, this can become challenging when trying to distinguish between primary and secondary defects, especially when cells or tissues interact with one another during development. For this reason and others, researchers rely on cell autonomous approaches. In zebrafish, one way to assess cell autonomous function of a gene is by using genome integration of reporters for overexpression in a cell specific manner (Tol2kit system). Our laboratory and others have successfully used the Tol2kit system in zebrafish to assess cell autonomous gene function in chondrocytes and other cells (Berger and Currie, 2013; Eames et al., 2011; Love and Prince, 2015; Melville et al., 2011; Unlu et al., 2020).

As reported here (Chapters III, IV) and elsewhere, *ERC1*/*erc1b* is broadly expressed in multiple tissues, including in the brain and craniofacial tissues. In this thesis, I report that loss of Erc1b in zebrafish results in defects in craniofacial muscle organization and cranial motor nerve growth and innervation. Previous work in the laboratory has shown that *erc1b*$^{-/-}$ mutants also display defects in chondrocyte cell shape and that mosaic overexpression of Erc1b is able to rescue mutant phenotype (D. Levic, unpublished). In the same manner, I developed cell specific Tol2 expression constructs to assesses the cell autonomous function of Erc1b in cranial motor nerves and the craniofacial muscles as described in Chapter III. However, our preliminary findings suggest that mosaic overexpression of Erc1b in either cranial motor neurons or craniofacial muscle fibers was not enough to rescue mutant cellular phenotype. One

potential explanation behind this finding could be that low expression mosaicism of the Tol2kit system is not enough to produce sufficient levels of cellular rescue to generate the desired effect. For example, fasciculation of axons that make up a nerve fiber requires axon-axon interactions to drive axonal growth and pathfinding, and loss of adhesion molecules results in fasciculation defects (Davis et al., 2017; Šmít et al., 2017). Mosaic overexpression of Erc1b in individual cranial motor neurons may not be sufficient to re-establish the axon-axon interactions needed to drive a rescued fasciculation phenotype when the majority of neurons remain *erc1b* deficient. In comparison, the cell autonomous function of Erc1b in a chondrocyte is likely due to chondrocytes relying less so on cell-cell interactions for their development, as the cells are enveloped by extracellular matrix that they produce and secrete themselves. Together, this finding suggests the need to establish stable, non-mosaic Tol2 overexpression lines to assess Erc1b function in cranial motor nerves.

Intercellular interactions may also play a role in the inconclusive mosaic overexpression analysis. As discussed in Chapter III, motor neurons and muscles function cooperatively during neuromuscular junction formation and maturation. As such, preliminary analysis of mosaic overexpression of Erc1b in individual craniofacial muscle fibers in *erc1b*$^{-/-}$ mutants did not rescue acetylcholine receptor field size compared to overexpression in wild-type larvae. This may indicate that Erc1b function is required on both cellular sides of the cranial neuromuscular junction. Ongoing experiments are evaluating neuromuscular junction size in patterning following global genetic replacement of *erc1b*.

This far, we have evaluated cell-specific Erc1b function in three different craniofacial tissues: cartilage, nerve, and muscle. It cannot be overlooked that other tissues or cell types may also be impacted by loss of Erc1b function in the zebrafish. One cell type of interest for future work are the craniofacial tenocytes, which are the tendon producing cells. Loss of Erc1b in zebrafish results in tendon disorganization and ectopic muscle fibers. However, establishing cell autonomous function for Erc1b in tenocytes may run into some of the same issues as discussed above as tenocytes interact with both muscle fibers and chondrocytes, both of which display phenotypes associated with loss of Erc1b function. In summary, while investigating gene function in a global knockout model has many advantages, determining cell-specific or autonomous function *in vivo* can be challenging.

Diverse ERC1 functions are mediated by protein-protein interactions

Historically, ERC1 has been considered to be a scaffold protein that interacts with Rab6 GTPase and functions as modulator of membrane-bound vesicle release in both neuronal and non-neuronal cells. More recent studies of ERC1 have greatly expanded not only ERC1's interacting protein network, but also diversified its functions. These newly discovered ERC1 functions, currently being studied mostly in *in vitro* contexts, would have implications on the function of Erc1b in zebrafish, especially in nerve outgrowth and neuromuscular junction patterning.

Recent evidence has proposed ERC1 as a core component of so called 'plasma membrane associated proteins (PMAPs)', a network of scaffold proteins that functions at the interface between the cytosol and plasma membrane to partition and localize cytoplasmic proteins into discrete condensates near the plasma membrane (Ramella et al.,

2022). Other core PMAP components include known ERC1 interacting proteins, liprin-α and LL5 proteins, among others (Ko et al., 2003; Lansbergen et al., 2006). PMAPs have been shown to be important in a number of cellular processes including focal cell adhesion turnover in migratory cells (Astro et al., 2014; Astro et al., 2016; Franchi et al., 2016), anchoring of microtubules to the cell cortex (Lansbergen et al., 2006), assembly and organization of presynaptic terminals (Mcdonald et al., 2020), degradation of extracellular matrix at invadosomes (Sala et al., 2018), and in the organization of acetylcholine receptor clusters in the postsynaptic muscle fiber (Kishi et al., 2005; Proszynski and Sanes, 2013).

Data from *in vitro* studies examining PMAPs function suggest the need for further investigation into Erc1b interactions with other PMAP components such as liprin-α and LL5β. Perturbation of either of these ERC1 interacting molecules in cultured myotubules resulted acetylcholine receptor clustering defects, similar to the neuromuscular junction defects observed in *erc1b*$^{-/-}$ mutants in Chapter II (Bernadzki et al., 2017; Kishi et al., 2005). PMAPs interact with focal cell adhesion molecules and facilitate adhesion turnover at protrusions of migrating cells and at tips of neurites in immature interneurons (Astro et al., 2016; Franchi et al., 2016; Sala et al., 2019). Knockdown of ERC1 or liprin- α in interneurons resulted in reduced branching and Sholl intersections (Franchi et al., 2016). This finding appears to be in contradiction to our finding that loss of Erc1b in zebrafish results in increased branching and Sholl intersections of cranial motor nerves (Chapter II). This discrepancy may be due to experimental setting where in an *in vivo* experiment signaling cues from other cells or tissues are present but are missing in an *in*

vitro setting. Our study emphasizes the need to perform future investigations into PMAP functions and protein interactions in an *in vivo* animal model system, such as zebrafish.

Future implications and concluding statement

In this dissertation, I utilized a known zebrafish craniofacial morphology mutant to discover new gene roles in craniofacial function using combined genetic and behavioral analyses. The craniofacial biology field has relied heavily on patient phenotypes and animal models to investigate genetic contributions to craniofacial form and function. Future work may consider employing phenome-wide and genome-wide association studies (PheWAS and GWAS) to uncover new gene associations with craniofacial dysmorphology and dysfunction. Excellent recent studies have successfully combined biobank data and electronic health records to inform both researchers and clinicians on the contribution of specific gene to a disease phenome, including cranio-dental phenotypes (Unlu et al., 2019; Unlu et al., 2020). However, computational genetic analysis alone is not sufficient to fully examine gene mechanism. Using combined genetic analysis and animal models like zebrafish can further strengthen associations between patient disease phenotypes and gene functions. These genetic approaches may help provide further insight into the biological and functional consequences of reduced ERC1 expression in patients and expand our basic cell biology knowledge base.

My findings and my proposed future studies will be of interest not only to cell and developmental biologists, but also geneticists and physicians to help understand the pathophysiology that underlie craniofacial abnormalities that impact craniofacial function.

List of other publications

Luderman LN*, Unlu G*****, Knapik EW (2017) 'Chapter Three: Zebrafish Developmental Models of Skeletal Diseases' in Zebrafish at the Interface of Development and Disease Research.
Current Topics in Developmental Biology, 124: 81-124, Edited by Kirsten Sadler Edepli, ISBN: 9780128033081, Academic Press, 10.1016/bs.ctdb.2016.11.004

Abstract: Zebrafish skeleton shares many similarities with human and other vertebrate skeletons. Over the past years the zebrafish model has contributed to understanding basic developmental mechanisms and cellular pathways directing skeletal development and homeostasis. This review will focus on the cell biology of cartilage and bone and how the basic cellular processes within chondrocytes and osteocytes function to assemble the structural frame of a vertebrate body. We will discuss fundamental functions of skeletal cells in production of extracellular matrix (ECM) and cellular activities leading to differentiation of progenitors to mature cells within the organ. We will aim to compare and contrast clinical findings in human skeletal syndromes and zebrafish developmental models to show the utility of zebrafish in unraveling molecular mechanisms of cellular functions necessary to maintain healthy human skeleton.

*co-first author.

BIBLIOGRAPHY

Abdelmoity, A.T., Hall, J.J., Bittel, D.C., Yu, S., 2011. 1.39 Mb inherited interstitial deletion in 12p13.33 associated with developmental delay. Eur J Med Genet 54, 198-203.

Abramyan, J., Richman, J., 2018. Craniofacial development: discoveries made in the chicken embryo. The International journal of developmental biology 62.

Abzhanov, A., Protas, M., Grant, B., Grant, P., Tabin, C., 2004. Bmp4 and morphological variation of beaks in Darwin's finches. Science (New York, N.Y.) 305.

Abzhanov, A., Tabin, C., 2004. Shh and Fgf8 act synergistically to drive cartilage outgrowth during cranial development. Developmental biology 273.

Adam, S., Coetzee, M., Honey, E., 2018. Pena-Shokeir syndrome: current management strategies and palliative care. The application of clinical genetics 11.

Akita, K., Sakaguchi-Kuma, T., Fukino, K., Ono, T., 2019. Masticatory Muscles and Branches of Mandibular Nerve: Positional Relationships Between Various Muscle Bundles and Their Innervating Branches. Anatomical record (Hoboken, N.J. : 2007) 302.

Alfandari, D., Cousin, H., Gaultier, A., Smith, K., White, J., Darribère, T., DeSimone, D., 2001. Xenopus ADAM 13 is a metalloprotease required for cranial neural crest-cell migration. Current biology : CB 11.

Andreeva, V., Connolly, M.H., Stewart-Swift, C., Fraher, D., Burt, J., Cardarelli, J., Yelick, P.C., 2011. Identification of adult mineralized tissue zebrafish mutants. Genesis 49, 360-366.

Asante, E., Hummel, D., Gurung, S., Kassim, Y., Al-Shakarji, N., Palaniappan, K., Sittaramane, V., Chandrasekhar, A., 2021. Defective Neuronal Positioning Correlates With Aberrant Motor Circuit Function in Zebrafish. Frontiers in neural circuits 15.

Astro, V., Chiaretti, S., Magistrati, E., Fivaz, M., de Curtis, I., 2014. Liprin-alpha1, ERC1 and LL5 define polarized and dynamic structures that are implicated in cell migration. J Cell Sci 127, 3862-3876.

Astro, V., Tonoli, D., Chiaretti, S., Badanai, S., Sala, K., Zerial, M., de Curtis, I., 2016. Liprin-α1 and ERC1 control cell edge dynamics by promoting focal adhesion turnover, Sci Rep.

Baker, E., Hinton, L., Callen, D.F., Haan, E.A., Dobbie, A., Sutherland, G.R., 2002. A familial cryptic subtelomeric deletion 12p with variable phenotypic effect. Clin Genet 61, 198-201.

Balice-Gordon, R., Lichtman, J., 1993. In vivo observations of pre- and postsynaptic changes during the transition from multiple to single innervation at developing

neuromuscular junctions. The Journal of neuroscience : the official journal of the Society for Neuroscience 13.

Barik, A., Li, L., Sathyamurthy, A., Xiong, W.-C., Mei, L., 2016. Schwann Cells in Neuromuscular Junction Formation and Maintenance. Journal of Neuroscience 36, 9770-9781.

Barlowe, C., d'Enfert, C., Schekman, R., 1993. Purification and characterization of SAR1p, a small GTP-binding protein required for transport vesicle formation from the endoplasmic reticulum. J Biol Chem 268, 873-879.

Barlowe, C., Schekman, R., 1993. SEC12 encodes a guanine-nucleotide-exchange factor essential for transport vesicle budding from the ER. Nature 365, 347-349.

Barrallo-Gimeno, A., Holzschuh, J., Driever, W., Knapik, E.W., 2004. Neural crest survival and differentiation in zebrafish depends on mont blanc/tfap2a gene function. Development 131, 1463-1477.

Barriga, E., Franze, K., Charras, G., Mayor, R., 2018. Tissue stiffening coordinates morphogenesis by triggering collective cell migration in vivo. Nature 554.

Bendixen, K., Gjørup, H., Baad-Hansen, L., Dahl, H.J., Harsløf, T., Schmidt, M., Langdahl, B., Haubek, D., 2018. Temporomandibular disorders and psychosocial status in osteogenesis imperfecta - a cross-sectional study. BMC oral health 18.

Berendsen, A.D., Olsen, B.R., 2015. Bone development. Bone 80, 14-18.

Berger, J., Currie, P., 2013. 503unc, a small and muscle-specific zebrafish promoter. Genesis (New York, N.Y. : 2000) 51.

Bernadzki, K.M., Gawor, M., Pęziński, M., Mazurek, P., Niewiadomski, P., Rędowicz, M.J., Prószyński, T.J., 2017. Liprin-α-1 is a novel component of the murine neuromuscular junction and is involved in the organization of the postsynaptic machinery. Scientific Reports 7.

Bernier, R., Golzio, C., Xiong, B., Stessman, H.A., Coe, B.P., Penn, O., Witherspoon, K., Gerdts, J., Baker, C., Vulto-van Silfhout, A.T., Schuurs-Hoeijmakers, J.H., Fichera, M., Bosco, P., Buono, S., Alberti, A., Failla, P., Peeters, H., Steyaert, J., Vissers, L., Francescatto, L., Mefford, H.C., Rosenfeld, J.A., Bakken, T., O'Roak, B.J., Pawlus, M., Moon, R., Shendure, J., Amaral, D.G., Lein, E., Rankin, J., Romano, C., de Vries, B.B.A., Katsanis, N., Eichler, E.E., 2014. Disruptive CHD8 mutations define a subtype of autism early in development. Cell 158, 263-276.

Bessell, A., Hooper, L., Shaw, W.C., Reilly, S., Reid, J., Glenny, A.-M., 2011. Feeding interventions for growth and development in infants with cleft lip, cleft palate or cleft lip and palate. Cochrane Database of Systematic Reviews.

Bi, X., Corpina, R.A., Goldberg, J., 2002. Structure of the Sec23/24-Sar1 pre-budding complex of the COPII vesicle coat. Nature 419, 271-277.

Bird, A., Cuntz, H., 2019. Dissecting Sholl Analysis into Its Functional Components. Cell reports 27.

Bourzgui, F., Aghoutan, H., Diouny, S., 2013. Craniomandibular Disorders and Mandibular Reference Position in Orthodontic Treatment. Int J Dent 2013.

Boyadjiev, S.A., Fromme, J.C., Ben, J., Chong, S.S., Nauta, C., Hur, D.J., Zhang, G., Hamamoto, S., Schekman, R., Ravazzola, M., Orci, L., Eyaid, W., 2006. Cranio-lenticulo-sutural dysplasia is caused by a SEC23A mutation leading to abnormal endoplasmic-reticulum-to-Golgi trafficking. Nat Genet 38, 1192-1197.

Brandizzi, F., Barlowe, C., 2013. Organization of the ER-Golgi interface for membrane traffic control. Nat Rev Mol Cell Biol 14, 382-392.

Breik, O., Tivey, D., Umapathysivam, K., Anderson, P., 2016a. Mandibular distraction osteogenesis for the management of upper airway obstruction in children with micrognathia: a systematic review. International journal of oral and maxillofacial surgery 45.

Breik, O., Umapathysivam, K., Tivey, D., Anderson, P., 2016b. Feeding and reflux in children after mandibular distraction osteogenesis for micrognathia: A systematic review. International journal of pediatric otorhinolaryngology 85.

Brugmann, S., Goodnough, L., Gregorieff, A., Leucht, P., ten Berge, D., Fuerer, C., Clevers, H., Nusse, R., Helms, J., 2007. Wnt signaling mediates regional specification in the vertebrate face. Development (Cambridge, England) 134.

Brunt, L., Norton, J., Bright, J., Rayfield, E., Hammond, C., 2015. Finite element modelling predicts changes in joint shape and cell behaviour due to loss of muscle strain in jaw development. Journal of biomechanics 48.

Brunt, L., Skinner, R., Roddy, K., Araujo, N., Rayfield, E., Hammond, C., 2016. Differential effects of altered patterns of movement and strain on joint cell behaviour and skeletal morphogenesis. Osteoarthritis and cartilage 24.

Buglo, E., Sarmiento, E., Martuscelli, N.B., Sant, D.W., Danzi, M.C., Abrams, A.J., Dallman, J.E., Züchner, S., 2020. Genetic compensation in a stable slc25a46 mutant zebrafish: A case for using F0 CRISPR mutagenesis to study phenotypes caused by inherited disease. PLOS ONE 15, e0230566.

Burg, M., Chai, Y., Yao, C., Magee, W., Figueiredo, J., 2016. Epidemiology, Etiology, and Treatment of Isolated Cleft Palate. Frontiers in physiology 7.

Bury, L., Sabo, S., 2011. Coordinated trafficking of synaptic vesicle and active zone proteins prior to synapse formation. Neural development 6.

Buvinic, S., Balanta-Melo, J., Kupczik, K., Vásquez, W., Beato, C., Toro-Ibacache, V., 2021. Muscle-Bone Crosstalk in the Masticatory System: From Biomechanical to Molecular Interactions. Frontiers in endocrinology 11.

Carette, M., Ferguson, M., 1992. The fate of medial edge epithelial cells during palatal fusion in vitro: an analysis by DiI labelling and confocal microscopy. Development (Cambridge, England) 114.

Chandrasekhar, A., 2004. Turning heads: development of vertebrate branchiomotor neurons. Dev Dyn 229, 143-161.

Chandrasekhar, A., Moens, C.B., Warren, J.T., Jr., Kimmel, C.B., Kuwada, J.Y., 1997. Development of branchiomotor neurons in zebrafish. Development 124, 2633-2644.

Chang, H.-P., Tseng, Y.-C., Chang, H.-F., 2006. Treatment of Mandibular Prognathism. Journal of the Formosan Medical Association 105, 781-790.

Chen, J., Galloway, J., 2014. The development of zebrafish tendon and ligament progenitors. Development (Cambridge, England) 141.

Chetty, M., Roberts, T.S., Stephen, L., Beighton, P., 2017. Craniofacial manifestations in osteogenesis imperfecta type III in South Africa. BDJ Open 3.

Chong, H., Young, N., Hu, D., Jeong, J., McMahon, A., Hallgrimsson, B., Marcucio, R., 2012. Signaling by SHH rescues facial defects following blockade in the brain. Developmental dynamics : an official publication of the American Association of Anatomists 241.

Collins, J.E., White, S., Searle, S.M.J., Stemple, D.L., 2012. Incorporating RNA-seq data into the zebrafish Ensembl genebuild. Genome Research 22, 2067-2078.

Compagnucci, C., Martinus, K., Griffin, J., Depew, M., 2021. Programmed Cell Death Not as Sledgehammer but as Chisel: Apoptosis in Normal and Abnormal Craniofacial Patterning and Development. Frontiers in cell and developmental biology 9.

Copic, A., Latham, C.F., Horlbeck, M.A., D'Arcangelo, J.G., Miller, E.A., 2012. ER cargo properties specify a requirement for COPII coat rigidity mediated by Sec13p. Science 335, 1359-1362.

Crump, J., Maves, L., Lawson, N., Weinstein, B., Kimmel, C., 2004. An essential role for Fgfs in endodermal pouch formation influences later craniofacial skeletal patterning. Development (Cambridge, England) 131.

Cuervo, R., Covarrubias, L., 2004. Death is the major fate of medial edge epithelial cells and the cause of basal lamina degradation during palatogenesis. Development (Cambridge, England) 131.

Cuervo, R., Valencia, C., Chandraratna, R., Covarrubias, L., 2002. Programmed cell death is required for palate shelf fusion and is regulated by retinoic acid. Developmental biology 245.

Darabid, H., Perez-Gonzalez, A., Robitaille, R., 2014. Neuromuscular synaptogenesis: coordinating partners with multiple functions. Nature reviews. Neuroscience 15.

Davis, O., Merrison-Hort, R., Soffe, S.R., Borisyuk, R., 2017. Studying the role of axon fasciculation during development in a computational model of the Xenopus tadpole spinal cord. Scientific Reports 7.

De Souza, A., Dai, X., Spencer, A., Reppen, T., Menzie, A., Roesch, P., He, Y., Caguyong, M., Bloomer, S., Herweijer, H., Wolff, J., Hagstrom, J., Lewis, D., Linsley, P., Ulrich, R., 2006. Transcriptional and phenotypic comparisons of Ppara knockout and siRNA knockdown mice. Nucleic acids research 34.

Deguchi-Tawarada, M., Inoue, E., Takao-Rikitsu, E., Inoue, M., Ohtsuka, T., Takai, Y., 2004. CAST2: identification and characterization of a protein structurally related to the presynaptic cytomatrix protein CAST. Genes to cells : devoted to molecular & cellular mechanisms 9.

Deken, S.L., Vincent, R., Hadwiger, G., Liu, Q., Wang, Z.W., Nonet, M.L., 2005. Redundant localization mechanisms of RIM and ELKS in Caenorhabditis elegans. The Journal of neuroscience : the official journal of the Society for Neuroscience 25, 5975-5983.

Diogo, R., Hinits, Y., Hughes, S., 2008. Development of mandibular, hyoid and hypobranchial muscles in the zebrafish: homologies and evolution of these muscles within bony fishes and tetrapods. BMC developmental biology 8.

Dixon, M., Marazita, M., Beaty, T., Murray, J., 2011. Cleft lip and palate: understanding genetic and environmental influences. Nature reviews. Genetics 12.

Dougherty, M., Kamel, G., Grimaldi, M., Gfrerer, L., Shubinets, V., Ethier, R., Hickey, G., Cornell, R.A., Liao, E.C., 2013. Distinct requirements for wnt9a and irf6 in extension and integration mechanisms during zebrafish palate morphogenesis. Development 140, 76-81.

Driever, W., Solnica-Krezel, L., Schier, A.F., Neuhauss, S.C., Malicki, J., Stemple, D.L., Stainier, D.Y., Zwartkruis, F., Abdelilah, S., Rangini, Z., Belak, J., Boggs, C., 1996. A genetic screen for mutations affecting embryogenesis in zebrafish. Development 123, 37-46.

Du, W., Bhojwani, A., Hu, J., 2021. FACEts of mechanical regulation in the morphogenesis of craniofacial structures. International journal of oral science 13.

Duarte, G., Ramos, R., Cardoso, M., 2016. Feeding methods for children with cleft lip and/or palate: a systematic review. Brazilian journal of otorhinolaryngology 82.

Eames, B.F., Yan, Y.L., Swartz, M.E., Levic, D.S., Knapik, E.W., Postlethwait, J.H., Kimmel, C.B., 2011. Mutations in fam20b and xylt1 reveal that cartilage matrix controls timing of endochondral ossification by inhibiting chondrocyte maturation. PLoS Genet 7, e1002246.

El-Brolosy, M.A., Stainier, D.Y.R., 2017. Genetic compensation: A phenomenon in search of mechanisms. PLOS Genetics 13, e1006780.

Faria, R.S., De Oliveira, C.P., Da Costa, M.M., Da S. Rosa, M.T.A., Córdoba, M.S., Pic-Taylor, A., Ferrari, I., De Oliveira, S.F., Mazzeu, J.F., 2016. Concurrent Loss of Heterozygosity and Mosaic Deletion of 12p13.32pter. Cytogenetic and Genome Research 148, 174-178.

Farnsworth, D., Saunders, L., Miller, A., 2020. A single-cell transcriptome atlas for zebrafish development. Developmental biology 459.

Feng, Z., Ko, C., 2008. The role of glial cells in the formation and maintenance of the neuromuscular junction. Annals of the New York Academy of Sciences 1132.

Fisher, S., Jagadeeswaran, P., Halpern, M.E., 2003. Radiographic analysis of zebrafish skeletal defects. Dev Biol 264, 64-76.

Flanagan-Steet, H., Fox, M., Meyer, D., Sanes, J., 2005. Neuromuscular synapses can form in vivo by incorporation of initially aneural postsynaptic specializations. Development (Cambridge, England) 132.

Fontinha, C., Engvall, M., Sjögreen, L., Kiliaridis, S., 2018. Craniofacial morphology and growth in young patients with congenital or childhood onset myotonic dystrophy. European journal of orthodontics 40.

Franchi, S.A., Astro, V., Macco, R., Tonoli, D., Barnier, J.V., Botta, M., de Curtis, I., 2016. Identification of a Protein Network Driving Neuritogenesis of MGE-Derived GABAergic Interneurons. Front Cell Neurosci 10, 289.

Gay, S., Muller, P.K., Lemmen, C., Remberger, K., Matzen, K., Kuhn, K., 1976. Immunohistological study on collagen in cartilage-bone metamorphosis and degenerative osteoarthrosis. Klin Wochenschr 54, 969-976.

Geiger, B., Bershadsky, A., Pankov, R., Yamada, K., 2001. Transmembrane crosstalk between the extracellular matrix--cytoskeleton crosstalk. Nature reviews. Molecular cell biology 2.

Geiger, M., Schoenebeck, J.J., Schneider, R.A., Schmidt, M.J., Fischer, M.S., Sánchez-Villagra, M.R., 2021. Exceptional Changes in Skeletal Anatomy under Domestication: The Case of Brachycephaly. Integrative Organismal Biology 3.

Glasauer, S.M.K., Neuhauss, S.C.F., 2014. Whole-genome duplication in teleost fishes and its evolutionary consequences. Molecular Genetics and Genomics 289, 1045-1060.

Golzio, C., Willer, J., Talkowski, M.E., Oh, E.C., Taniguchi, Y., Jacquemont, S., Reymond, A., Sun, M., Sawa, A., Gusella, J.F., Kamiya, A., Beckmann, J.S., Katsanis, N., 2012. KCTD13 is a major driver of mirrored neuroanatomical phenotypes of the 16p11.2 copy number variant. Nature 485, 363-367.

Gong, Y., Mo, C., Fraser, S., 2004. Planar cell polarity signalling controls cell division orientation during zebrafish gastrulation. Nature 430.

Goody, M.F., Carter, E.V., Kilroy, E.A., Maves, L., Henry, C.A., 2017. "Muscling" Throughout Life: Integrating Studies of Muscle Development, Homeostasis, and Disease in Zebrafish. Curr Top Dev Biol 124, 197-234.

Granero-Moltó, F., Sarmah, S., O'Rear, L., Spagnoli, A., Abrahamson, D., Saus, J., Hudson, B., Knapik, E., 2008. Goodpasture antigen-binding protein and its spliced variant, ceramide transfer protein, have different functions in the modulation of apoptosis during zebrafish development. The Journal of biological chemistry 283.

Grant, P., Moens, C., 2010. The neuroepithelial basement membrane serves as a boundary and a substrate for neuron migration in the zebrafish hindbrain. Neural development 5.

Grenier, J., Teillet, M., Grifone, R., Kelly, R., Duprez, D., 2009. Relationship between neural crest cells and cranial mesoderm during head muscle development. PloS one 4.

Grigoriev, I., Splinter, D., Keijzer, N., Wulf, P.S., Demmers, J., Ohtsuka, T., Modesti, M., Maly, I.V., Grosveld, F., Hoogenraad, C.C., Akhmanova, A., 2007. Rab6 regulates transport and targeting of exocytotic carriers. Dev Cell 13, 305-314.

Gross-Thebing, T., 2020. RNAscope™ Multiplex Detection in Zebrafish, Methods in Molecular Biology. Springer US, pp. 195-202.

Gross-Thebing, T., Paksa, A., Raz, E., 2014. Simultaneous high-resolution detection of multiple transcripts combined with localization of proteins in whole-mount embryos. BMC Biology 12.

Gurniak, C., Perlas, E., Witke, W., 2005. The actin depolymerizing factor n-cofilin is essential for neural tube morphogenesis and neural crest cell migration. Developmental biology 278.

Guthrie, S., 2007. Patterning and axon guidance of cranial motor neurons. Nat Rev Neurosci 8, 859-871.

Hall, B., Herring, S., 1990. Paralysis and growth of the musculoskeletal system in the embryonic chick. Journal of morphology 206.

Hall, J., 2014. Arthrogryposis (multiple congenital contractures): diagnostic approach to etiology, classification, genetics, and general principles. European journal of medical genetics 57.

Han, J.Y., Park, J., 2021. Variable Phenotypes of Epilepsy, Intellectual Disability, and Schizophrenia Caused by 12p13.33–p13.32 Terminal Microdeletion in a Korean Family: A Case Report and Literature Review. Genes 12, 1001.

Harris, A., 1981. Embryonic growth and innervation of rat skeletal muscles. III. Neural regulation of junctional and extra-junctional acetylcholine receptor clusters. Philosophical transactions of the Royal Society of London. Series B, Biological sciences 293.

Hassan, M., Kaler, H., Zhang, B., Cox, T., Young, N., Jheon, A., 2020. Effects of Multi-Generational Soft Diet Consumption on Mouse Craniofacial Morphology. Frontiers in physiology 11.

Held, R., Kaeser, P., 2018. ELKS active zone proteins as multitasking scaffolds for secretion. Open biology 8.

Held, R.G., Liu, C., Kaeser, P.S., 2016. ELKS controls the pool of readily releasable vesicles at excitatory synapses through its N-terminal coiled-coil domains. Elife 5.

Hernandez, L.P., 2002. Functional Morphology and Developmental Biology of Zebrafish: Reciprocal Illumination from an Unlikely Couple. Integrative and Comparative Biology 42, 222-231.

Hida, Y., Ohtsuka, T., 2010. CAST and ELKS proteins: structural and functional determinants of the presynaptic active zone. Journal of biochemistry 148, 131-137.

Higashijima, S., Hotta, Y., Okamoto, H., 2000. Visualization of cranial motor neurons in live transgenic zebrafish expressing green fluorescent protein under the control of the islet-1 promoter/enhancer. J Neurosci 20, 206-218.

Hinits, Y., Williams, V., Sweetman, D., Donn, T., Ma, T., Moens, C., Hughes, S., 2011. Defective cranial skeletal development, larval lethality and haploinsufficiency in Myod mutant zebrafish. Developmental biology 358.

Houssin, N., Martin, J., Coppola, V., Yoon, S., Plageman , T., 2020. Formation and contraction of multicellular actomyosin cables facilitate lens placode invagination. Developmental biology 462.

Howe, K., Clark, M.D., Torroja, C.F., Torrance, J., Berthelot, C., Muffato, M., Collins, J.E., Humphray, S., McLaren, K., Matthews, L., McLaren, S., Sealy, I., Caccamo, M., Churcher, C., Scott, C., Barrett, J.C., Koch, R., Rauch, G.J., White, S., Chow, W., Kilian, B., Quintais, L.T., Guerra-Assuncao, J.A., Zhou, Y., Gu, Y., Yen, J., Vogel, J.H., Eyre, T., Redmond, S., Banerjee, R., Chi, J., Fu, B., Langley, E., Maguire, S.F., Laird, G.K., Lloyd, D., Kenyon, E., Donaldson, S., Sehra, H., Almeida-King, J., Loveland, J., Trevanion, S., Jones, M., Quail, M., Willey, D., Hunt, A., Burton, J., Sims, S., McLay, K., Plumb, B., Davis, J., Clee, C., Oliver, K., Clark, R., Riddle, C., Elliot, D., Threadgold, G., Harden, G., Ware, D., Begum, S., Mortimore, B., Kerry, G., Heath, P., Phillimore, B., Tracey, A., Corby, N., Dunn, M., Johnson, C., Wood, J., Clark, S., Pelan,

S., Griffiths, G., Smith, M., Glithero, R., Howden, P., Barker, N., Lloyd, C., Stevens, C., Harley, J., Holt, K., Panagiotidis, G., Lovell, J., Beasley, H., Henderson, C., Gordon, D., Auger, K., Wright, D., Collins, J., Raisen, C., Dyer, L., Leung, K., Robertson, L., Ambridge, K., Leongamornlert, D., McGuire, S., Gilderthorp, R., Griffiths, C., Manthravadi, D., Nichol, S., Barker, G., Whitehead, S., Kay, M., Brown, J., Murnane, C., Gray, E., Humphries, M., Sycamore, N., Barker, D., Saunders, D., Wallis, J., Babbage, A., Hammond, S., Mashreghi-Mohammadi, M., Barr, L., Martin, S., Wray, P., Ellington, A., Matthews, N., Ellwood, M., Woodmansey, R., Clark, G., Cooper, J., Tromans, A., Grafham, D., Skuce, C., Pandian, R., Andrews, R., Harrison, E., Kimberley, A., Garnett, J., Fosker, N., Hall, R., Garner, P., Kelly, D., Bird, C., Palmer, S., Gehring, I., Berger, A., Dooley, C.M., Ersan-Urun, Z., Eser, C., Geiger, H., Geisler, M., Karotki, L., Kirn, A., Konantz, J., Konantz, M., Oberlander, M., Rudolph-Geiger, S., Teucke, M., Lanz, C., Raddatz, G., Osoegawa, K., Zhu, B., Rapp, A., Widaa, S., Langford, C., Yang, F., Schuster, S.C., Carter, N.P., Harrow, J., Ning, Z., Herrero, J., Searle, S.M., Enright, A., Geisler, R., Plasterk, R.H., Lee, C., Westerfield, M., de Jong, P.J., Zon, L.I., Postlethwait, J.H., Nusslein-Volhard, C., Hubbard, T.J., Roest Crollius, H., Rogers, J., Stemple, D.L., 2013. The zebrafish reference genome sequence and its relationship to the human genome. Nature 496, 498-503.

Hu, D., Marcucio, R., 2009. Unique organization of the frontonasal ectodermal zone in birds and mammals. Developmental biology 325.

Hu, D., Marcucio, R., Helms, J., 2003. A zone of frontonasal ectoderm regulates patterning and growth in the face. Development (Cambridge, England) 130.

Huijbers, M.G., Lipka, A.F., Potman, M., Hensbergen, P.J., Titulaer, M.J., Niks, E.H., van der Maarel, S.M., Klooster, R., Verschuuren, J.J., 2013. Antibodies to active zone protein ERC1 in Lambert-Eaton myasthenic syndrome. Hum Immunol 74, 849-851.

Huycke, T., Eames, B., Kimmel, C., 2012. Hedgehog-dependent proliferation drives modular growth during morphogenesis of a dermal bone. Development (Cambridge, England) 139.

Ingold, E., Vom Berg-Maurer, C., Burckhardt, C., Lehnherr, A., Rieder, P., Keller, P., Stelzer, E., Greber, U., Neuhauss, S., Gesemann, M., 2015. Proper migration and axon outgrowth of zebrafish cranial motoneuron subpopulations require the cell adhesion molecule MDGA2A. Biology open 4.

Inoue, E., Deguchi-Tawarada, M., Takao-Rikitsu, E., Inoue, M., Kitajima, I., Ohtsuka, T., Takai, Y., 2006. ELKS, a protein structurally related to the active zone protein CAST, is involved in Ca2+-dependent exocytosis from PC12 cells. Genes Cells 11, 659-672.

Isola, G., Anastasi, G., Matarese, G., Williams, R., Cutroneo, G., Bracco, P., Piancino, M., 2018. Functional and molecular outcomes of the human masticatory muscles. Oral diseases 24.

Iwase, M., Ohashi, M., Tachibana, H., Toyoshima, T., Nagumo, M., 2006. Bite force, occlusal contact area and masticatory efficiency before and after orthognathic surgical

correction of mandibular prognathism. International journal of oral and maxillofacial surgery 35.

Jin, J., Ding, J., 2006. Analysis of cell migration, transdifferentiation and apoptosis during mouse secondary palate fusion. Development (Cambridge, England) 133.

Jing, L., Gordon, L., Shtibin, E., Granato, M., 2010. Temporal and spatial requirements of unplugged/MuSK function during zebrafish neuromuscular development. PloS one 5.

Jones, N., Lynn, M., Gaudenz, K., Sakai, D., Aoto, K., Rey, J., Glynn, E., Ellington, L., Du, C., Dixon, J., Dixon, M., Trainor, P., 2008. Prevention of the neurocristopathy Treacher Collins syndrome through inhibition of p53 function. Nature medicine 14.

Juranek, J., Mukherjee, K., Rickmann, M., Martens, H., Calka, J., Sudhof, T.C., Jahn, R., 2006. Differential expression of active zone proteins in neuromuscular junctions suggests functional diversification. Eur J Neurosci 24, 3043-3052.

Kaeser, P.S., Deng, L., Chavez, A.E., Liu, X., Castillo, P.E., Sudhof, T.C., 2009. ELKS2alpha/CAST deletion selectively increases neurotransmitter release at inhibitory synapses. Neuron 64, 227-239.

Kamel, G., Hoyos, T., Rochard, L., Dougherty, M., Kong, Y., Tse, W., Shubinets, V., Grimaldi, M., Liao, E., 2013. Requirement for frzb and fzd7a in cranial neural crest convergence and extension mechanisms during zebrafish palate and jaw morphogenesis. Developmental biology 381.

Kanzaki, H., Wada, S., Kumazawa, M., Yamada, Y., Sudo, T., Ozawa, E., Seko, T., Akaike, S., Murakami, M., Oikawa, T., Okumura, S., Nakamura, Y., Tomonari, H., 2019. Mandibular prognathism attenuates brain blood flow induced by chewing. Scientific Reports 9.

Katzel, E., Basile, P., Koltz, P., Marcus, J., Girotto, J., 2009. Current surgical practices in cleft care: cleft palate repair techniques and postoperative care. Plastic and reconstructive surgery 124.

Kaucka, M., Ivashkin, E., Gyllborg, D., Zikmund, T., Tesarova, M., Kaiser, J., Xie, M., Petersen, J., Pachnis, V., Nicolis, S., Yu, T., Sharpe, P., Arenas, E., Brismar, H., Blom, H., Clevers, H., Suter, U., Chagin, A., Fried, K., Hellander, A., Adameyko, I., 2016. Analysis of neural crest-derived clones reveals novel aspects of facial development. Science advances 2.

Kaucka, M., Zikmund, T., Tesarova, M., Gyllborg, D., Hellander, A., Jaros, J., Kaiser, J., Petersen, J., Szarowska, B., Newton, P., Dyachuk, V., Li, L., Qian, H., Johansson, A., Mishina, Y., Currie, J., Tanaka, E., Erickson, A., Dudley, A., Brismar, H., Southam, P., Coen, E., Chen, M., Weinstein, L., Hampl, A., Arenas, E., Chagin, A., Fried, K., Adameyko, I., 2017. Oriented clonal cell dynamics enables accurate growth and shaping of vertebrate cartilage. eLife 6.

Kawabe, H., Mitkovski, M., Kaeser, P.S., Hirrlinger, J., Opazo, F., Nestvogel, D., Kalla, S., Fejtova, A., Verrier, S.E., Bungers, S.R., Cooper, B.H., Varoqueaux, F., Wang, Y., Nehring, R.B., Gundelfinger, E.D., Rosenmund, C., Rizzoli, S.O., Sudhof, T.C., Rhee, J.S., Brose, N., 2017. ELKS1 localizes the synaptic vesicle priming protein bMunc13-2 to a specific subset of active zones. J Cell Biol 216, 1143-1161.

Ke, F., Vanyai, H., Cowan, A., Delbridge, A., Whitehead, L., Grabow, S., Czabotar, P., Voss, A., Strasser, A., 2018. Embryogenesis and Adult Life in the Absence of Intrinsic Apoptosis Effectors BAX, BAK, and BOK. Cell 173.

Kiefer, J., 2005. Planar cell polarity: heading in the right direction. Developmental dynamics : an official publication of the American Association of Anatomists 233.

Kiliaridis, S., Katsaros, C., 1998. The effects of myotonic dystrophy and Duchenne muscular dystrophy on the orofacial muscles and dentofacial morphology. Acta odontologica Scandinavica 56.

Kim, N., Burden, S.J., 2007. MuSK controls where motor axons grow and form synapses. Nature Neuroscience 11, 19-27.

Kim, N., Stiegler, A., Cameron, T., Hallock, P., Gomez, A., Huang, J., Hubbard, S., Dustin, M., Burden, S., 2008. Lrp4 is a receptor for Agrin and forms a complex with MuSK. Cell 135.

Kimmel, C., Miller, C., Moens, C., 2001. Specification and morphogenesis of the zebrafish larval head skeleton. Developmental biology 233.

Kimmel, C.B., Ballard, W.W., Kimmel, S.R., Ullmann, B., Schilling, T.F., 1995a. Stages of embryonic development of the zebrafish. Dev Dyn 203, 253-310.

Kimmel, C.B., Ballard, W.W., Kimmel, S.R., Ullmann, B., Schilling, T.F., 1995b. Stages of embryonic development of the zebrafish. Developmental Dynamics 203, 253-310.

Kimmel, C.B., Miller, C.T., Kruze, G., Ullmann, B., BreMiller, R.A., Larison, K.D., Snyder, H.C., 1998. The shaping of pharyngeal cartilages during early development of the zebrafish. Dev Biol 203, 245-263.

Kishi, M., Kummer, T., Eglen, S., Sanes, J., 2005. LL5beta: a regulator of postsynaptic differentiation identified in a screen for synaptically enriched transcripts at the neuromuscular junction. The Journal of cell biology 169.

Kittel, R.J., Wichmann, C., Rasse, T.M., Fouquet, W., Schmidt, M., Schmid, A., Wagh, D.A., Pawlu, C., Kellner, R.R., Willig, K.I., Hell, S.W., Buchner, E., Heckmann, M., Sigrist, S.J., 2006. Bruchpilot promotes active zone assembly, Ca2+ channel clustering, and vesicle release. Science (New York, N.Y.) 312, 1051-1054.

Knapik, E.W., 2000. ENU mutagenesis in zebrafish--from genes to complex diseases. Mamm Genome 11, 511-519.

Ko, J., Na, M., Kim, S., Lee, J.R., Kim, E., 2003. Interaction of the ERC family of RIM-binding proteins with the liprin-alpha family of multidomain proteins. J Biol Chem 278, 42377-42385.

Kobayashi, T., Honma, K., Shingaki, S., Nakajima, T., 2001. Changes in masticatory function after orthognathic treatment in patients with mandibular prognathism. British Journal of Oral and Maxillofacial Surgery 39, 260-265.

Koolstra, J., van Eijden, T., 1997. Dynamics of the human masticatory muscles during a jaw open-close movement. Journal of biomechanics 30.

Korfage, J., Koolstra, J., Langenbach, G., van Eijden, T., 2005. Fiber-type composition of the human jaw muscles--(part 2) role of hybrid fibers and factors responsible for inter-individual variation. Journal of dental research 84.

Kwan, K.M., Fujimoto, E., Grabher, C., Mangum, B.D., Hardy, M.E., Campbell, D.S., Parant, J.M., Yost, H.J., Kanki, J.P., Chien, C.B., 2007. The Tol2kit: a multisite gateway-based construction kit for Tol2 transposon transgenesis constructs. Dev Dyn 236, 3088-3099.

Lane, J., Yumoto, K., Azhar, M., Ninomiya-Tsuji, J., Inagaki, M., Hu, Y., Deng, C., Kim, J., Mishina, Y., Kaartinen, V., 2015. Tak1, Smad4 and Trim33 redundantly mediate TGF-β3 signaling during palate development. Developmental biology 398.

Lang, M.R., Lapierre, L.A., Frotscher, M., Goldenring, J.R., Knapik, E.W., 2006. Secretory COPII coat component Sec23a is essential for craniofacial chondrocyte maturation. Nat Genet 38, 1198-1203.

Lansbergen, G., Grigoriev, I., Mimori-Kiyosue, Y., Ohtsuka, T., Higa, S., Kitajima, I., Demmers, J., Galjart, N., Houtsmuller, A.B., Grosveld, F., Akhmanova, A., 2006. CLASPs attach microtubule plus ends to the cell cortex through a complex with LL5beta. Dev Cell 11, 21-32.

Larson, T., Gordon, T., Lau, H., Parichy, D., 2010. Defective adult oligodendrocyte and Schwann cell development, pigment pattern, and craniofacial morphology in puma mutant zebrafish having an alpha tubulin mutation. Developmental biology 346.

Le Pabic, P., Ng, C., Schilling, T., 2014. Fat-Dachsous signaling coordinates cartilage differentiation and polarity during craniofacial development. PLoS genetics 10.

LeClair, E., Mui, S., Huang, A., Topczewska, J., Topczewski, J., 2009. Craniofacial skeletal defects of adult zebrafish Glypican 4 (knypek) mutants. Developmental dynamics : an official publication of the American Association of Anatomists 238.

Leyser, M., Dias, B.L., Coelho, A.L., Vasconcelos, M., Nascimento, O.J.M., 2016. 12p deletion spectrum syndrome: a new case report reinforces the evidence regarding the potential relationship to autism spectrum disorder and related developmental impairments. Molecular Cytogenetics 9.

Li, M., Zhao, L., Page-McCaw, P.S., Chen, W., 2016. Zebrafish Genome Engineering Using the CRISPR-Cas9 System. Trends Genet 32, 815-827.

Li, R., Gundersen, G.G., 2008. Beyond polymer polarity: how the cytoskeleton builds a polarized cell. Nature Reviews Molecular Cell Biology 9, 860-873.

Li, S.W., Prockop, D.J., Helminen, H., Fassler, R., Lapvetelainen, T., Kiraly, K., Peltarri, A., Arokoski, J., Lui, H., Arita, M., et al., 1995. Transgenic mice with targeted inactivation of the Col2 alpha 1 gene for collagen II develop a skeleton with membranous and periosteal bone but no endochondral bone. Genes Dev 9, 2821-2830.

Lin, S., Landmann, L., Ruegg, M.A., Brenner, H.R., 2008. The Role of Nerve- versus Muscle-Derived Factors in Mammalian Neuromuscular Junction Formation. Journal of Neuroscience 28, 3333-3340.

Lin, W., Burgess, R.W., Dominguez, B., Pfaff, S.L., Sanes, J.R., Lee, K.-F., 2001. Distinct roles of nerve and muscle in postsynaptic differentiation of the neuromuscular synapse. Nature 410, 1057-1064.

Liu, C., Bickford, L.S., Held, R.G., Nyitrai, H., Sudhof, T.C., Kaeser, P.S., 2014. The active zone protein family ELKS supports Ca2+ influx at nerve terminals of inhibitory hippocampal neurons. The Journal of neuroscience : the official journal of the Society for Neuroscience 34, 12289-12303.

Liu, D., Wang, W., Melville, D., Cha, Y., Yin, Z., Issaeva, N., Knapik, E., Yarbrough, W., 2011. Tumor suppressor Lzap regulates cell cycle progression, doming, and zebrafish epiboly. Developmental dynamics : an official publication of the American Association of Anatomists 240.

Liu, N., Troconis, E., Kalmar, L., Price, D., Wright, H., Adams, V., Sargan, D., Ladlow, J., 2017a. Conformational risk factors of brachycephalic obstructive airway syndrome (BOAS) in pugs, French bulldogs, and bulldogs. PloS one 12.

Liu, P., Ma, S., Zhang, H., Liu, C., Lu, Y., Chen, L., Qin, C., 2017b. Specific ablation of mouse Fam20C in cells expressing type I collagen leads to skeletal defects and hypophosphatemia. Scientific Reports 7.

Liu, S., Narumi, R., Ikeda, N., Morita, O., Tasaki, J., 2020. Chemical-induced craniofacial anomalies caused by disruption of neural crest cell development in a zebrafish model. Developmental Dynamics 249, 794-815.

Liu, W., Selever, J., Murali, D., Sun, X., Brugger, S., Ma, L., Schwartz, R., Maxson, R., Furuta, Y., Martin, J., 2005. Threshold-specific requirements for Bmp4 in mandibular development. Developmental biology 283.

Love, C.E., Prince, V.E., 2015. Rest represses maturation within migrating facial branchiomotor neurons. Dev Biol 401, 220-235.

Lu, J., Peatman, E., Tang, H., Lewis, J., Liu, Z., 2012. Profiling of gene duplication patterns of sequenced teleost genomes: evidence for rapid lineage-specific genome expansion mediated by recent tandem duplications. BMC Genomics 13, 246.

Luderman, L., Unlu, G., Knapik, E., 2017. Zebrafish Developmental Models of Skeletal Diseases. Current Topics in Developmental Biology.

Lumsden, A., Sprawson, N., Graham, A., 1991. Segmental origin and migration of neural crest cells in the hindbrain region of the chick embryo. Development (Cambridge, England) 113.

Lüchinger, A.B., Hadders-Algra, M., Van Kan, C.M., De Vries, J.I.P., 2008. Fetal Onset of General Movements. Pediatric Research 63, 191-195.

Macdonald, A.H., Rodriguez, L., Acena, I., Martinez-Fernandez, M.L., Sanchez-Izquierdo, D., Zuazo, E., Martinez-Frias, M.L., 2010. Subtelomeric deletion of 12p: Description of a third case and review. Am J Med Genet A 152a, 1561-1566.

Machado, R.G., Eames, B.F., 2017. Using Zebrafish to Test the Genetic Basis of Human Craniofacial Diseases. J Dent Res 96, 1192-1199.

Mameli, C., Zichichi, G., Mahmood, N., Elalaoui, S., Mirza, A., Dharmaraj, P., Burrone, M., Cattaneo, E., Sheth, J., Gandhi, A., Kochar, G., Alkuraya, F., Kabra, M., Mercurio, G., Zuccotti, G., 2020. Natural history of non-lethal Raine syndrome during childhood. Orphanet journal of rare diseases 15.

Mao, Y., Baum, B., 2015. Tug of war--the influence of opposing physical forces on epithelial cell morphology. Developmental biology 401.

Mapp, O., Wanner, S., Rohrschneider, M., Prince, V., 2010. Prickle1b mediates interpretation of migratory cues during zebrafish facial branchiomotor neuron migration. Developmental dynamics : an official publication of the American Association of Anatomists 239.

Mapp, O.M., Walsh, G.S., Moens, C.B., Tada, M., Prince, V.E., 2011. Zebrafish Prickle1b mediates facial branchiomotor neuron migration via a farnesylation-dependent nuclear activity. Development 138, 2121-2132.

Marcucio, R., Cordero, D., Hu, D., Helms, J., 2005. Molecular interactions coordinating the development of the forebrain and face. Developmental biology 284.

Marlow, F., Topczewski, J., Sepich, D., Solnica-Krezel, L., 2002. Zebrafish Rho kinase 2 acts downstream of Wnt11 to mediate cell polarity and effective convergence and extension movements. Current biology : CB 12.

Martelli-Junior, H., Coletta, R., Miranda, R., Barros, L., Swerts, M., Bonan, P., 2009. Orofacial features of Treacher Collins syndrome. Medicina oral, patologia oral y cirugia bucal 14.

Martin, A., Kaschube, M., Wieschaus, E., 2009. Pulsed contractions of an actin-myosin network drive apical constriction. Nature 457.

Martinelli, M., Palmieri, A., Carinci, F., Scapoli, L., 2020. Non-syndromic Cleft Palate: An Overview on Human Genetic and Environmental Risk Factors. Frontiers in cell and developmental biology 8.

Matsui, M., Klingensmith, J., 2014. Multiple tissue-specific requirements for the BMP antagonist Noggin in development of the mammalian craniofacial skeleton. Developmental biology 392.

Matsuo, K., Palmer, J.B., 2008. Anatomy and Physiology of Feeding and Swallowing: Normal and Abnormal. Physical Medicine and Rehabilitation Clinics of North America 19, 691-707.

Mcdonald, N.A., Fetter, R.D., Shen, K., 2020. Assembly of synaptic active zones requires phase separation of scaffold molecules. Nature 588, 454-458.

McGurk, P., Swartz, M., Chen, J., Galloway, J., Eberhart, J., 2017. In vivo zebrafish morphogenesis shows Cyp26b1 promotes tendon condensation and musculoskeletal patterning in the embryonic jaw. PLoS genetics 13.

Melville, D.B., Knapik, E.W., 2011. Traffic jams in fish bones: ER-to-Golgi protein transport during zebrafish development. Cell Adh Migr 5, 114-118.

Melville, D.B., Montero-Balaguer, M., Levic, D.S., Bradley, K., Smith, J.R., Hatzopoulos, A.K., Knapik, E.W., 2011. The feelgood mutation in zebrafish dysregulates COPII-dependent secretion of select extracellular matrix proteins in skeletal morphogenesis. Dis Model Mech 4, 763-776.

Michalk, A., Stricker, S., Becker, J., Rupps, R., Pantzar, T., Miertus, J., Botta, G., Naretto, V., Janetzki, C., Yaqoob, N., Ott, C., Seelow, D., Wieczorek, D., Fiebig, B., Wirth, B., Hoopmann, M., Walther, M., Körber, F., Blankenburg, M., Mundlos, S., Heller, R., Hoffmann, K., 2008. Acetylcholine receptor pathway mutations explain various fetal akinesia deformation sequence disorders. American journal of human genetics 82.

Mihaylova, V., Salih, M.A.M., Mukhtar, M.M., Abuzeid, H.A., El-Sadig, S.M., Von Der Hagen, M., Huebner, A., Nurnberg, G., Abicht, A., Muller, J.S., Lochmuller, H., Guergueltcheva, V., 2009. REFINEMENT OF THE CLINICAL PHENOTYPE IN MUSK-RELATED CONGENITAL MYASTHENIC SYNDROMES. Neurology 73, 1926-1928.

Mildinhall, S., 2012. Speech and language in the patient with cleft palate. Frontiers of oral biology 16.

Mio, C., Passon, N., Baldan, F., Bregant, E., Monaco, E., Mancini, L., Demori, E., Damante, G., 2020. CACNA1C haploinsufficiency accounts for the common features of interstitial 12p13.33 deletion carriers. European journal of medical genetics 63.

Miyashita, T., 2016. Fishing for jaws in early vertebrate evolution: a new hypothesis of mandibular confinement. Biological reviews of the Cambridge Philosophical Society 91.

Moens, C., Prince, V., 2002. Constructing the hindbrain: insights from the zebrafish. Developmental dynamics : an official publication of the American Association of Anatomists 224.

Monier, S., Jollivet, F., Janoueix-Lerosey, I., Johannes, L., Goud, B., 2002. Characterization of novel Rab6-interacting proteins involved in endosome-to-TGN transport. Traffic 3, 289-297.

Montague, T.G., Cruz, J.M., Gagnon, J.A., Church, G.M., Valen, E., 2014. CHOPCHOP: a CRISPR/Cas9 and TALEN web tool for genome editing. Nucleic Acids Res 42, W401-407.

Montero-Balaguer, M., Lang, M.R., Sachdev, S.W., Knappmeyer, C., Stewart, R.A., De La Guardia, A., Hatzopoulos, A.K., Knapik, E.W., 2006. The mother superior mutation ablates foxd3 activity in neural crest progenitor cells and depletes neural crest derivatives in zebrafish. Dev Dyn 235, 3199-3212.

Mori, Y., Matsui, T., Fukuda, M., 2013. Rabex-5 protein regulates dendritic localization of small GTPase Rab17 and neurite morphogenesis in hippocampal neurons. The Journal of biological chemistry 288.

Motch Perrine, S.M., Wu, M., Holmes, G., Bjork, B.C., Jabs, E.W., Richtsmeier, J.T., 2020. Phenotypes, Developmental Basis, and Genetics of Pierre Robin Complex. Journal of Developmental Biology 8, 30.

Muncie, J.M., Weaver, V.M., 2018. The Physical and Biochemical Properties of the Extracellular Matrix Regulate Cell Fate, Current Topics in Developmental Biology. Elsevier, pp. 1-37.

Müller, I., Melville, D., Tanwar, V., Rybski, W., Mukherjee, A., Shoemaker, M., Wang, W., Schoenhard, J., Roden, D., Darbar, D., Knapik, E., Hatzopoulos, A., 2013. Functional modeling in zebrafish demonstrates that the atrial-fibrillation-associated gene GREM2 regulates cardiac laterality, cardiomyocyte differentiation and atrial rhythm. Disease models & mechanisms 6.

Nakata, T., Kitamura, Y., Shimizu, K., Tanaka, S., Fujimori, M., Yokoyama, S., Ito, K., Emi, M., 1999. Fusion of a novel gene, ELKS, to RET due to translocation t(10;12)(q11;p13) in a papillary thyroid carcinoma. Genes Chromosomes Cancer 25, 97-103.

Nayak, S., Kadavigere, R., Mathew, M., Kumar, P., Hall, J., Girisha, K., 2014. Fetal akinesia deformation sequence: expanding the phenotypic spectrum. American journal of medical genetics. Part A 164A.

Neff, M., Turk, E., Kalishman, M., 2002. Web-based primer design for single nucleotide polymorphism analysis. Trends in genetics : TIG 18.

Neuhauss, S.C., Solnica-Krezel, L., Schier, A.F., Zwartkruis, F., Stemple, D.L., Malicki, J., Abdelilah, S., Stainier, D.Y., Driever, W., 1996. Mutations affecting craniofacial development in zebrafish. Development 123, 357-367.

Nie, S., Kee, Y., Bronner-Fraser, M., 2009. Myosin-X is critical for migratory ability of Xenopus cranial neural crest cells. Developmental biology 335.

Nie, S., Kee, Y., Bronner-Fraser, M., 2011. Caldesmon regulates actin dynamics to influence cranial neural crest migration in Xenopus. Molecular biology of the cell 22.

Nishimune, H., 2012. Molecular Mechanism of Active Zone Organization at Vertebrate Neuromuscular Junctions. Mol Neurobiol 45, 1-16.

Nishimune, H., Shigemoto, K., 2018. Practical Anatomy of the Neuromuscular Junction in Health and Disease. Neurologic clinics 36.

Noden, D., 1983. The role of the neural crest in patterning of avian cranial skeletal, connective, and muscle tissues. Developmental biology 96.

Noden, D., 1988. Interactions and fates of avian craniofacial mesenchyme. Development (Cambridge, England) 103 Suppl.

Noden, D., Francis-West, P., 2006. The differentiation and morphogenesis of craniofacial muscles. Developmental dynamics : an official publication of the American Association of Anatomists 235.

Noden, D., Trainor, P., 2005. Relations and interactions between cranial mesoderm and neural crest populations. Journal of anatomy 207.

Nomura, H., Ohtsuka, T., Tadokoro, S., Tanaka, M., Hirashima, N., 2009. Involvement of ELKS, an active zone protein, in exocytotic release from RBL-2H3 cells. Cell Immunol 258, 204-211.

Nowlan, N., Dumas, G., Tajbakhsh, S., Prendergast, P., Murphy, P., 2012. Biophysical stimuli induced by passive movements compensate for lack of skeletal muscle during embryonic skeletogenesis. Biomechanics and modeling in mechanobiology 11.

Nowlan, N., Sharpe, J., Roddy, K., Prendergast, P., Murphy, P., 2010. Mechanobiology of embryonic skeletal development: Insights from animal models. Birth defects research. Part C, Embryo today : reviews 90.

Nyitrai, H., Wang, S., Kaeser, P., 2020. ELKS1 Captures Rab6-Marked Vesicular Cargo in Presynaptic Nerve Terminals. Cell reports 31.

Odent, S., Attie-Bitach, T., Blayau, M., Mathieu, M., Auge, J., Delezoide, A.L., Le Gall, J.Y., Le Marec, B., Munnich, A., David, V., Vekemans, M., 1999. Expression of the Sonic hedgehog (SHH) Gene during Early Human Development and Phenotypic Expression of New Mutations Causing Holoprosencephaly. Human Molecular Genetics 8, 1683-1689.

Ohara-Imaizumi, M., Ohtsuka, T., Matsushima, S., Akimoto, Y., Nishiwaki, C., Nakamichi, Y., Kikuta, T., Nagai, S., Kawakami, H., Watanabe, T., Nagamatsu, S., 2005. ELKS, a protein structurally related to the active zone-associated protein CAST, is expressed in pancreatic beta cells and functions in insulin exocytosis: interaction of ELKS with exocytotic machinery analyzed by total internal reflection fluorescence microscopy. Mol Biol Cell 16, 3289-3300.

Ohtsuka, T., Takao-Rikitsu, E., Inoue, E., Inoue, M., Takeuchi, M., Matsubara, K., Deguchi-Tawarada, M., Satoh, K., Morimoto, K., Nakanishi, H., Takai, Y., 2002. Cast: a novel protein of the cytomatrix at the active zone of synapses that forms a ternary complex with RIM1 and munc13-1. J Cell Biol 158, 577-590.

Ono, F., Higashijima, S., Shcherbatko, A., Fetcho, J., Brehm, P., 2001. Paralytic zebrafish lacking acetylcholine receptors fail to localize rapsyn clusters to the synapse. The Journal of neuroscience : the official journal of the Society for Neuroscience 21.

Paes, E.C., De Vries, I.A.C., Penris, W.M., Hanny, K.H., Lavrijsen, S.W., Van Leerdam, E.K., Rademaker, M.M., Veldhoen, E.S., Eijkemans, R.M.J.C., Kon, M., Breugem, C.C., 2017. Growth and prevalence of feeding difficulties in children with Robin sequence: a retrospective cohort study. Clinical Oral Investigations 21, 2063-2076.

Panzer, J., Song, Y., Balice-Gordon, R., 2006. In vivo imaging of preferential motor axon outgrowth to and synaptogenesis at prepatterned acetylcholine receptor clusters in embryonic zebrafish skeletal muscle. The Journal of neuroscience : the official journal of the Society for Neuroscience 26.

Panzer, J.A., Gibbs, S.M., Dosch, R., Wagner, D., Mullins, M.C., Granato, M., Balice-Gordon, R.J., 2005. Neuromuscular synaptogenesis in wild-type and mutant zebrafish. Dev Biol 285, 340-357.

Paradowska-Stolarz, A., Kawala, B., 2014. Occlusal disorders among patients with total clefts of lip, alveolar bone, and palate. BioMed research international 2014.

Perissinotto, D., Iacopetti, P., Bellina, I., Doliana, R., Colombatti, A., Pettway, Z., Bronner-Fraser, M., Shinomura, T., Kimata, K., Mörgelin, M., Löfberg, J., Perris, R., 2000. Avian neural crest cell migration is diversely regulated by the two major hyaluronan-binding proteoglycans PG-M/versican and aggrecan. Development (Cambridge, England) 127.

Perris, R., Perissinotto, D., 2000. Role of the extracellular matrix during neural crest cell migration. Mechanisms of development 95.

Peterson, B., Rolfe, R., Kunselman, A., Murphy, P., Szczesny, S., 2021. Mechanical Stimulation via Muscle Activity Is Necessary for the Maturation of Tendon Multiscale Mechanics During Embryonic Development. Frontiers in cell and developmental biology 9.

Phelan, K., Hollyday, M., 1990. Axon guidance in muscleless chick wings: the role of muscle cells in motoneuronal pathway selection and muscle nerve formation. The Journal of neuroscience : the official journal of the Society for Neuroscience 10.

Pietri, T., Eder, O., Breau, M., Topilko, P., Blanche, M., Brakebusch, C., Fässler, R., Thiery, J., Dufour, S., 2004. Conditional beta1-integrin gene deletion in neural crest cells causes severe developmental alterations of the peripheral nervous system. Development (Cambridge, England) 131.

Poets, C., Bacher, M., 2011. Treatment of upper airway obstruction and feeding problems in Robin-like phenotype. The Journal of pediatrics 159.

Ponomareva, O., Eliceiri, K., Halloran, M., 2016. Charcot-Marie-Tooth 2b associated Rab7 mutations cause axon growth and guidance defects during vertebrate sensory neuron development. Neural development 11.

Proszynski, T.J., Sanes, J.R., 2013. Amotl2 interacts with LL5beta, localizes to podosomes and regulates postsynaptic differentiation in muscle. J Cell Sci 126, 2225-2235.

Ramella, M., Ribolla, L., de Curtis, I., 2022. Liquid-Liquid Phase Separation at the Plasma Membrane-Cytosol Interface: Common Players in Adhesion, Motility, and Synaptic Function. Journal of molecular biology 434.

Reddi, A.H., Gay, R., Gay, S., Miller, E.J., 1977. Transitions in collagen types during matrix-induced cartilage, bone, and bone marrow formation. Proc Natl Acad Sci U S A 74, 5589-5592.

Richardson, J., Gauert, A., Briones, M., L, Fanlo, L., Alhashem, Z., Assar, R., Marti, E., Kabla, A., Härtel, S., Linker, C., 2016. Leader Cells Define Directionality of Trunk, but Not Cranial, Neural Crest Cell Migration. Cell reports 15.

Richardson, R., Dixon, J., Jiang, R., Dixon, M., 2009. Integration of IRF6 and Jagged2 signalling is essential for controlling palatal adhesion and fusion competence. Human molecular genetics 18.

Ridenour, D.A., Mclennan, R., Teddy, J.M., Semerad, C.L., Haug, J.S., Kulesa, P.M., 2014. The neural crest cell cycle is related to phases of migration in the head. Development 141, 1095-1103.

Rooryck, C., Stef, M., Burgelin, I., Simon, D., Souakri, N., Thambo, J.B., Chateil, J.F., Lacombe, D., Arveiler, B., 2009. 2.3 Mb terminal deletion in 12p13.33 associated with oculoauriculovertebral spectrum and evaluation of WNT5B as a candidate gene. Eur J Med Genet 52, 446-449.

Rossi, A., Kontarakis, Z., Gerri, C., Nolte, H., Hölper, S., Krüger, M., Stainier, D.Y.R., 2015. Genetic compensation induced by deleterious mutations but not gene knockdowns. Nature 524, 230-233.

Saadi, I., Alkuraya, F., Gisselbrecht, S., Goessling, W., Cavallesco, R., Turbe-Doan, A., Petrin, A., Harris, J., Siddiqui, U., Grix, A., Hove, H., Leboulch, P., Glover, T., Morton, C., Richieri-Costa, A., Murray, J., Erickson, R., Maas, R., 2011. Deficiency of the cytoskeletal protein SPECC1L leads to oblique facial clefting. American journal of human genetics 89.

Sabo, S., Gomes, R., McAllister, A., 2006. Formation of presynaptic terminals at predefined sites along axons. The Journal of neuroscience : the official journal of the Society for Neuroscience 26.

Sai, X., Yonemura, S., Ladher, R., 2014. Junctionally restricted RhoA activity is necessary for apical constriction during phase 2 inner ear placode invagination. Developmental biology 394.

Sala, K., Corbetta, A., Minici, C., Tonoli, D., Murray, D., Cammarota, E., Ribolla, L., Ramella, M., Fesce, R., Mazza, D., Degano, M., de Curtis, I., 2019. The ERC1 scaffold protein implicated in cell motility drives the assembly of a liquid phase. Scientific reports 9.

Sala, K., Raimondi, A., Tonoli, D., Tacchetti, C., de Curtis, I., 2018. Identification of a membrane-less compartment regulating invadosome function and motility. Scientific reports 8.

Sanes, J.R., Lichtman, J.W., 1999. DEVELOPMENT OF THE VERTEBRATE NEUROMUSCULAR JUNCTION. Annual Review of Neuroscience 22, 389-442.

Sanes, J.R., Lichtman, J.W., 2001. Induction, assembly, maturation and maintenance of a postsynaptic apparatus. Nat Rev Neurosci 2, 791-805.

Sarmah, S., Barrallo-Gimeno, A., Melville, D.B., Topczewski, J., Solnica-Krezel, L., Knapik, E.W., 2010. Sec24D-dependent transport of extracellular matrix proteins is required for zebrafish skeletal morphogenesis. PLoS One 5, e10367.

Schekman, R., Orci, L., 1996. Coat proteins and vesicle budding. Science 271, 1526-1533.

Schilling, T., Kimmel, C., 1994. Segment and cell type lineage restrictions during pharyngeal arch development in the zebrafish embryo. Development (Cambridge, England) 120.

Schilling, T.F., Kimmel, C.B., 1997. Musculoskeletal patterning in the pharyngeal segments of the zebrafish embryo. Development 124, 2945-2960.

Schilling, T.F., Piotrowski, T., Grandel, H., Brand, M., Heisenberg, C.P., Jiang, Y.J., Beuchle, D., Hammerschmidt, M., Kane, D.A., Mullins, M.C., van Eeden, F.J., Kelsh, R.N., Furutani-Seiki, M., Granato, M., Haffter, P., Odenthal, J., Warga, R.M., Trowe, T., Nusslein-Volhard, C., 1996. Jaw and branchial arch mutants in zebrafish I: branchial arches. Development 123, 329-344.

Schlager, M., Kapitein, L., Grigoriev, I., Burzynski, G., Wulf, P., Keijzer, N., de Graaff, E., Fukuda, M., Shepherd, I., Akhmanova, A., Hoogenraad, C., 2010. Pericentrosomal targeting of Rab6 secretory vesicles by Bicaudal-D-related protein 1 (BICDR-1) regulates neuritogenesis. The EMBO journal 29.

Schlosser, G., 2006. Induction and specification of cranial placodes. Developmental biology 294.

Scott, J.E., 2003. Elasticity in extracellular matrix ‘shape modules’ of tendon, cartilage, etc. A sliding proteoglycan-filament model. The Journal of Physiology 553, 335-343.

Sepich, D., Usmani, M., Pawlicki, S., Solnica-Krezel, L., 2011. Wnt/PCP signaling controls intracellular position of MTOCs during gastrulation convergence and extension movements. Development (Cambridge, England) 138.

Shankland, W., 2001. The trigeminal nerve. Part IV: the mandibular division. Cranio : the journal of craniomandibular practice 19.

Sholl, D., 1953. Dendritic organization in the neurons of the visual and motor cortices of the cat. Journal of anatomy 87.

Shwartz, Y., Blitz, E., Zelzer, E., 2013. One load to rule them all: mechanical control of the musculoskeletal system in development and aging. Differentiation; research in biological diversity 86.

Shwartz, Y., Farkas, Z., Stern, T., Aszódi, A., Zelzer, E., 2012. Muscle contraction controls skeletal morphogenesis through regulation of chondrocyte convergent extension. Developmental biology 370.

Silva, I.M., Rosenfeld, J., Antoniuk, S.A., Raskin, S., Sotomaior, V.S., 2014. A 1.5Mb terminal deletion of 12p associated with autism spectrum disorder. Gene 542, 83-86.

Singh, D., Bartlett, S., 2005. Congenital mandibular hypoplasia: analysis and classification. The Journal of craniofacial surgery 16.

Singh, V.P., Moss, T.P., 2015. Psychological impact of visible differences in patients with congenital craniofacial anomalies. Progress in Orthodontics 16.

Sjögreen, L., Engvall, M., Ekström, A.-B., Lohmander, A., Kiliaridis, S., Tulinius, M., 2006. Orofacial dysfunction in children and adolescents with myotonic dystrophy. Developmental Medicine & Child Neurology 49, 18-22.

Skorpen, J., Lafond-Benestad, S., Lømo, T., 1999. Regulation of the size and distribution of ectopic neuromuscular junctions in adult skeletal muscle by nerve-derived trophic factor and electrical muscle activity. Molecular and cellular neurosciences 13.

Slater, C.R., 2017. The Structure of Human Neuromuscular Junctions: Some Unanswered Molecular Questions, Int J Mol Sci.

Stottmann, R., Anderson, R., Klingensmith, J., 2001. The BMP antagonists Chordin and Noggin have essential but redundant roles in mouse mandibular outgrowth. Developmental biology 240.

Strachan, L., Condic, M., 2003. Neural crest motility and integrin regulation are distinct in cranial and trunk populations. Developmental biology 259.

Strachan, L.R., Condic, M.L., 2004. Cranial neural crest recycle surface integrins in a substratum-dependent manner to promote rapid motility. Journal of Cell Biology 167, 545-554.

Strachan, L.R., Condic, M.L., 2008. Neural crest motility on fibronectin is regulated by integrin activation. Experimental Cell Research 314, 441-452.

Straube, A., Merdes, A., 2007. EB3 regulates microtubule dynamics at the cell cortex and is required for myoblast elongation and fusion. Current biology : CB 17.

Subramanian, A., Kanzaki, L., Galloway, J., Schilling, T., 2018. Mechanical force regulates tendon extracellular matrix organization and tenocyte morphogenesis through TGFbeta signaling. eLife 7.

Subramanian, A., Schilling, T., 2014. Thrombospondin-4 controls matrix assembly during development and repair of myotendinous junctions. eLife 3.

Subramanian, A., Schilling, T., 2015. Tendon development and musculoskeletal assembly: emerging roles for the extracellular matrix. Development (Cambridge, England) 142.

Sudhof, T.C., 2012. The presynaptic active zone. Neuron 75, 11-25.

Sugimoto, Y., Takimoto, A., Akiyama, H., Kist, R., Scherer, G., Nakamura, T., Hiraki, Y., Shukunami, C., 2013. Scx+/Sox9+ progenitors contribute to the establishment of the junction between cartilage and tendon/ligament. Development (Cambridge, England) 140.

Szabo-Rogers, H., Smithers, L., Yakob, W., Liu, K., 2010. New directions in craniofacial morphogenesis. Developmental biology 341.

Szabó, A., Mayor, R., 2018. Mechanisms of Neural Crest Migration. Annual review of genetics 52.

Szabó, A., Melchionda, M., Nastasi, G., Woods, M.L., Campo, S., Perris, R., Mayor, R., 2016. In vivo confinement promotes collective migration of neural crest cells. Journal of Cell Biology 213, 543-555.

Szokol, K., Glover, J., Perreault, M., 2008. Differential origin of reticulospinal drive to motoneurons innervating trunk and hindlimb muscles in the mouse revealed by optical recording. The Journal of physiology 586.

Szul, T., Sztul, E., 2011. COPII and COPI traffic at the ER-Golgi interface. Physiology (Bethesda) 26, 348-364.

Szyszka-Sommerfeld, L., Budzyńska, A., Lipski, M., Kulesza, S., Woźniak, K., 2020. Assessment of Masticatory Muscle Function in Patients with Bilateral Complete Cleft Lip and Palate and Posterior Crossbite by means of Electromyography. Journal of healthcare engineering 2020.

Szyszka-Sommerfeld, L., Woźniak, K., Matthews-Brzozowska, T., Kawala, B., Mikulewicz, M., Machoy, M., 2018. The electrical activity of the masticatory muscles in children with cleft lip and palate. International journal of paediatric dentistry 28.

Tan, Y., Fu, R., Liu, J., Wu, Y., Wang, B., Jiang, N., Nie, P., Cao, H., Yang, Z., Fang, B., 2016. ADAM10 is essential for cranial neural crest-derived maxillofacial bone development. Biochemical and biophysical research communications 475.

Tanaka, H., Maeda, R., Shoji, W., Wada, H., Masai, I., Shiraki, T., Kobayashi, M., Nakayama, R., Okamoto, H., 2007. Novel mutations affecting axon guidance in zebrafish and a role for plexin signalling in the guidance of trigeminal and facial nerve axons. Development 134, 3259-3269.

Taylor, R.W., Qi, J.Y., Talaga, A.K., Ma, T.P., Pan, L., Bartholomew, C.R., Klionsky, D.J., Moens, C.B., Gamse, J.T., 2011. Asymmetric Inhibition of Ulk2 Causes Left-Right Differences in Habenular Neuropil Formation. Journal of Neuroscience 31, 9869-9878.

Thevenon, J., Callier, P., Andrieux, J., Delobel, B., David, A., Sukno, S., Minot, D., Mosca Anne, L., Marle, N., Sanlaville, D., Bonnet, M., Masurel-Paulet, A., Levy, F., Gaunt, L., Farrell, S., Le Caignec, C., Toutain, A., Carmignac, V., Mugneret, F., Clayton-Smith, J., Thauvin-Robinet, C., Faivre, L., 2013. 12p13.33 microdeletion including ELKS/ERC1, a new locus associated with childhood apraxia of speech. Eur J Hum Genet 21, 82-88.

Thisse, B., Thisse, C., 2014. In Situ Hybridization on Whole-Mount Zebrafish Embryos and Young Larvae, Methods in Molecular Biology. Springer New York, pp. 53-67.

Tjakkes, G.H., Reinders, J.J., Tenvergert, E.M., Stegenga, B., 2010. TMD pain: the effect on health related quality of life and the influence of pain duration. Health Qual Life Outcomes 8, 46.

Tokoro, T., Higa, S., Deguchi-Tawarada, M., Inoue, E., Kitajima, I., Ohtsuka, T., 2007. Localization of the active zone proteins CAST, ELKS, and Piccolo at neuromuscular junctions. Neuroreport 18, 313-316.

tom Dieck, S., Specht, D., Strenzke, N., Hida, Y., Krishnamoorthy, V., Schmidt, K.F., Inoue, E., Ishizaki, H., Tanaka-Okamoto, M., Miyoshi, J., Hagiwara, A., Brandstatter, J.H., Lowel, S., Gollisch, T., Ohtsuka, T., Moser, T., 2012. Deletion of the presynaptic scaffold CAST reduces active zone size in rod photoreceptors and impairs visual processing. The Journal of neuroscience : the official journal of the Society for Neuroscience 32, 12192-12203.

Trainor, P., 2005. Specification and patterning of neural crest cells during craniofacial development. Brain, behavior and evolution 66.

Trainor, P., Tam, P., 1995. Cranial paraxial mesoderm and neural crest cells of the mouse embryo: co-distribution in the craniofacial mesenchyme but distinct segregation in branchial arches. Development (Cambridge, England) 121.

Trainor, P.A., 2010. Craniofacial birth defects: The role of neural crest cells in the etiology and pathogenesis of Treacher Collins syndrome and the potential for prevention. American Journal of Medical Genetics Part A 152A, 2984-2994.

Tropepe, V., Sive, H.L., 2003. Can zebrafish be used as a model to study the neurodevelopmental causes of autism? Genes Brain Behav 2, 268-281.

Twigg, S., Wilkie, A., 2015. New insights into craniofacial malformations. Human molecular genetics 24.

Uemura, O., Okada, Y., Ando, H., Guedj, M., Higashijima, S., Shimazaki, T., Chino, N., Okano, H., Okamoto, H., 2005. Comparative functional genomics revealed conservation and diversification of three enhancers of the isl1 gene for motor and sensory neuron-specific expression. Dev Biol 278, 587-606.

Umemoto, G., Nakamura, H., Oya, Y., Kikuta, T., 2009. Masticatory dysfunction in patients with myotonic dystrophy (type 1): a 5-year follow-up. Special Care in Dentistry 29, 210-214.

Unlu, G., Gamazon, E., Qi, X., Levic, D., Bastarache, L., Denny, J., Roden, D., Mayzus, I., Breyer, M., Zhong, X., Konkashbaev, A., Rzhetsky, A., Knapik, E., Cox, N., 2019. GRIK5 Genetically Regulated Expression Associated with Eye and Vascular Phenomes: Discovery through Iteration among Biobanks, Electronic Health Records, and Zebrafish. American journal of human genetics 104.

Unlu, G., Levic, D.S., Melville, D.B., Knapik, E.W., 2014. Trafficking mechanisms of extracellular matrix macromolecules: insights from vertebrate development and human diseases. Int J Biochem Cell Biol 47, 57-67.

Unlu, G., Qi, X., Gamazon, E., Melville, D., Patel, N., Rushing, A., Hashem, M., Al-Faifi, A., Chen, R., Li, B., Cox, N., Alkuraya, F., Knapik, E., 2020. Phenome-based approach identifies RIC1-linked Mendelian syndrome through zebrafish models, biobank associations and clinical studies. Nature medicine 26.

Vacaru, A.M., Unlu, G., Spitzner, M., Mione, M., Knapik, E.W., Sadler, K.C., 2014. In vivo cell biology in zebrafish - providing insights into vertebrate development and disease. J Cell Sci 127, 485-495.

Van De Lande, L.S., Caron, C.J.J.M., Pluijmers, B.I., Joosten, K.F.M., Streppel, M., Dunaway, D.J., Koudstaal, M.J., Padwa, B.L., 2018. Evaluation of Swallow Function in Patients with Craniofacial Microsomia: A Retrospective Study. Dysphagia 33, 234-242.

van Eijden, T., Turkawski, S., 2001. Morphology and physiology of masticatory muscle motor units. Critical reviews in oral biology and medicine : an official publication of the American Association of Oral Biologists 12.

Van Otterloo, E., Williams, T., Artinger, K.B., 2016. The old and new face of craniofacial research: How animal models inform human craniofacial genetic and clinical data. Dev Biol 415, 171-187.

Varshney, G.K., Pei, W., LaFave, M.C., Idol, J., Xu, L., Gallardo, V., Carrington, B., Bishop, K., Jones, M., Li, M., Harper, U., Huang, S.C., Prakash, A., Chen, W., Sood, R., Ledin, J., Burgess, S.M., 2015. High-throughput gene targeting and phenotyping in zebrafish using CRISPR/Cas9. Genome Res.

Vermillion, K., Lidberg, K., Gammill, L., 2014. Expression of actin-binding proteins and requirement for actin-depolymerizing factor in chick neural crest cells. Developmental dynamics : an official publication of the American Association of Anatomists 243.

Villarroel-Campos, D., Bronfman, F.C., Gonzalez-Billault, C., 2016. Rab GTPase signaling in neurite outgrowth and axon specification. Cytoskeleton (Hoboken) 73, 498-507.

Vogt, J., Morgan, N., Marton, T., Maxwell, S., Harrison, B., Beeson, D., Maher, E., 2009. Germline mutation in DOK7 associated with fetal akinesia deformation sequence. Journal of medical genetics 46.

von Cramon-Taubadel, N., 2011. Global human mandibular variation reflects differences in agricultural and hunter-gatherer subsistence strategies. Proceedings of the National Academy of Sciences of the United States of America 108.

Wada, N., Javidan, Y., Nelson, S., Carney, T., Kelsh, R., Schilling, T., 2005. Hedgehog signaling is required for cranial neural crest morphogenesis and chondrogenesis at the midline in the zebrafish skull. Development (Cambridge, England) 132.

Wagh, D.A., Rasse, T.M., Asan, E., Hofbauer, A., Schwenkert, I., Durrbeck, H., Buchner, S., Dabauvalle, M.C., Schmidt, M., Qin, G., Wichmann, C., Kittel, R., Sigrist, S.J., Buchner, E., 2006. Bruchpilot, a protein with homology to ELKS/CAST, is required for structural integrity and function of synaptic active zones in Drosophila. Neuron 49, 833-844.

Walker, L., Roque, R., Navarro, M., Granato, M., 2021. Agrin/Lrp4 signal constrains MuSK-dependent neuromuscular synapse development in appendicular muscle. Development (Cambridge, England) 148.

Walker, M.B., Kimmel, C.B., 2007. A two-color acid-free cartilage and bone stain for zebrafish larvae. Biotech Histochem 82, 23-28.

Walsh, M., Lichtman, J., 2003. In vivo time-lapse imaging of synaptic takeover associated with naturally occurring synapse elimination. Neuron 37.

Wang, H., Luo, X., Leighton, J., 2015. Extracellular Matrix and Integrins in Embryonic Stem Cell Differentiation. Biochemistry Insights 8s2, BCI.S30377.

Wang, S.S., Held, R.G., Wong, M.Y., Liu, C., Karakhanyan, A., Kaeser, P.S., 2016. Fusion Competent Synaptic Vesicles Persist upon Active Zone Disruption and Loss of Vesicle Docking. Neuron 91, 777-791.

Wang, Y., Liu, X., Biederer, T., Sudhof, T.C., 2002. A family of RIM-binding proteins regulated by alternative splicing: Implications for the genesis of synaptic active zones. Proc Natl Acad Sci U S A 99, 14464-14469.

Wang, Y., Zheng, Y., Chen, D., Chen, Y., 2013. Enhanced BMP signaling prevents degeneration and leads to endochondral ossification of Meckel's cartilage in mice. Developmental biology 381.

Wansleeben, C., Meijlink, F., 2011. The planar cell polarity pathway in vertebrate development. Developmental dynamics : an official publication of the American Association of Anatomists 240.

Webb, B.D., Manoli, I., Engle, E.C., Jabs, E.W., 2021. A framework for the evaluation of patients with congenital facial weakness. Orphanet Journal of Rare Diseases 16.

Welby, L., Caudill, H., Yitsege, G., Hamad, A., Bunyak, F., Zohn, I., Maynard, T., LaMantia, A., Mendelowitz, D., Lever, T., 2020. Persistent Feeding and Swallowing Deficits in a Mouse Model of 22q11.2 Deletion Syndrome. Frontiers in neurology 11.

Westerfield, M., 2000. The zebrafish book. A guide for the laboratory use of zebrafish (Danio rerio), 4th edition ed. University of Oregon Press, Eugene.

Wilbe, M., Ekvall, S., Eurenius, K., Ericson, K., Casar-Borota, O., Klar, J., Dahl, N., Ameur, A., Annerén, G., Bondeson, M., 2015. MuSK: a new target for lethal fetal akinesia deformation sequence (FADS). Journal of medical genetics 52.

Wu, H., Xiong, W.C., Mei, L., 2010. To build a synapse: signaling pathways in neuromuscular junction assembly. Development 137, 1017-1033.

Wu, P., Jiang, T., Shen, J., Widelitz, R., Chuong, C., 2006. Morphoregulation of avian beaks: comparative mapping of growth zone activities and morphological evolution. Developmental dynamics : an official publication of the American Association of Anatomists 235.

Wyngaarden, L., Vogeli, K., Ciruna, B., Wells, M., Hadjantonakis, A., Hopyan, S., 2010. Oriented cell motility and division underlie early limb bud morphogenesis. Development (Cambridge, England) 137.

Yamaguchi, T., Bradley, A., McMahon, A., Jones, S., 1999. A Wnt5a pathway underlies outgrowth of multiple structures in the vertebrate embryo. Development (Cambridge, England) 126.

Yang, X., Arber, S., William, C., Li, L., Tanabe, Y., Jessell, T., Birchmeier, C., Burden, S., 2001. Patterning of muscle acetylcholine receptor gene expression in the absence of motor innervation. Neuron 30.

Yin, X., Yu, T., Chen, B., Xu, J., Chen, W., Qi, Y., Zhang, P., Li, Y., Kou, Y., Ma, Y., Han, N., Wan, P., Luo, Q., Zhu, D., Jiang, B., 2019. Spatial Distribution of Motor Endplates and its Adaptive Change in Skeletal Muscle. Theranostics 9.

Yoshihisa, T., Barlowe, C., Schekman, R., 1993. Requirement for a GTPase-activating protein in vesicle budding from the endoplasmic reticulum. Science 259, 1466-1468.

Zhang, J., Lefebvre, J.L., Zhao, S., Granato, M., 2004. Zebrafish unplugged reveals a role for muscle-specific kinase homologs in axonal pathway choice. Nature Neuroscience 7, 1303-1309.

Šmít, D., Fouquet, C., Pincet, F., Zapotocky, M., Trembleau, A., 2017. Axon tension regulates fasciculation/defasciculation through the control of axon shaft zippering. eLife 6.